

Peptide Modification of Polyimide-Insulated Microwires for Reducing Glial Scarring

by

Sangita Sridar

A thesis submitted in partial fulfillment of the requirements for the degree of

Master of Science

in

Materials Engineering

Department of Chemical and Materials Engineering  
University of Alberta

© Sangita Sridar, 2015

## **Abstract**

Neuroprosthetic devices are either stimulation or recording electrodes that are used to restore functionality of the human body after neural injury or disease. The long-term utility of these devices is limited by their viability and stability within the central nervous system due to foreign body response from glial cells, namely microglia and astrocytes. During this response, these glial cells form scar tissue (glial scar) around the implant (to isolate the device and electrically insulate from the neurons). These cells also secrete chemicals to inhibit the outgrowth of neuron processes, which affects the electrode function. This work focuses on a method for modulating the responses from the microglia and astrocyte to reduce scarring around microstimulation electrodes comprised of polyimide-insulated platinum (Pt) / iridium (Ir) metal alloy. The surface of the electrodes are functionalized with a specific peptide – with the sequence KHIFSDDSSSE – to modulate the glial scar. This peptide is similar to the homophilic binding site of neural cell adhesion molecules (NCAM). In this work, it was shown that this peptide reduced the proliferation of microglia and astrocytes (when added in solution to pure astrocyte cultures). The responses of microglia and astrocytes to both peptide-coated and uncoated electrodes were tested in 3D gels. From these tests, fewer microglia were found in the region surrounding peptide-coated electrodes than uncoated electrodes. The modulation of microglial response is indicative of modulation of the acute response. Astrocytes preferentially attached to the peptide-coated electrode, and the number of attached astrocytes remained the same up to 2 weeks post implantation compared to the uncoated electrode. The modulation of astrocyte response is indicative of modulation of the initial stages of the chronic response. These results suggest that this peptide could be used to modulate scar tissue formation by glial cells.

## **Dedication**

This thesis is dedicated to my family, and friends for their continued support, and motivation during this challenging research career.

## **Acknowledgements**

I would like to thank my supervisor Dr. Anastasia Elias for her support, encouragement and guidance throughout my research to make it successful. I would also like thank Dr. Kathryn Todd for her support and guidance in the field of neuroscience. She helped me learn new aspects in the field of neuroscience and her guidance ensured in making my project successful.

I would also like to extend a special thanks to Dr. Matthew Churchward, who helped a lot in guiding, training and advising me through my experiments. I would also like to thank Dr. Kamaldeep Dhama, Dr. Dimitre Karpuzov, Andrea Jeffery, Kyle Koss, Preetam Anbukarasu, who played an essential role in training and advising me through my research. I would like to thank my other lab mates Diana Martinez Tobon, Dr. Chan Chan Wang, Theodore Ng, Dr. Ben Nearingburg, Joshua Cunningham, Sam Joshua, and Erika Johnson who supported me during my work time in the labs.

Finally, I would like to acknowledge the funding agencies Alberta Health Services (AHS) and Alberta Innovates Health Solutions (AIHS) that contributed significantly to the progress of my research.

# Table of Contents

<b>Chapter 1.0</b> .....	1
<b>Introduction</b> .....	1
1.1 Overview:.....	2
1.2 Neuroprosthetic devices.....	3
1.3 Biocompatibility of the neuroprosthetic devices.....	4
1.4 Strategies to improve biocompatibility.....	6
1.4.1. Electrode design.....	7
1.4.2. Drug delivery systems.....	10
1.4.3. Surface functionalization of electrodes.....	11
1.4.3.1. Nanoporous gold coatings.....	11
1.4.3.2. Hydrogel coatings.....	12
1.4.3.3. Peptides and proteins.....	12
1.5 Experimental outline.....	15
<b>Chapter 2.0</b> .....	17
<b>Effect of peptide in 2D mixed glial cultures</b> .....	17
2.1 Introduction to effect of peptide in 2D mixed glial cultures.....	18
2.2 Glial cell extraction and their growth in 2D culture plates.....	19
2.3 Treatment with solution containing peptide.....	22
2.4 Characterisation of the 2D cultures to visualize the effect of peptide.....	23
2.5 Peptide dependence on cell seeding density.....	31
2.6 Summary.....	32
<b>Chapter 3.0</b> .....	33
<b>Peptide attachment on the microwires</b> .....	33

3.1 Introduction to peptide attachment on microwires.....	34
3.2 Process steps of the peptide attachment process .....	34
3.2.1 Oxygen plasma treatment step.....	36
3.2.2 Silane attachment step .....	36
3.2.2.1 X-ray photoelectron spectroscopy (XPS) .....	39
3.2.2.2 Fluorescence microscope.....	39
3.2.2.3 Optimization of APTES layer on the glass substrate.....	40
3.2.2.4 APTES deposition on PI wire .....	49
3.2.3 Peptide attachment step .....	51
3.3. Summary .....	57
<b>Chapter 4.0</b> .....	<b>58</b>
<b>Testing peptide-coated wire in 3D mixed glial cultures</b> .....	<b>58</b>
4.1 Introduction to responses of glial cells to peptide-coated wire in 3D mixed glial cultures	59
4.2 Glial cell extraction and their growth in 3D gels .....	59
4.3 Peptide coating on the wire and insertion into the gel .....	61
4.4 Characterization of 3D gels with cells .....	62
4.4.1. Viability of cells in 3D gels.....	63
4.4.2. Morphology of cells in 3D gels .....	70
4.5 Responses of glial cells to the peptide-coated wire.....	72
4.5.1. Microglia counts near the wire .....	77
4.5.2. GFAP signal intensity from the astrocytes attached to the wire.....	79
4.5.3. Morphology of microglia and astrocytes after wire insertion .....	81
4.6 Summary .....	84
<b>Chapter 5.0</b> .....	<b>85</b>
<b>Future work and conclusion</b> .....	<b>85</b>

5.1. Overview .....	86
5.2. Future work .....	86
5.2.1. Improving peptide attachment process .....	86
5.2.2. Studies on peptide stability .....	87
5.2.3. Measurement of indicators contributing to glial scar .....	88
5.3. Conclusion.....	89
<b>Reference</b> .....	<b>93</b>

## List of tables

<b>Table 3.1:</b> Comparative table of the BE values of the samples deposited under pH 6 to that of the BE values in the literature [50], [59]–[63] for elements like C, O, N, and Si (2p).....	<b>40</b>
---	-----------

## List of figures

<b>Figure 1.1:</b> Schematic of glial scar formation. Microglia cells (Red) first become activated and morphology changes from ramified to amoeboid. Astrocytes (Green) react at a later point in time and forms scar tissue [10]. Reprinted with permission from dx.doi.org/10.1021/bm500318d   Biomacromolecules 2014, 15, 2157–2165}. Copyright 2014 American Chemical Society. ....	<b>5</b>
<b>Figure 2.1:</b> Schematic of Hemocytometer grid. The five regions used for cell counting are marked as blue squares in the large central grid. One of the regions is zoomed to show an example for counting cells. The live cells (in light blue circles) and the dead cells (in dark blue circles) are present in this region and the letter ‘X’ is marked to show that cells falling in that region would not count.....	<b>21</b>
<b>Figure 2.2:</b> Fluorescence microscope images showing nuclei of all cells labeled with Hoechst stain (HS) and nuclei of proliferating cells with EdU for various concentrations of peptide i.e. 0 µg/mL (control) and 50 µg/mL of media in 2 D mixed glial cultures. The enlarged section shows purple colored and blue colored circular structures which are nuclei of proliferating and non-proliferating glial cells respectively.....	<b>26</b>
<b>Figure 2.3:</b> Fluorescence microscope images showing microglial labeled with Iba1 and astrocytes labeled with GFAP for various concentrations of peptide i.e. 0 µg/mL (control) and 50 µg/mL of media in 2 D mixed glial cultures. ....	<b>27</b>
<b>Figure 2.4:</b> Plot showing the percentage of proliferating glial cell for various peptide concentrations. Each bar is based on the average of 5 samples (3 independent experiments). The one-way ANOVA showing a statistical significance for the entire raw data and Dunnett’s comparison test showing that the sample treated with 50 µg/mL peptide concentration reduces the proliferation of glial cells when compared to the sample treated with 0 µg/mL peptide concentration (P=0.0449, >95 %confidence interval).The significance bar (Labeled with *) indicates the difference between the 0 (control) and 50 µg/mL is significant.....	<b>29</b>

**Figure 2.5:** a) Comparative plot showing the percentage of proliferating total glial cell for peptide concentrations 0  $\mu\text{g/mL}$  and 50  $\mu\text{g/mL}$  (Unpaired t-test, P-value =0.007, >95 % confidence interval). The significance bar (Labeled with \*\*) indicates the difference between the 0 (control) and 50  $\mu\text{g/mL}$  is very significant. b) Comparative plot showing the percentage of proliferating microglial cell for peptide concentrations 0  $\mu\text{g/mL}$  and 50  $\mu\text{g/mL}$  (Unpaired t-test, P-value =0.0394, >95 % confidence interval). The significance bar (Labeled with \*) indicates the difference between the 0 (control) and 50  $\mu\text{g/mL}$  is significant. c) Comparative plot showing the percentage of proliferating astrocytes for peptide concentrations 0  $\mu\text{g/mL}$  and 50  $\mu\text{g/mL}$  (Unpaired t-test, P-value =0.0413, >95 % confidence interval). The significance bar (Labeled with \*) indicates the difference between the 0 (control) and 50  $\mu\text{g/mL}$  is significant..... **30**

**Figure 2.6:** Plots showing the percentage of proliferating glial cells for peptide concentrations 0  $\mu\text{g/mL}$  and 50  $\mu\text{g/mL}$  at two seeding densities ( $8 \times 10^6$  cells/mL and  $2 \times 10^4$  cells/mL). a) High seeding density of  $8 \times 10^6$  cells/mL. The unpaired t-test showing no statistical significance in percentage of proliferating glial cells between 0  $\mu\text{g/mL}$  and 50  $\mu\text{g/mL}$  peptide concentrations (P=0.5028, >95 %confidence interval). b) Low seeding density  $2 \times 10^4$  cells/mL. The unpaired t-test showing a statistical significance in percentage of proliferating glial cells for the low seeding density raw data, and the result showing that the peptide at 50  $\mu\text{g/mL}$  peptide concentration reduces the proliferation of glial cells when compared to the sample with 0  $\mu\text{g/mL}$  peptide concentration (P=0.0449, >95 %confidence interval). The significance bar (Labeled with \*\*) indicates the difference between the 0 (control) and 50  $\mu\text{g/mL}$  is very significant..... **31**

**Figure 3.1:** Schematic of peptide attachment process a) Polyimide-insulated microwire (PI wire) cleaned with isopropanol and acetone b) The oxygen plasma treatment of the polyimide wire c) The covalent bonding of silane to the oxygen plasma treated wires d) The amide bond formation ( marked by black circle ) between the peptide and the silane using EDC. .... **35**

**Figure 3.2:** Schematic of oxygen plasma treatment step. The image showing the schematic of micro-etch RIE equipment with the chamber containing wire sample (zoomed portion in the image). .... **36**

**Figure 3.3:** Schematic of APTES attachment process a) APTES molecule dissolved in ethanol and water mixture (95mL: 5mL) b) Hydrolysis of the APTES molecule produced silanols c) The condensation of two or more APTES molecules on the plasma treated PI wire after removal of water molecules d) The condensation process leads to hydrogen bond formation between hydroxyl

group on the wire and the silanols e) Application of heat resulted in water removal and covalent bond formation between hydroxyl group on the wire and the silanols.....	37
<b>Figure 3.4:</b> Schematic of multilayer and monolayer silane attachment on the plasma treated the surface.....	38
<b>Figure 3.5:</b> Carbon spectra (obtained using XPS) of samples treated with (pH 6) and without (pH 4) acetic acid during treatment.....	41
<b>Figure 3.6:</b> Nitrogen spectra (collected by XPS, peak at 399 eV) of a) plasma treated samples b) sample deposited under pH 6 c) sample deposited under pH 4 d) graph showing the atomic percentages of nitrogen under each condition. ....	42,43
<b>Figure 3.7:</b> Graphs show a) the C/Si ratio and b) the N/Si ratio of samples deposited under pH 6, and pH 4, and control samples before and after incubation in 0.9 % NaCl at 37° C for four days. ....	44
<b>Figure 3.8:</b> Carbon spectra (obtained using XPS) of a) sample deposited under pH 6 condition before and after incubation in 0.9 % NaCl at 37° C for four days b) sample deposited under pH 4 condition before and after incubation in 0.9 % NaCl at 37° C for four days.....	45
<b>Figure 3.9:</b> Nitrogen spectra (obtained using XPS) of a) sample deposited under pH 6 condition before and after incubation in 0.9 % NaCl at 37° C for four days b) sample deposited under pH 6 condition before and after incubation in 0.9 % NaCl at 37° C for four days.....	46
<b>Figure 3.10:</b> a) Fluorescent images (obtained using fluorescent microscope) of a plasma treated sample (control), and silane-treated samples deposited under pH 6 and silane-treated samples deposited under pH 4 before and after incubation in NaCl solution b) graph showing the number of edges i.e. corresponding to the number of FITC dye for each condition shown in the fluorescent images (figure a of this image). ....	48
<b>Figure 3.11:</b> Silicon spectra (obtained using XPS) of a) plasma treated sample without silane b) silane-attached sample deposited under pH 4 condition.....	50
<b>Figure 3.12:</b> a) Fluorescent images (obtained using fluorescent microscope) of the silane-coated sample deposited under pH 4 before and after incubation in 0.9 % NaCl solution for four days at 37°C. ....	51
<b>Figure 3.13:</b> a) Graph showing the percentage of peptide coverage on the PI wire for various peptide concentrations (1 µg/mL, 10 µg/mL and 100 µg/mL) b) Fluorescent images (obtained	

using fluorescent microscope) of silane-coated sample (control), and the peptide-coated wires at different concentrations. .... 53

**Figure 3.14:** a) Graph showing the percentage of peptide coverage on the PI wire by varying reaction parameters including EDC concentration, process time and temperature for 100 µg/mL peptide concentration. b) Fluorescent images (obtained using fluorescent microscope) of peptide-coated sample for the same conditions as shown in the graph. .... 55

**Figure 3.15:** a) Graph showing the normalized fluorescent intensity data for the PI wire samples placed in 0.9 % NaCl solution at 37°C for ten and fourteen days and PI wire sample before placing in the NaCl solution (Day 0) b) Fluorescent images (obtained using fluorescent microscope) of peptide-coated sample for the same conditions as shown in the graph. .... 57

**Figure 4.1:** Confocal images of the 0.75 wt% HAMA gel with various cell seeding densities  $1 \times 10^7$ ,  $5 \times 10^6$  and  $1 \times 10^6$  cells/mL. The images show that the gel with seeding density  $1 \times 10^7$  has the least viability when compared to the other seeding densities. .... 65

**Figure 4.2:** The graph showing the quantified value of the percentage of living cells in the 0.75 wt% HAMA gel with various seeding densities of densities  $1 \times 10^7$ ,  $5 \times 10^6$  and  $1 \times 10^6$  cells/mL (independent experiments N=3). The graph showing that percentage of living cells in seeding densities  $5 \times 10^6$  and  $1 \times 10^6$  cells/mL were significantly higher than  $1 \times 10^7$  cells/mL. (One- way ANOVA with Turkey post-test was performed, and the P value was 0.0073 (<0.05) in 95 %confidence interval) The significance bar (Labeled with \*) indicates the difference between the  $5 \times 10^6$  cells/mL and  $1 \times 10^7$  cells/mL is significant and the significance bar (Labeled with \*\*) indicates the difference between the  $1 \times 10^6$  cells/mL and  $1 \times 10^7$  cells/mL is very significant. .... 66

**Figure 4.3:** Confocal images of the 0.5 wt% and 0.75 wt% HAMA gels seeded with  $5 \times 10^6$  cells/mL. The images show that 0.5 wt% HAMA gel has the higher viability when compared to 0.75 wt% HAMA gel. .... 67

**Figure 4.4:** The graph showing the quantified value of the percentage of living cells in the 0.5 wt% HAMA gel and 0.75 wt% HAMA gel seeded with  $5 \times 10^6$  cells/mL (independent experiments N=3). The graph showing that the percentage of living cells in 0.5 wt% HAMA gel was significantly higher than 0.75 wt% HAMA gel. (The unpaired t-test was performed and the P value was 0.0031 (<0.05) in 95 %confidence interval). The significance bar (Labeled with \*\*) indicates the difference between the 0.5 wt% HAMA gel and 0.75 wt% HAMA gel is very significant. ... 68

**Figure 4.5:** Confocal images of the 0.5 wt% HAMA gels seeded with  $5 \times 10^6$  cells/mL at various time points 5, 12 and 18 days post cell encapsulation. The images show that 0.5 wt% HAMA gel has the high viability at all time points. .... **69**

**Figure 4.6:** The graph showing the quantified value of the percentage of living cells in the 0.5 Wt % HAMA gels at various time points (independent experiments N=3). The graph showing that the percentage of living cells in 0.5 wt% HAMA gel were approximately the same at all time points. .... **70**

**Figure 4.7:** Confocal images of the 0.5 wt% HAMA gel with cell seeding density of  $5 \times 10^6$  cells/mL at days 5, 12 and 18 post cell encapsulation. The antibodies labeled for microglia (Iba1), astrocytes (GFAP) and nuclei of all cells labeled with Hoechst stain ..... **71**

**Figure 4.8:** Confocal images show autofluorescence signal of the Pt/Ir metal in the PI wire when looked under Iba1 channel and GFAP channel and the wires were not inserted into a gel. The solid line (Solid green line and solid pink line) seen in the image correspond to the auto-fluorescence signal. .... **73**

**Figure 4.9:** Confocal images of the 0.5 wt% HAMA gel (cell seeding density of  $5 \times 10^6$  cells/mL) with wires treated at 0 (control), 1  $\mu\text{g/mL}$ , 10  $\mu\text{g/mL}$  and 100  $\mu\text{g/mL}$  peptide solution at days 1, 7 and 14 post cell encapsulation. The antibodies labeled for microglia (Iba1), astrocytes (GFAP). .... **75**

**Figure 4.10:** Confocal image showing wires treated with GFAP (primary and secondary antibody) and the solid pink line in the image is an auto-fluorescence signal of the Pt/Ir metal in GFAP channel (wires were not inserted into the gel). .... **77**

**Figure 4.11:** Graph showing microglial counts near the wire that is inserted into the 0.5 wt% HAMA gel with cell seeding density of  $5 \times 10^6$  cells/mL at days 1, 7 and 14 post insertion. The wires were treated with 0  $\mu\text{g/mL}$  (control), 1  $\mu\text{g/mL}$ , 10  $\mu\text{g/mL}$  and 100  $\mu\text{g/mL}$  peptide solution. 2 way ANOVA with Bonferroni post-test, significance of days post insertion \*\*\* (highly significant), peptide concentration \* (significant) and their interaction \*\* (very significant). .... **79**

**Figure 4.12:** Graph showing GFAP signal intensity from the astrocytes attached on the wire that is inserted into the 0.5 wt% HAMA gel with cell seeding density of  $5 \times 10^6$  cells/mL at days 1, 7 and 14 post wire insertion into the gel. The wires were treated with 0  $\mu\text{g/mL}$  (control), 1  $\mu\text{g/mL}$ , 10  $\mu\text{g/mL}$  and 100  $\mu\text{g/mL}$  peptide solutions. 2 way ANOVA with Bonferroni post-test, the

significance of days post insertion \*\*\* (highly significant), peptide concentration \*(significant). The interaction between the days post insertion and peptide concentration is not significant. .... **81**

**Figure 4.13:** Confocal images of the 0.5 wt% HAMA gel (cell seeding density of  $5 \times 10^6$  cells/mL) with wires treated at 0  $\mu\text{g/mL}$  (control), 1  $\mu\text{g/mL}$ , 10  $\mu\text{g/mL}$  and 100  $\mu\text{g/mL}$  peptide solution at days 7 and 14 post cell encapsulation (imaged at zoom factor 1.5). The antibodies labeled for microglia (Iba1), astrocytes (GFAP)..... **83**

# List of abbreviations

2D	two-dimensional
3D	three-dimensional
ANOVA	analysis of variance
APTES	(3-aminopropyl) triethoxysilane
AUTMS	(11-aminoundecyl) trimethoxysilane
BBB	blood brain barrier
BE	binding energy
BMP	bone morphogenetic protein
BSA	bovine serum albumin
CD	cell density
CNS	central nervous system
CPS	counts per second
CSPGs	chondroitin sulfate proteoglycans
Dde	bis-N-[1-(4, 4- dimethyl-2, 6-dioxocyclohexylidene) ethyl
DEX	dexamethasone
DI water	distilled water
DMEM	Dulbecco's modified Eagle's medium
DMF	N, N-dimethylformamide
DMSO	dimethyl sulfoxide
DNA	deoxyribonucleic acid
DRIE	deep reactive ion etching
ECM	extracellular matrix
EDC	1-ethyl-3-(3-dimethylaminopropyl)carbodiimide
EDTA	ethylenediaminetetraacetic acid
EdU	5-ethynyl-2 –deoxyuridine
EM	4-ethyl morpholine
EO-EPI	ethylene oxide epichlorohydrin
EtOH	ethanol

EY	eosin Y
FBS	fetal bovine serum
FITC	fluorescein isothiocyanate
FMOC	fluorenylmethyloxycarbonyl group
GFAP	glial fibrillary acidic protein
HA	hyaluronic acid
HAMA	methacrylated hyaluronic acid
HPLC	high-performance liquid chromatography
HS	Hoechst stain
Iba 1	ionized calcium-binding adapter molecule 1
IL	interleukin
Ir	iridium
ISMS	intraspinal microstimulation
KE	kinetic energy
LC-MS	liquid chromatography mass spectrometry
MA	methacrylic anhydride
MS	mass spectrometry
NaCl	sodium chloride
NaOH	sodium hydroxide
NCAM	neural cell adhesion molecule
NCD	nanocrystalline diamond
NHS	normal horse serum
NO	nitric oxide
NVP	1-vinyl-2-pyrrolidinone
PBS	phosphate buffered solution
PC12 cells	pheochromocytoma cells
PDGF	plant derived growth factors
PDMS	polydimethylsioxane
PEDOT	poly(3,4-ethylenedioxythiophene)
PEG	poly ethylene glycol
PI	polyimide

PI wire	polyimide insulated wire
PLGA	poly lactic-co-glycolic acid
PLL	poly-L-lysine
PNS	peripheral nervous system
PPy	polypyrrole
PS	penicillin-streptomycin
Pt	platinum
PU	polyurethane
PVAc	poly (vinyl acetate)
SCI	spinal cord injury
Si	silicon
TAMRA	5-caboxytetramethylrhodamine
TEA	triethanolamine
TNF- $\alpha$	tumor necrosis factor alpha
TRIS buffer	tris (hydroxymethyl) aminomethane
V	volume
wt%	weight percent (w/v)
XPS	x-ray photoelectron spectroscopy

# Chapter 1.0

## Introduction

## 1.1 Overview:

Neuroprosthetic devices are used to restore functionality of the human body after neural injury or disease. These devices can be interfaced with the central nervous system (CNS) or peripheral nervous system (PNS) to stimulate neurons or record neural signals. The long-term utility of neuroprosthetic devices is limited by the viability and stability of the devices within the body. When a foreign body (such as a neuroprosthetic device) is implanted in the CNS, it initiates a foreign body response from glial cells in the central nervous system (this involves mainly astrocytes and microglia) through chemical signalling. The microglial cells get activated, and they start the process of phagocytosis, to try and break down the device. These activated microglial cell signal the astrocytes, causing them to activate and form scar tissue around the implanted device (to isolate the device). Activated astrocytes also secrete chemicals to inhibit neurite outgrowth in the region [1]. The inhibition of neurite outgrowth in the implanted region affects function of electrode, as the scar tissue electrically insulates the device from the cells. It is expected that modulation of the responses from microglia and astrocytes would enhance the compatibility of the device with the nervous system. One feature of the glial scar is increased proliferation of glial cells (mainly astrocytes), near the region of neural injury. Reduction in the proliferation of glial cells is expected to influence the extent of scar tissue formed around the implant and this is expected to increase the viability of wires in the CNS. This work focuses on a method for modulating the responses of the microglia and astrocytes to reduce scarring around intraspinal microstimulation electrodes made of polyimide-insulated platinum (Pt) / iridium (Ir) metal alloy. These electrodes are used to stimulate neuron pools to restore lower-limb movements in patients who have experienced injury to their lumbar region in the spinal cord. In my work, the electrodes were modified with a specific peptide – with the sequence KHIFSDDSSE – to modulate the glial scar. In this work, the peptide reduced proliferation of both glial cells when tested in two-dimensional (2D) mixed glial cultures. The number of microglia near the peptide-coated wire electrode was reduced compared to the uncoated wire when tested in a three-dimensional (3D) gel containing mixed glial cell. These microglia cells that were found near the electrode site had a circular morphology similar to the activated state of the microglia. In the same 3D gel, increased number of astrocytes attached to peptide-coated wires even at day 1 post implantation, as compared to uncoated wires. The number of astrocytes (as determined using immunostaining for GFAP antibody) attached to the peptide-coated wires and the number of microglia near the peptide-coated

wires remained the same even two weeks post implantation of the peptide-coated wire. These effects could be due to the reduced proliferation of glial cells near the electrode, similar to the 2D cultures. Based on these results, I expect that this peptide could be used to modulate scar tissue formation by glial cells.

## 1.2 Neuroprosthetic devices

All of the functions of the human body are regulated through specific electrical signals from the central nervous system (CNS). The CNS is comprised of the brain and spinal cord. The electrical signals are transferred from the spinal cord to the target organs through the peripheral nervous system (PNS). The CNS and PNS can be affected by disorders such as vascular disorders (*e.g.* stroke or transient ischemic attacks), structural disorders (*e.g.* brain or spinal cord injuries or auditory nerve dysfunction), infections (*e.g.* meningitis or encephalitis), functional disorders (*e.g.* epilepsy or neuralgia) and degenerative disorders (*e.g.* Parkinson's disease or Alzheimer's disease). These neurological disorders can result in a severe loss of function. The recovery of lost function of body parts is challenging; one approach utilizes stimulation of the affected region in the CNS or PNS. In recent years, this has been achieved through the use of neuroprosthetic devices such as deep brain stimulators (to treat motor symptoms of Parkinson's disease) [2]; cochlear implants (to stimulate auditory nerve to treat sensorineural deafness) [3]; brain-machine interface systems (for controlling robotic limbs) [4] intraspinal microstimulation electrodes (to stimulate the injured lumbar region of the spinal cord to restore lower-limb movements in patients) [5].

In spinal cord injury affecting the lumbar region of the spinal cord, patients can lose both sensation and motion control after injury. These losses are due to the disruption of communication between the brain and peripheral nerves as the central communication system of the CNS (*i.e.* the spinal cord) is injured. Mushahwar *et al.* suggested that the motor neurons and networks of interneurons (which enable communication between sensory and motor pathways for reflexes) below the level of the lesion (*i.e.* injury) remains intact [5]. Therefore, stimulation of these surviving neurons below the lesion site may restore some function following the injury. They have demonstrated (in a cat model) that the surviving neurons could be stimulated to restore function using ultrafine intraspinal microstimulation electrodes [5]. These electrodes were implanted into the lumbar

region of the spinal cord [5]. The functional electrical stimulators were under simple finite state control, which were implemented using external sensors. Since these external sensors were bulky and uncomfortable to use, microelectrode arrays instead were used to record signals from sensory nerves to aid with the continuous feedback control [6]. Microelectronic devices were implanted in the dorsal root ganglion (in the same cat model) to read the electrical signal from the neurons [6].

### **1.3 Biocompatibility of the neuroprosthetic devices**

Virtually any neuroprosthetic device implanted into the brain, spinal cord or PNS faces problems in terms of long-term viability and stability [7]. In the CNS, both of these problems are due to the responses of the glial cells, which limit the biocompatibility of the device. Biocompatibility in the case of long-term implanted devices is defined as the ability of the implanted device “not to elicit any undesirable local or systemic effects in that host” [8]. If the device can modulate the response from CNS, it is considered to be more biocompatible with the CNS.

The responses of the CNS to chronically implanted electrodes has two parts: the initial acute response and chronic response [9], [10]. The initial acute response is the result of mechanical trauma to the tissue that occurs when an implant is inserted. The chronic response results in scarring caused by a specific type of CNS cells called glial cells around the implanted electrodes. There are three types of glial cells in CNS, namely microglia, astrocytes, and oligodendrocytes. The microglia and astrocytes are the glial cells that react to a neural injury, whereas the oligodendrocytes aide in myelin formation [9]. The microglia constitutes 5-10% of the glial cells [7], whereas astrocytes constitute 30-65% of the glial cells [11].

The mechanism of the initial acute response ensures rebuilding of tissue that is severed from the insertion of electrodes and activation of cells in the foreign body response. The blood vessels damaged during insertion release erythrocytes, which activate platelets and clotting factors. This activation results in macrophage recruitment and the initiation of tissue rebuilding. The response from the CNS includes the activation and proliferation of the microglia, which are the first cells to respond to the neural injury. The activated microglia start eating the cellular debris and excess fluid present in the lesion site [12]. The activated microglia attempt to phagocytose the foreign body, ideally causing degradation of the material.

The activation of microglia initiates the chronic response of the CNS. They further activate astrocytes around the implant site [13]. The morphology of the glial cells changes owing to activation. The activated microglia changes from ramified (in the resting state) to amoeboid form (in the activated state) as shown in Figure 1.1. The activated astrocytes show increased glial fibrillary acid protein (GFAP) filaments and hypertrophy of cells (*i.e.* increase in cell volume) as shown in Figure 1.1 [13]. Both cell types undergo active proliferation. The activated astrocytes encapsulate electrodes by forming a compact sheath around the electrodes [9], [10]. This encapsulation layer is referred to as glial scar (Figure 1.1). Polikov *et al.* have suggested that the glial scar may play a role in isolating necrotic neural tissue from the rest of the body, and may also prevent infiltration of lymphocytes [9]. Thus, the scar tissue helps in maintaining a blood-brain barrier (BBB). The blood-brain barrier is a highly selective permeability barrier to separate the blood vessel (*i.e.* capillaries going to brain) and the extracellular fluid of the brain. Thus, this barrier acts as a protective layer against passage of foreign substances into the brain. They also mentioned that the scar tissue prevents the diffusion of nearby neurons into the implant site, thus increasing the impedance to measure the neural signal [9]. The glial components might also create a new pathway that shunts current from the stimulating electrodes and away from the intended neuronal targets [14].

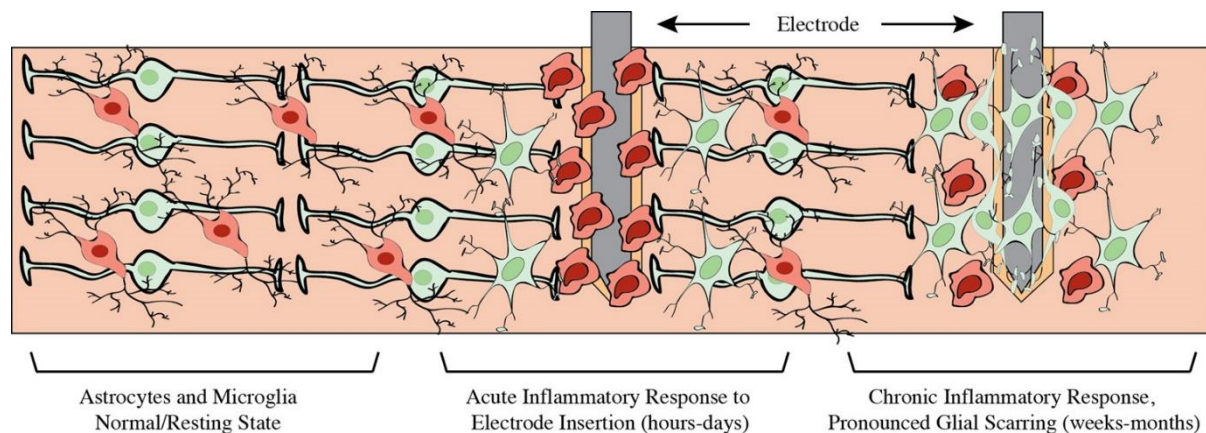


**Figure 1.1: Schematic of glial scar formation. Microglia cells (Red) first become activated and morphology changes from ramified to amoeboid. Astrocytes (Green) react at a later point in time and forms scar tissue [10]. Reprinted with permission from dx.doi.org/10.1021/bm500318d | Biomacromolecules 2014, 15, 2157–2165}. Copyright 2014 American Chemical Society.**

Turner *et al.* have shown the time course of astrogliosis with passive silicon electrode into the rat cerebral cortex [15]. First, they implanted the electrodes and then explanted them at 2, 4, 6 and 12-

week time points. For the electrode that was explanted after the 2<sup>nd</sup> week, immunostaining for GFAP showed a region around the implant that contained reactive astrocytes. This region extended from 500 to 600  $\mu\text{m}$  around the implant. The layers of cells that were adjacent to the implant showed a dense and organized structure as compared to the regions far away (beyond 600  $\mu\text{m}$  from the implant surface). During 2<sup>nd</sup> and 4<sup>th</sup> week, the reactive astrocytes extended their processes towards the insertion site (active proliferation of glial cells). During 6<sup>th</sup> and 12<sup>th</sup> week, the processes became stronger and more compact. They also suggested that the formation of the glial sheath (scarring) around the implant was complete in 6 weeks post implantation and it remained intact till the implant remains *in situ* [15]. This time course of glial scar formation was confirmed by Szarowski *et al.* [10].

Griffith *et al.* also identified reactive glia cells as far as 1 cm away from the chronically implanted platinum electrode tracks in Rhesus macaque motor cortices [14]. The astrocytes within 1 cm distance from the electrodes exhibited hypertrophy while those from areas beyond 1 cm showed normal growth. The reactions of the astrocytes were significant even during 3<sup>rd</sup>-year post implantation while the reactions of the microglial (which increased after three months) were not significant during 3<sup>rd</sup>-year post implantation. Thus, they concluded that the microglial reactions were more transient than the astrocytic reactions. Reactive astrocytes were found to secrete chondroitin-6-sulfate proteoglycans (CSPGs) and cytotactin / tenascin that inhibit the growth of neuron in injured brain and spinal cord models [1]. These reactive astrocytes secretions might not allow the growth of neurite in the regions severed by the implant and also in the regions around the implant [14]. In contrast, non-activated astrocyte monolayers were observed to help in the growth of neurons in the culture. The neural processes extended along the tracks provided by these astrocytes regardless of the materials beneath the astrocytes [16], [17]. Thus, the approaches that are aimed at electrode integration and long-term viability must consider improving neuronal survival and the reducing effects of gliosis [14].

#### **1.4 Strategies to improve biocompatibility**

The strategies to improve the biocompatibility of chronically implanted electrodes are discussed in this section. These strategies focus on minimizing the damage to the neural and vascular cells during insertion, reducing glial proliferation around the implant (if implanted in the CNS), and improving the neural growth around the implant for better recording or stimulation. Apart from

the reduction of glial scarring, there should be a reduction in the inflammatory response to the implanted electrodes. The engineering strategies to achieve biocompatibility must systemically result in progressively better implantable devices for chronic neural interfaces, *i.e.* the device should have consistent and measurable performance improvements with successive versions [18]. The following strategies have been adopted to improve the biocompatibility of device implanted in the CNS:

1. Change the properties of the electrodes (including dimensions, material, and stiffness) to minimize the foreign body response from microglia and astrocytes.
2. Delivery of drugs to modulate foreign body response from microglia and astrocytes.
3. Functionalize the surface of the electrode to modulate cell behavior.

#### **1.4.1. Electrode design**

The impact of some electrode design properties on the foreign body response from microglia and astrocytes has been studied. Electrode parameters that can be varied include size, shape, and material. For arrays of electrodes (in which electrodes joined by a base), the number of electrodes can also be varied. Finally, whether or not the electrodes are connected to each other or another object has been examined (*i.e.* whether the electrodes are tethered or untethered)[19].

Various studies have been involved in changing size and shape of the electrode. They studied the initial glial response, initial wound healing response and the chronic glial response to these changes [10], [14], [20]. In the study conducted by Szarowski *et al.*, electrode tips of different shape and cross-sectional area were implanted in the cortex of the adult male Wistar and Sprague–Dawley rat brain. The electrode tips had different shapes such as an ellipse, square and trapezoid with cross-sectional areas of 2500, 10,000 and 16900  $\mu\text{m}^2$  respectively [10]. They found that the initial glial and wound healing responses decreased as the cross-sectional area of the silicon electrode decreased. The electrodes with trapezoidal tips had a larger surface area, sharp corners, and more irregularities than smaller electrodes with ellipsoidal tips. They suggested that this could have also contributed to the difference in the initial wound response. They concluded from these results that the decrease in initial glial and wound healing responses was due to the various geometries of the tips and cross-sectional area of these tips [10]. A study by Kozai *et al.* have also confirmed that the difference in size influences the initial acute response from the glial cells [20]. They tested and

found that the initial glial response decreased in the case of ultra-small implantable composite with the cross-sectional area-  $58.1 \mu\text{m}^2$ . The ultra-small electrodes were made of a carbon fiber core, a poly(*p*-xylylene) based thin-film coating. Both electrode types were inserted in the motor cortex of adult male Sprague-Dawley rats [20] to test the foreign body response from microglia and astrocytes. Apart from the initial wound healing response, Szarowski *et al.* concluded that sustained or *chronic glial response* was independent of various geometries and sizes of the electrodes [10]. However, Kozai *et al.* [20] showed that reducing the cross-sectional area of the electrodes further from  $2500 \mu\text{m}^2$  (suggested in the work by Szarowski *et al.* [10]) to the size of ultra-thin electrodes (of diameter  $\sim 8.5 \mu\text{m}$  and cross-sectional area of  $58.1 \mu\text{m}^2$ ) reduced the chronic reactive tissue response [20]. Seymour *et al.* have also studied the influence of shape and size on the chronic reactive tissue response [21]. They placed parylene-based electrodes of two sizes (thicker and thinner electrodes of size  $48 \mu\text{m}$  by  $68 \mu\text{m}$  and  $5 \mu\text{m}$  by  $100 \mu\text{m}$  respectively) in the cerebral cortex of the adult male Sprague–Dawley rat brains [21]. They found that the thinner electrode caused a smaller chronic reactive tissue response [21]. Griffith *et al.* studied the extent of sustained glial response to the six platinum wires (of  $50 \mu\text{m}$  in diameter each and varying length) connected using cannon wafer connectors [14]. They implanted these electrodes in Rhesus macaque motor cortices [14]. They suggested that apart from electrode design, a comprehensive approach encompassing both electrode design and pharmacological management of gliosis was required to decrease the chronic glial response. All the above studies showed that the electrode designs such as electrode shape and size played an essential role influencing the *initial wound healing* response. In contrast, the chronic response remained relatively unaffected, and was reduced only when the electrode size was ultra-small (cross-sectional area roughly in hundreds of  $\mu\text{m}^2 \sim <500 \mu\text{m}^2$ ) [10], [14], [20], [21]. However, it is not possible to reduce dimensions of the electrode beyond a certain value. If the electrode is made too small, problems such as buckling (during insertion) and internal stresses can arise due to the very small dimensions, and these can affect the performance of the device in a long term. Also, in the case of stimulation, electrodes that are too small in cross-sectional area may not be able to carry the required current.

Connections between one electrode and other electrodes, a tethering site and/or the electronics can also contribute to the foreign body response from the microglia and astrocytes. Ersen *et al.* have conducted a study on the influence of floating electrodes to the chronic response of the CNS, and

they have concluded that these electrodes elicited a smaller less chronic tissue response compared to connected electrodes [19]. They used passive (without any stimulating current) parylene C coated silicon floating electrodes implanted in both cervical spinal cords and motor cortices [19]. Further work is required to test this effect both in active electrodes and for longer implantation times. Thelin *et al.* have studied the combined effect of size of the electrodes and tethering between them on the long term tissue reaction [22]. They implanted the electrodes into the cerebral cortex of the adult female Sprague-Dawley rats [22]. They used two types of implants; smaller untethered implants (50  $\mu\text{m}$  in diameter) and larger tethered implants (200  $\mu\text{m}$  in diameter). They have found that the untethered electrodes with small diameter caused the smallest tissue reactions as opposed to the tethered electrodes with larger diameter [22].

The use of various materials to improve biocompatibility has also been reported previously. The materials include silicon [10], various metals such as brass, gold, platinum, iridium, palladium and tantalum [23], and nanocrystalline diamond films (NCD) [24], [25]. The most commonly used materials of the above listing are the metals, due to their high surface charge density and corrosion resistance. Ignatius *et al.* have shown that various metal electrodes did not have any significant differences in the attachment of neurons on these electrodes when tested in primary central nervous system neuron cultures [23]. Metals are typically selected based on the electrical properties such as surface charge density.

Other alternative approaches involve coating NCD onto the electrode. NCD films have both good electrical properties and bio-inertness, which make them good candidates for improving biocompatibility [25]. NCD films with a high surface roughness ( $320\pm 17$  nm) have been coated onto titanium metal. This high roughness was significant in reducing adhesion of fibroblasts (the cells that caused initial foreign body response from vascular system due to severed blood vessels). The films were tested in primary human fibroblasts cultures (CRL2429) [26]. The NCD films were also doped with boron using microwave chemical vapor deposition for much higher electrochemical performance [24]. The major drawback of these film coatings is the challenge in depositing these coatings onto surfaces that are not flat. NCD coatings are relatively expensive when compared to materials such as silicon and metals.

With the limitations in controlling the dimensions and material of the electrode, alternate approaches are looked at to increase biocompatibility of implants. These include delivering drugs

to the lesion site, or modifying the surface of the implant with chemical coatings. Researchers are therefore exploring molecular and cell biological approaches to modulate foreign body response from microglia and astrocytes and integrate the neuroprosthetic devices.

### **1.4.2. Drug delivery systems**

Microchannels or wells, or nanofibers can be used to deliver drugs to the site surrounding an implant. Drugs can be stored in wells or microchannels created on an electrode; a few examples of this type of system are given below. For delivery of bioactive molecules (like peptides, or proteins), wells have been etched in polyimide electrode array [27]. The bioactive molecules have been either simply adhered or covalently attached to the polyimide surface [27]. Similar to biomolecules, whole cells can also be introduced through these wells.

Purcell *et al.* have developed parylene devices (or probes) with wells to deliver cells. These wells contained an alginate hydrogel seeded with E14 murine cortical neural stem cells [28]. They tested them *in vivo* in male Sprague-Dawley rat brain [28]. These probes were seeded with neural stem cells to integrate the device with the surrounding brain tissue. The device was integrated with tissue due to secretions of neuroprotective and neurotrophic factors (*i.e.* factors that help in the growth of neurons) by the neural stem cells [28]. The limitation of etching wells is that it requires increasing the dimensions of the neural electrodes, and only small quantities of biomolecules can be introduced (as determined by the volume of the reservoir).

3D- probe structures made of silicon with microfluidic channels were fabricated using surface micromachining and deep reactive ion etching (DRIE). These channels enabled the delivery of transferrin (a glycoprotein that helps to target drugs) and dextran (a polysaccharide molecule that also acts as drug carriers) [29]. The group that developed these 3D probes studied the drug release mechanism *in vitro* using agarose brain phantoms and *in vivo* in the premotor cortex of adult male rat brain. They found that diffusion-mediated delivery of drugs was an effective intervention strategy for reducing the reactive tissue response process [29].

A drug-loaded nanofiber was developed by Abidian *et al.* [30]. They developed silicon-based microelectrode coated with degradable electrospun nanofibers loaded with dexamethasone (DEX), a synthetic corticosteroid was used as an anti-inflammatory drug [31] [30]. DEX-loaded PLGA nanofibers were prepared by electrospinning, and they were coated with an alginate hydrogel using

dipping method. Finally, the hydrogels were coated with the conducting polymer poly (3, 4-ethylenedioxythiophene) (PEDOT) using electrochemical polymerization around the electrospun nanofibers within the hydrogel scaffold. The final devices had excellent electrical characteristics in terms of impedance and charge storage capacity, and the DEX was shown to release slowly from the devices over weeks. *In vivo* testing was not performed.

In terms of reducing the foreign body response from microglia and astrocytes to neural interfaces, delivery of anti-inflammatory drugs or chemical factors encourage the growth of neurons near the implant. Whether drug-loaded electrodes can affect the long-term biocompatibility of neural devices is not yet understood.

### **1.4.3. Surface functionalization of electrodes**

Surface functionalization of electrodes for neural interfaces has been done with various chemicals, including bioactive molecules, hydrogels, and polymers. Coatings are selected based on the function that they can perform at the site of implantation. Some of the various functions performed by these coating are: reduce inflammation, promote adhesion of neural cells, encourage adhesion and reduce glial scarring. Adhesion of neural cells improves recording of neural signals or the stimulation of neurons.

Multiple functions may be combined to improve the biocompatibility of a device. A combination of chemicals can be applied to target different functions. When a new coating is developed, it is essential to characterize the chemical state of the modified surface and to test the efficacy of the coating (*in vitro* and/or *in vivo*). Characterization of the coating ensures that the coating was successful. Some different types of coatings intended to improve the biocompatibility of implant surface interfacing with the CNS are described below.

#### **1.4.3.1. Nanoporous gold coatings**

Nanoporous (np) gold coatings were produced by an alloy corrosion process [32]. In one study, np gold with  $87.11 \pm 4.55$  pores was produced, and primary rat cells were cultured on the surface. This coating was shown to reduce gliosis (*i.e.* the change in non-reactive glial cells to the reactive state when the CNS was damaged). The topography of the surface of the nanoporous gold allowed

increased attachment of neurons while reducing the attachment of astrocytes. The authors of the study suggested that a similar coating could be used on the surface of recording electrodes to encourage the selective attachment of neurons, enabling the recording of signals from these cells.

#### **1.4.3.2. Hydrogel coatings**

Hydrogels are a three-dimensional hydrophilic polymeric network which absorb a high percentage of water. Hydrogels have been coated on the neural electrodes to modulate the immunoreactivity of cells in the CNS or PNS. Polyethylene glycol (PEG)-containing polyurethane (PU) hydrogel coatings for polydimethylsiloxane (PDMS)-based neural electrodes were developed by Rao *et al.* [33]. These coatings were found to have higher conductivity and better electrochemical performance than bare electrodes. The PEG-containing PU coating reduced astrocyte immunoreactivity in both Rat pheochromocytoma (PC12) cells (*in vitro*) and cortex of rat (*in vivo*). Coating stability is essential if the hydrogels are to have a long-term effect on the foreign body response from microglia and astrocytes; in the aforementioned study, the stability of the coating was not analyzed [33]. Polypyrrole (PPy) conducting polymer was coated on gold electrodes through an alginate hydrogel matrix by Kim *et al.* [34]. These electrodes were tested for the electrochemical properties by implanting on guinea pig's brain. Though the biocompatibility of these electrodes was not studied in the work by Kim *et al.*, the alginate hydrogels are themselves biocompatible [34]. Alginate gel by itself has been shown to help in reducing the connective tissue scar formation in a completely transected rat Spinal Cord Injury (SCI) model [35], [36]. Hydrogels could potentially be used to modify the foreign body response from microglia and astrocytes.

#### **1.4.3.3. Peptides and proteins**

Peptides are short chains of amino acids linked together by amide bonds. Peptides sequences can be naturally occurring (*i.e.* derived from proteins in the body), or can be artificially constructed. Both kinds of peptide sequences can be used to modify surfaces to improve their biocompatibility. A few examples of peptide sequences that occur naturally are the RGD sequence of the extracellular matrix or ECM (and associated with cell adhesion), the YIGSR and IKVAV peptide sequences of laminin protein, the  $\alpha$ -MSH peptide secreted by astrocytes [37], and the KHIFSDDSSSE sequence [38] of the neural cell adhesion molecules (NCAM). An example of a synthetically constructed peptide is one in which the GAGAGS peptide sequence of silk was

alternated with the cell-binding sequence RGD [39]. Peptides are produced using the solid phase peptide synthesis method, and can be covalently attached to the surface of a substrate [40]–[43]. In the peptide attachment process, peptide sequences can be covalently attached to either silane-functionalized surfaces [41]–[43], or dextran-functionalized surface [40]. In some cases, whole proteins have been attached covalently to substrates [23], [44], [45].

Peptides are good candidates for improving the biocompatibility of neural interfaces as they can affect how cells recognize surfaces. The peptide sequences of the ECM (*i.e.* RGD) and laminin (*i.e.* YIGSR, IKVAV) attract and adhere neural cells, as has been shown *in vitro* testing using neuronal-like PC12 cells [40]. The attachment of neurons on the electrode surface could help in achieving better recordings of the neuronal signals (for recording electrode), or improve the precision in stimulation of the neurons (for stimulation electrodes). The tridecapeptide  $\alpha$ -MSH acts as an anti-inflammatory biomolecule by reducing inflammation. It has been shown that this peptide reduces the number of reactive microglia *in vivo* (implanted into the motor cortex of the rat brain) when compared to uncoated silicon electrodes [37].

Peptides have been attached directly to electrodes for reducing the inflammatory response and the number of reactive microglia near the electrodes. In one study, the  $\alpha$ -MSH peptide was attached to silicon surfaces to measure the effect of this peptide on activated microglia (*in vitro*). Lipopolysaccharide was used to increase the activation and proliferation of microglial cells in cultures from neonatal Sprague–Dawley rat cerebral hemispheres [37]. Peptide-functionalized silicon surfaces were placed in these cultures. The effect of the peptide was assessed by the measurement of nitric oxide (NO) and a pro-inflammatory cytokine tumor necrosis factor alpha (TNF-  $\alpha$ ). The peptide-coated substrate showed a decrease in the quantity of both NO and TNF-  $\alpha$  when compared to uncoated sample, indicating a reduction in the level of microglia activation [37]. Peptide-coated electrodes were also placed *in vivo* in rat brains. Immunostaining of the tissues was carried out to identify reactive microglia; the peptide-coated samples showed reduced numbers of reactive microglia [37]. Peptides and adhesive proteins have been integrated with polymers on the surfaces of electrodes for enhancing neural cell attachment, and a few examples are given below. Both anionically modified laminin peptides (DEDEDYFQRYLI and DCDPGYIGSR) and the whole laminin protein were used to dope PEDOT electrodeposited on platinum (Pt) electrodes. Both of the laminin peptides exhibited good neural cell attachment and outgrowth when tested in PC12 cells. However, higher amounts of attachment and outgrowth were

achieved using whole native laminin proteins [44]. Ignatius *et al.* co-adsorbed laminin and poly-D-lysine on various metals and glass to improve cell attachment, spreading and growth [23]. A synthetic peptide DCDPGYIGSR was co-deposited with the conducting polymer polypyrrole on an electrode surface by electrochemical polymerization; the electrodes were then implanted in guinea pig brains [46]. Initially, the electrode had good neuronal attachment, and during 2<sup>nd</sup> week (after implantation) there were fibroblast and ECM proteins on the electrode surface [46]. 83 % of the electrodes coated with peptide had better neuronal processes when compared to the uncoated electrodes. This peptide did not influence the scarring reaction of the electrode site, and both the electrodes (with and without the peptide) had same scarring pattern [46]. In another study, the CDPGYIGSR peptide sequence from laminin was attached to PPy coated recording sites. The electrodes were placed in the culture of neuroblastoma cells (SH-SY5Y). An enhanced attachment of the neuroblastoma cells to peptide-coated recording sites was observed as compared with sites that were not coated with peptide [39]. Webb *et al.* attached the L1 protein (a cell adhesion molecule expressed in the developing CNS and PNS) to a substrate [45]. They cultured hippocampal neurons from a rat on these substrates, as well as on substrates coated with fibronectin. Cells cultured on L1-coated substrates showed a higher number of neurite growth when compared to those cultured on substrates coated with fibronectin [45].

Peptides have also been used to modify surfaces (with and without polymers) to enhance the attachment of astrocytes. A few examples are given below. In one study, silk-like polymer fibronectin (with GAGAGS peptide sequences of silk alternated with the cell-binding sequence RGD) was attached to PPy. Modified and unmodified PPy surfaces were placed in the culture of rat glial cells (C6), and preferential attachment of astrocytes to the coated substrates was seen as compared to uncoated electrodes [39]. It has been shown that when the peptide KHIFSDDSSE was added (in solution) to pure astrocyte cultures, the proliferation of the astrocytes was reduced [47]. In another study, the peptide KHIFSDDSSE was attached to a substrate surface and was found to bind specifically astrocytes when tested *in vitro* in rat cerebral astrocyte cultures [41]. The surface modified by this peptide exhibited a reduced surface neuron attachment compared to IKVAV when tested *in vitro* in E16 hippocampal neurons [48]. This effect was observed due to the signal leading to the intracellular response, and the signal was mediated by homophilic binding to the peptide at the glial surface. Based on these results, the peptide KHIFSDDSSE could help limit glial scarring due to the reduction in proliferation of astrocytes. Increased attachment of

astrocytes to the surface of electrodes could also help to anchor the electrodes in the tissue. Overall, peptides such as KHIFSDDSSE can potentially reduce both acute response and chronic response of the CNS.

## 1.5 Experimental outline

The purpose of this work is to enhance the biocompatibility of the intraspinal microstimulation electrodes (50  $\mu\text{m}$  in diameter and made of polyimide-insulated Pt/Ir wires) by reducing the level of glial scarring around the electrode. In this work, I describe the development of a method to apply stable coatings of the peptide KHIFSDDSSE to polyimide-insulated Pt/Ir wires. The peptide KHIFSDDSSE mimics bioactive domain of the neural cell adhesion molecules (NCAM), and Sporns *et al.* have tested the efficacy of this peptide (in solution) in reducing the proliferation of astrocytes in 2D pure astrocyte cultures [47]. Since activated astrocytes are a major constituent of a glial scar, it is anticipated that a coating of this peptide could reduce the glial scar formed around an implant. Furthermore, Kam *et al.* have shown that peptide KHIFSDDSSE coated on glass substrates increased astrocytes adhesion *in vitro* in cultures [41]. They suggest that the increased astrocytes adhesion could help in the anchorage of neural implants to the neural tissue. Here, it is hypothesized that coating the peptide onto the microwires will adhere astrocytes to the wire surface, and reduce the proliferation of glial cells around the implant.

Chapter 2 of this work describes the effects of adding peptide KHIFSDDSSE to 2D mixed glial cultures, which represent more realistic heterogeneous environment in the spinal cord than the pure astrocyte cultures used by Sporns *et al.* [47]. It is hypothesized that in these cultures, the proliferation of glial cells will be reduced.

Chapter 3 describes the development of a method to covalently attach the peptide KHIFSDDSSE to polyimide-insulated platinum (Pt) / iridium (Ir) electrodes. The peptide modification process includes oxygen plasma treatment of the polyimide surface [49], [50], covalent attachment of (3-aminopropyl) triethoxysilane (APTES) to this plasma-treated surface, and attachment of the peptide to the silane surface through 1-Ethyl-3-(3-dimethylaminopropyl)carbodiimide (EDC) chemistry [43]. A variety of parameters in this process was optimized to achieve high surface

coverage of the wire. In addition, the stability of the coating under physiological conditions is examined, and the deposition parameters are varied to maximize stability.

In Chapter 4, the ability of the peptide KHIFSDDSSSE to modify cell-electrode interactions is tested *in vitro* using a 3D model of a glial scar. This model was developed by Jeffery *et al.*, and consists of a crosslinked hyaluronic acid hydrogel seeded with astrocytes and microglia [13]. In the first part of the work, the characteristics of the 3D methacrylated hyaluronic acid (HAMA) gel (including gel density in PBS and cell seeding density) were optimized to achieve high cell viability. Subsequently, the peptide-coated electrodes (coated at various peptide concentrations) are inserted into the gels, and the resulting scars are observed at 1, 7 and 14 days post implantation. The number of microglia around the electrode and the intensity of glial fibrillary acidic protein (GFAP, an antibody labelling) signal from astrocytes attached to the electrodes is measured for each condition. These values are compared to measurements from the uncoated electrode to observe the effect of peptide coating on the glial scarring process.

## Chapter 2.0

# Effect of peptide in 2D mixed glial cultures

## 2.1 Introduction to effect of peptide in 2D mixed glial cultures

The purpose of this chapter is to explore whether KHIFSDDSSSE – a peptide sequence that mimics a homophilic binding domain of neural cell adhesion molecules (NCAM) that are present on the surface of neural and glial cells – affects the proliferation of glial cells (both microglia and astrocytes) in 2D cultures. Later in this thesis, this peptide will be coated on the microwires and its effect on the glial cells (in 3D gels) will be characterized.

Sporns *et al.* have shown that this peptide is effective in reducing the proliferation of astrocytes in primary rat astrocyte cultures [47]. They have also shown that whole NCAM molecule inhibited proliferation of astrocytes in pure astrocyte cultures. These NCAM molecules have shown dependency on cell seeding density to reduce proliferation astrocytes. When exposed to NCAM, cells plated at a lower cell density showed greater reduction in proliferation when compared to cells plated at a higher cell density due to the fact that the high cell density cultures reached confluence (the low cell density cultures did not reach confluence) [47]. They suggested that the NCAM molecule exhibited this behavior due to the contact inhibition from the astrocytes [47]. In contact inhibition phenomenon, the cells show reduced proliferation when there is no space to grow (*i.e.* when confluence is reached) [51].

In this chapter, the number of proliferating cells in the presence and absence of peptide (in solution) was measured using a nucleotide called 5-ethynyl-2 –deoxyuridine (EdU) that was dissolved in DMEM/F12 [52]. EdU gets incorporated into the deoxyribonucleic acid (DNA) of the proliferating cells, where EdU can be visualized using a fluorescent azide [1]. The presence of fluorescent azide-labeled EdU in a cell is indicative of proliferation.

For these experiments, mixed glial cells (consisting of astrocytes and microglia) were extracted from CNS tissue and were grown in culture flasks. The cells in the culture flasks were re-plated in 12 well plates at a lower cell density ( $2 \times 10^4$  cells/mL). The peptide was dissolved in media solution and was injected into the well plates containing glial cells at lower seeding density. Simultaneously, EdU was poured into the well plates. The EdU was later labeled with the fluorescent azide (dye), where the dye forms a covalent bond with EdU using click chemistry [52]. In order to specify which type of cell (either microglia or astrocytes) was proliferating, both cells types were labeled with their respective primary and secondary antibodies. The influence of

peptide (at various concentrations) on the proliferation of glial cells was studied. Since the peptide KHIFSDDSSSE is a part of NCAM molecule, it could exhibit a dependency on cell seeding density to reduce the proliferation of glial cells when tested in mixed glial culture. In this work, the dependency of this peptide on cell seeding density (at two cell densities  $8 \times 10^6$  cells/mL and  $2 \times 10^4$  cells/mL) was studied.

## **2.2 Glial cell extraction and their growth in 2D culture plates**

Mixed glial cells were obtained from the brain tissue of postnatal day one Sprague –Dawley rat pups and they were grown in cell culture flasks with poly-L-lysine (PLL). The well plates were maintained in media solution containing Dulbecco's Modified Eagle's Medium and Ham's nutrient mixture F-12 (DMEM/F12) along with 10 % Fetal Bovine Serum (FBS) and 2% Penicillin-streptomycin (PS) (this is prepared as standard for entire experiments) for ten days at 37°C in 5 % CO<sub>2</sub> humidified incubator [53]–[55].

At day 10, the cells were extracted from culture flasks and re-plated in 12 well plates at a cell density of  $2 \times 10^4$  cells/mL of media solution. The re-plating was done to lower seeding density. The seeding density was lowered to reduce the contact inhibition effect by the glial cells. Before lowering the seeding density, 12 well plates (made of polystyrene) were treated with solution containing 40 mL of filtered distilled (DI) water (filtered with 22 µm filter) and 1 mL of poly-L-lysine (PLL). The volume of the PLL/filtered DI water mixture (which was stirred vigorously) added to the well plates was 1mL/ well. After 20 minutes, the PLL/ filtered DI water mixture was removed from the wells and the wells were allowed to dry at room temperature.

For re-plating the cells into the 12 well plates, the following steps were carried out. The media solution was removed completely from the flask (containing cells), and the cells were washed in DMEM-F12 solution to remove residual media which could interfere with subsequent steps. The cells were dissociated from the culture flask by adding 25 mL (per flask) solution containing 0.025 % Trypsin and 0.01 % Ethylenediaminetetraacetic acid (Trypsin-EDTA, Gibco) and left at 37°C in the incubator for 10 minutes. After 10 minutes, the cells were lifted off from the bottom of the culture flask as a thin film. The film (containing cells) was collected using a 1000 µL pipette and

poured into two centrifuge tube each of volume 15 mL. The trypsin-EDTA solution was spun down using centrifuge for two minutes to get pellet cells.

The Trypsin-EDTA solution was decanted, and the cells were resuspended in 1mL of the media solution into each centrifuge tube. These cells were further dissociated into a single cell suspension via trituration. Both volumes were poured into a single 15 mL centrifuge tube. 8 mL of media was added to the volume in the centrifuge tube and were triturated one more time. Then, the media solution was spun down using centrifuge for two minutes. The media solution was decanted to reduce residual Trypsin-EDTA. The cells were again resuspended in 1mL of media solution, and the trituration step was carried out to break cells. 9 mL of media solution was added to this suspension.

Before plating these cells into 12 well plates treated with PLL, both the number of living cells and the cell density (CD) were assessed using the Trypan Blue exclusion assay. The trypan blue dye enters the cell membranes that are not intact *i.e.* the dead cells. Under light microscopy, the dead cells appeared dark whereas the live cells appeared light. The trypan blue dye was added to a small sample of the cell suspension. 50  $\mu$ L volume of cell suspension was placed in a microcentrifuge tube and to this 50  $\mu$ L of 0.4 wt% (wt/volume) trypan blue was added and triturated well using 200  $\mu$ L pipettes. Out of the 100  $\mu$ L, 12  $\mu$ L volume of the solution was poured to a Hemocytometer to count the number of live cells in the suspension and hence the cell density. The cells on the upper and right lines (marked by the symbol X in Figure 2.1) were not counted to avoid counting cells twice.

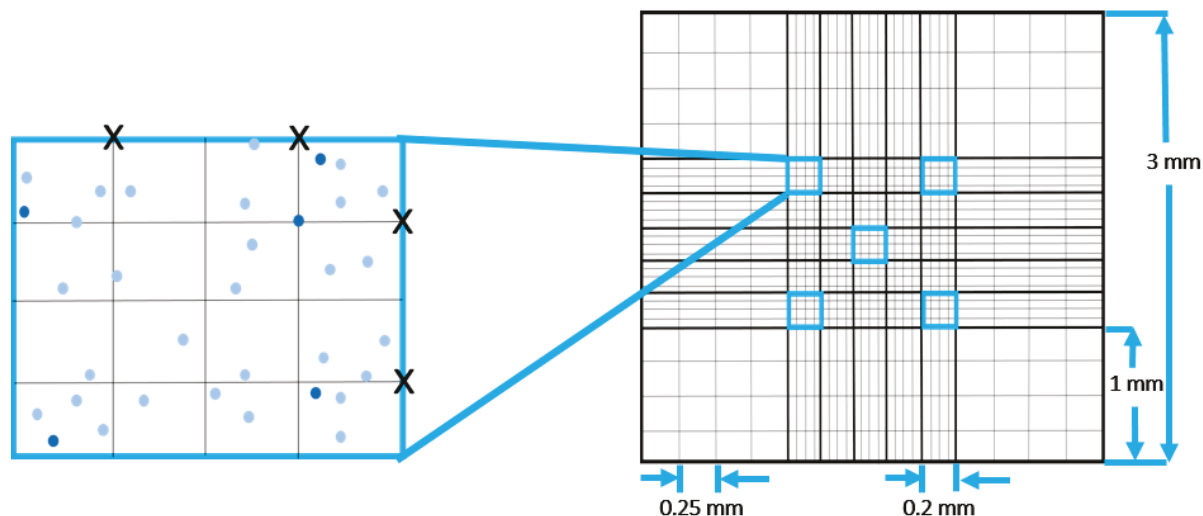


**Figure 2.1: Schematic of Hemocytometer grid. The five regions used for cell counting are marked as blue squares in the large central grid. One of the regions is zoomed to show an example for counting cells. The live cells (in light blue circles) and the dead cells (in dark blue circles) are present in this region and the letter 'X' is marked to show that cells falling in that region would not count.**

The live cells were counted from all the 5 section of the large central grid (see fig. 2.1) and the average value of all the sections was multiplied by the value 50,000 (based on the volume of the grid) to obtain the cell density (number of cells/mL). Equations 2.1 and 2.2 show the calculation of initial cell density.

$$\text{Cell density (CD}_{\text{initial}}) = \text{Average live cell count} \times \text{Dilution factor} \times 10^4 \text{ cells/mL} \quad [2.1]$$

$$\text{Cell density (CD}_{\text{initial}}) = \text{Average live cell count} \times 50,000 \text{ (cell/mL)} \quad [2.2]$$

Based on this CD, the cell suspension solution was diluted further by adding media solution to obtain a  $\text{CD}_{\text{final}}$  of  $2 \times 10^4$  cells/mL. Equations 2.3 and 2.4 can be used to calculate the volume of cell suspension required for dilution ( $V_1$ , in mL), in order to obtain enough solution to fill a certain number of well plates (each of which can hold 1 mL).

$$\text{CD}_{\text{initial}} \times V_1 = 2 \times 10^4 \text{ (cells/mL)} \times \text{Number of well plates} \times 1\text{mL} \quad [2.3]$$

$$V_1 = \frac{2 \times 10^4 (\text{cells/mL}) \times \text{Number of well plates} \times 1\text{mL}}{CD_{\text{initial}} (\text{cells/mL})}$$

[2.4]

From the volume of cell suspension needed for dilution, the volume of media solution required for dilution ( $V_2$ , in mL) was calculated, and it is shown in equation 2.5.

$$V_2 = (\text{Number of well plates} \times 1\text{mL}) - V_1$$

[2.5]

The volume  $V_2$  was added to the volume  $V_1$  in a 15 mL centrifuge tube and triturated. Thus, a cell suspension with cell density  $2 \times 10^4$  cells/mL was obtained. The final cell suspensions were added to the well plates treated with PLL with the volume of the cell suspension as 1mL per well. The cells were later stored at 37°C in 5 % CO<sub>2</sub> humidified incubator for four days before treating with the peptide.

### 2.3 Treatment with solution containing peptide

The peptide KHIFSDDSSSE was bought from the company Biomatik, and it was built using solid state peptide synthesis. The company determined the peptide purity to be 96 % using the mass spectrometry (MS) and high-performance liquid chromatography (HPLC).

Peptide solutions of varying concentration were added to well plates in which the cells were being cultured to test the effect of the peptide on the cell cultures. At day 14, the media was removed from the wells containing the cells, and peptide solutions of concentrations 100 µg/mL, 50 µg/mL, 25 µg/mL, 10 µg/mL, 0.2 µg/mL and 0.002 µg/mL (peptide in media solution) were added (1mL/well). In order to measure the proliferation of cells, simultaneously 500 µM of EdU was added to each well (with/without peptide) with the volume of 10 µL/mL (EdU in DMEM/F12). The 12 well plates were placed at 37°C in 5 % CO<sub>2</sub> humidified incubator for one day. The entire experiment was performed thrice from three set of animals (N=3).

Four control samples were also utilized to ensure the validity of the results. One control sample was used to test the specificity of the peptide to produce a response from the glial cells. No peptide

solution was added to this control; characterization was performed with EdU as for the other samples. A second control was used for testing the specificity in the reaction between EdU and the EdU labeling dye. EdU was not added to this control. Since the second control did not test the specificity of the peptide, the peptide solution was also not added to this sample. The third and fourth set of controls were used to test the cross-reactivity of the primary and secondary antibodies. In these controls, the primary antibody and secondary antibody were added to separate wells. The purpose of the third control (exposed to the primary antibody only) was to prove that the primary antibody cannot react alone to produce fluorescence in the cells *i.e.* secondary antibody was required to label the primary sample for the secondary antibody. Similarly, the purpose of the fourth control (exposed to the secondary antibody only) was to prove that secondary cannot label the cell without the primary antibody. Neither of these controls was exposed to EdU or peptide, as they were only to test the response of the primary and secondary antibody.

## **2.4 Characterisation of the 2D cultures to visualize the effect of peptide**

At day 1 post peptide treatment, the well plates were removed from the incubator and fixed by the treating cells with 10% formalin for 20 minutes at room temperature. Formalin enables crosslinking of surface proteins of cells. After fixing, cells were washed with phosphate-buffered saline (PBS) three times and then treated with blocking buffer solution containing PBS 0.5% Triton X-100 and 10 % normal horse serum (NHS) for 1 hour at room temperature. Cells were again washed with PBS thrice.

The cells treated with EdU were labeled with Alexa Fluor® 488 azide dye [52]. Cells were first washed in 3% bovine serum albumin (BSA) protein before EdU treatment. They were then treated with click reaction cocktail (500  $\mu$ L /well), consisting of 100 mM click reaction buffer or Tris(hydroxymethyl)aminomethane (TRIS) buffer, 100 mM copper sulfate pentahydrate, 4.2 mM of Alexa Fluor® 488 azide dye and 100 mM ascorbic acid or the reaction buffer additive (each component is added in the same order to make up the reaction cocktail)[52]. This reaction proceeded for 30 minutes at room temperature, during which the well plates were placed on a shaker for uniform treatment throughout the well. The wells were again washed in 3 % BSA (twice) and then washed with PBS (thrice). In order to validate the specificity of the reaction

between the EdU and the reaction cocktail, a control well was used. EdU was not added to this control well during the experiment (as described in section 2.3). In the characterization step, the reaction cocktail solution was added to the control well. If the reaction between the reaction cocktail and the EdU is specific, then the control well (which does not have EdU) will not react with the reaction cocktail.

After the washing step, cells were treated with primary antibodies anti-mouse Glial fibrillary acidic protein (GFAP) and anti-rabbit ionized calcium-binding adapter molecule 1 (Iba1) for labeling astrocytes and microglia cells, respectively. The primary antibody for the astrocytes – namely anti-mouse GFAP – was diluted 1:500 in PBS and the anti-rabbit Iba1 antibody was diluted 1:1000 in PBS and both were added together with 0.1 % Triton X-100 and 1% NHS (the volume of the mixture containing primary antibodies, Triton X-100, and NHS added to each well was 350  $\mu$ L). The cells were incubated overnight (over 18 hours) at 4°C with mild shaking. The control sample for secondary antibody was added to both the primary antibodies.

A day after the treatment with primary antibodies, wells were washed with PBS (thrice) and secondary antibodies such as Alexa Fluor 647 anti-mouse (Molecular Probes) and Alexa Fluor 488 donkey anti-rabbit (Molecular Probes) were applied to label the primary antibodies of the astrocytes and microglia, respectively. The secondary antibodies were diluted 1:250 in PBS with 1% NHS and 350  $\mu$ L/ well was added. The wells were left at room temperature for one hour with mild shaking. The wells were again washed with PBS thrice. The control sample for primary antibody was added to both the secondary antibodies.

The nucleus of all the cells were also labeled using Hoechst stain (HS) with the dilution of 1:1000 in PBS and with the volume of 1mL/well. The Hoechst stain (chemical compound: Bis-benzimidides) is a dye that stains the DNA of the cells. The samples were left at room temperature for five minutes and washed with PBS thrice later. Before viewing the cells under a fluorescent microscope, the cells were mounted with fluoromount. Images of the cells were taken on a Leica DMI6000B inverted fluorescent microscope, and they were analyzed using Image J using a method developed by Churchward *et al.* [53].

Each well was imaged at 21 different positions and these different positions form a grid. The total number of cells was found using the nuclear staining (blue channel, DAPI filter). The microglia, astrocytes, and EdU were imaged using GFP filter (green channel), CY5 filter (purple channel)

and CY3 filter (red channel) respectively. The backgrounds of all the channels were subtracted; the channels were filtered, and the region of interest (ROI) of each channel was defined to get the fluorescent intensity values in that region. With the blue channel as a reference channel, ROI of the blue channel was matched with the ROIs of other channels. Based on a threshold, the intensity values in a grid (21 positions/well) were integrated to get the counts that were positive (positive for number of cells that were proliferating) and the counts that were negative (negative for number of cells that were proliferating *i.e.* the counts were equal to the number of cells that were not proliferating). From the positive counts, the percentage of positive counts was found [2].

In Figure 2.2, the blue channel was superimposed on the red channel (merging of channels) to measure the number of glial cells proliferating. In Figure 2.2, the nuclei of the proliferating cells are the pink colored circular structures (this color results due to the merging of red and blue channels) in the enlarged image and the nuclei of non-proliferating cells are the blue colored circular structures. The merged image of blue and red channels was used to determine the percentage of proliferating glial cells under various peptide concentrations. The merged channels did not specify the cell type *i.e.* it did not specify if the proliferating glial cells were microglia or astrocytes. In order to verify the cell type, the purple (indicates astrocytes) and the green channel (indicates microglia) were superimposed individually on the already merged blue-red channels (Figure 2.3). The second superimposition was used to determine the percentage of proliferating microglial cells and the percentage of the proliferating astrocytes under various peptide concentrations.

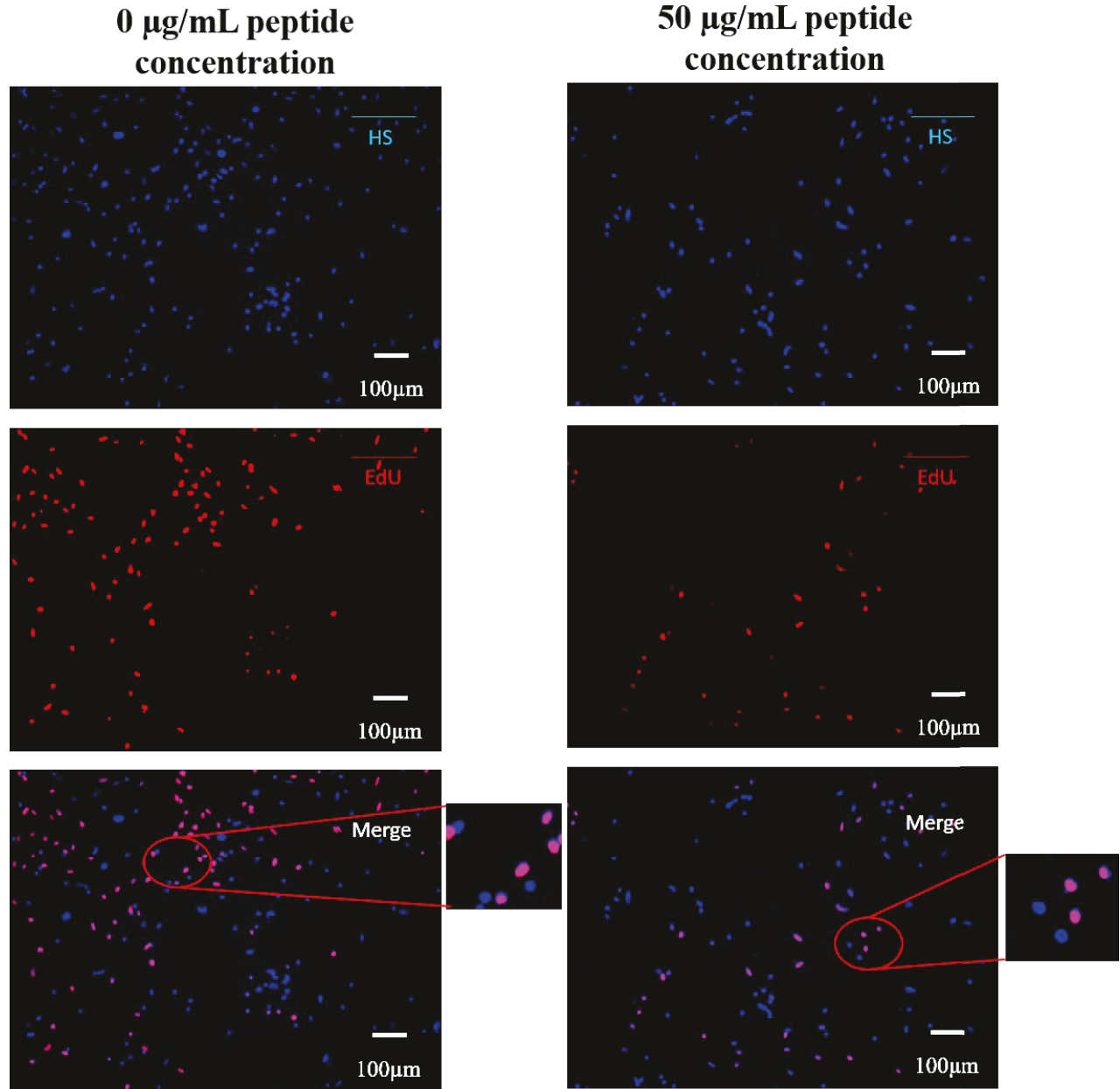


Figure 2.2: Fluorescence microscope images showing nuclei of all cells labeled with Hoechst stain (HS) and nuclei of proliferating cells with EdU for various concentrations of peptide *i.e.* 0 µg/mL (control) and 50 µg/mL of media in 2 D mixed glial cultures. The enlarged section showing purple colored and blue colored circular structures which are nuclei of proliferating and non-proliferating glial cells respectively.

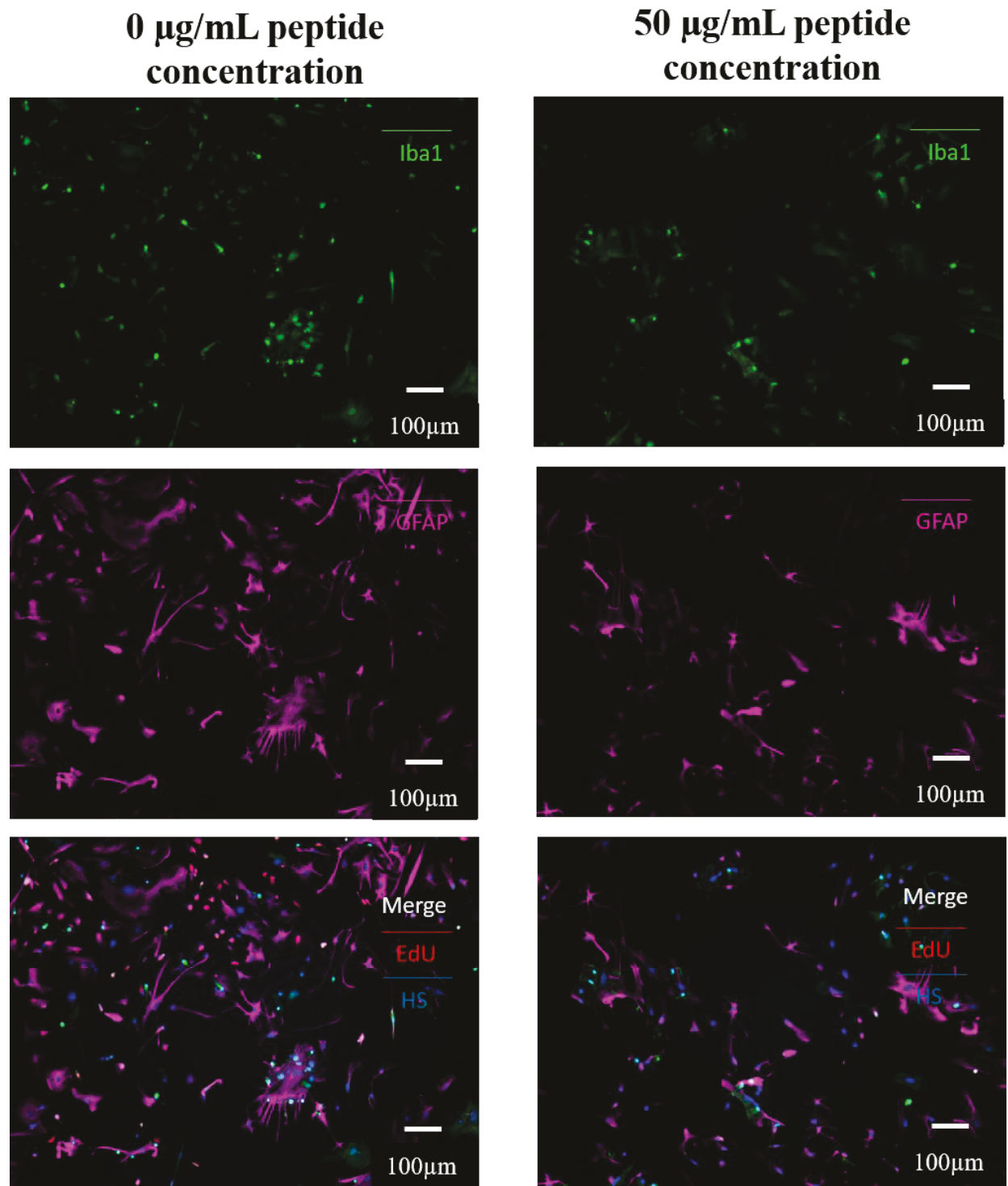
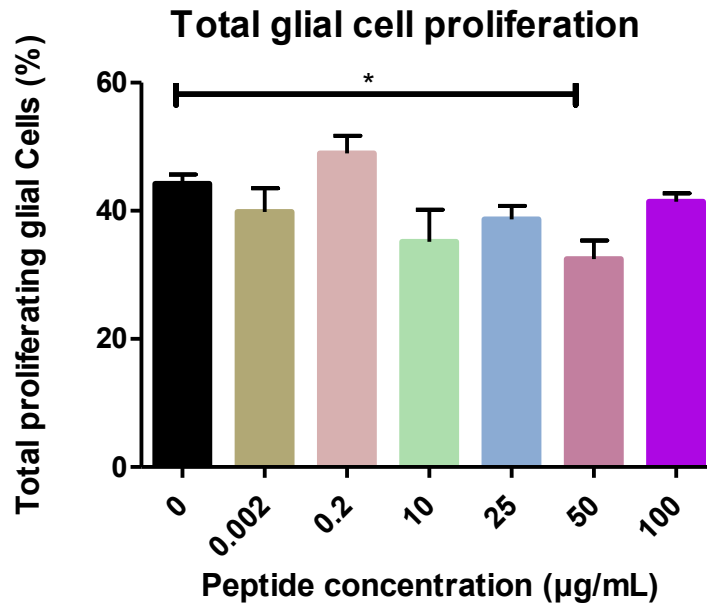


Figure 2.3: Fluorescence microscope images showing microglial labeled for Iba1 and astrocytes immunostained for GFAP for various concentrations of peptide *i.e.* 0  $\mu\text{g/mL}$  (control) and 50  $\mu\text{g/mL}$  of media in 2 D mixed glial cultures.

The fluorescent images in Figure 2.2 and 2.3 show two peptide concentrations 0  $\mu\text{g/mL}$  and 50  $\mu\text{g/mL}$  of peptide-treated mixed glial cultures. Figure 2.2 shows that the 50  $\mu\text{g/mL}$  peptide-treated mixed glial cultures have less proliferation of glial cells than the 0  $\mu\text{g/mL}$  peptide-treated mixed glial cultures (control). Both microglia and astrocytes extend their processes in the 50  $\mu\text{g/mL}$  and 0  $\mu\text{g/mL}$  peptide-treated mixed glial cultures as shown in Figure 2.3. Similar to these peptide concentrations, the percentage of the proliferation of microglia and astrocytes were quantified for other peptide treatment conditions, and the results are discussed below.

The percentage of proliferating glial cells (both cell types) were plotted against various peptide concentrations (Figure 2.4). In the control sample (to which no peptide was added), 44.3 % of the glial cells were found to be proliferating. In general, the addition of different concentrations of the peptide reduced the number of proliferating cells except 0.2  $\mu\text{g/mL}$  (49%) of the peptide. For this concentration of peptide, a slight increase in proliferation was seen. One way analysis of variance (ANOVA) test was performed on this raw data. It shows a statistical significance across samples with the P value of 0.0123, which is less than 0.05 (P value summary is \*(significant)). Dunnett's comparison test on this raw data shows a statistically significant reduction in the proliferation of glial cells at 50  $\mu\text{g/mL}$  peptide concentration (32.5 %) when compared to the sample at 0  $\mu\text{g/mL}$  peptide concentration (44.3 %).



**Figure 2.4:** Plot showing the percentage of proliferating glial cell for various peptide concentrations. Each bar is based on the average of 5 samples (3 independent experiments). The one-way ANOVA showing a statistical significance for the entire raw data and Dunnett's comparison test showing that the sample treated with 50 µg/mL peptide concentration reduces the proliferation of glial cells when compared to the sample treated with 0 µg/mL peptide concentration ( $P=0.0449$ , >95 %confidence interval).The significance bar (Labeled with \*) indicates the difference between the 0 (control) and 50 µg/mL is significant.

Apart from the one-way ANOVA test, the comparative t-test was performed for peptide concentrations 0 µg/mL and 50 µg/mL with three set of data, namely (1) proliferating glial cells (addition of both microglia and astrocytes) (Figure 2.5 a), (2) proliferating microglial cells (Figure 2.5 b) and (3) proliferating astrocytes (Figure 2.5 c). Since the data set collected was independent of time point, the unpaired t-test was carried out. All the three data sets shows a statistical significance for confidence interval >95%. The percentage of proliferating glial cells (sum of microglia and astrocytes) for 0 µg/mL and 50 µg/mL peptide-treated samples are  $44.3 \pm 1.6$  and  $32.5 \pm 3.3$  respectively (Figure 2.5 a). This result indicates that the peptide (at 50 µg/mL) is effective in reducing the proliferation of both microglia and astrocytes. The percentage of proliferating microglia cells for 0 µg/mL and 50 µg/mL peptide-treated samples are  $21 \pm 2.5$  and  $13 \pm 3$  respectively (Figure 2.5 b). The decrease in proliferation at 50 µg/mL peptide concentration indicates that the peptide (at 50 µg/mL) is effective in reducing the proliferation of microglia. The percentage of proliferating astrocytes for 0 µg/mL and 50 µg/mL peptide-treated samples are  $23 \pm$

1 and  $20 \pm 1$  respectively (Figure 2.5 c). The decrease in proliferation at 50  $\mu\text{g}/\text{mL}$  peptide concentration indicates that the peptide (at 50  $\mu\text{g}/\text{mL}$ ) is effective in reducing the proliferation of astrocyte.

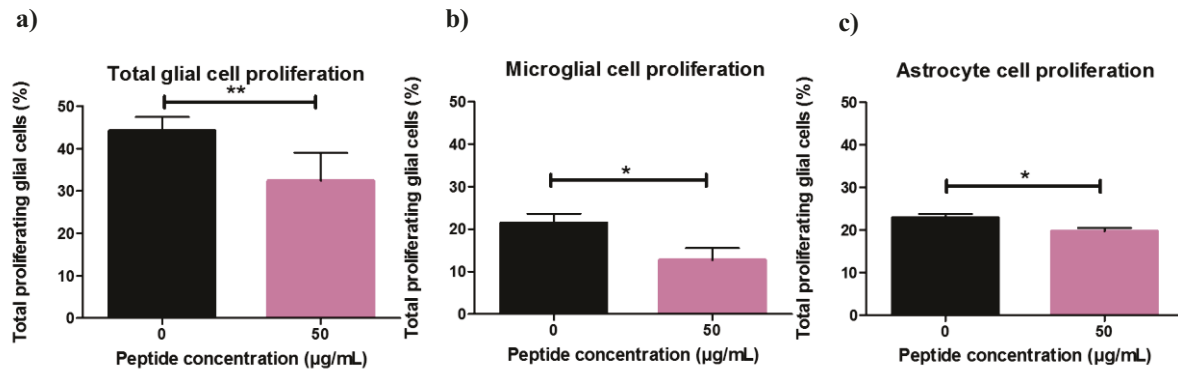


**Figure 2.5:** a) Comparative plot showing the percentage of proliferating total glial cell for peptide concentrations 0  $\mu\text{g}/\text{mL}$  and 50  $\mu\text{g}/\text{mL}$  (Unpaired t-test, P-value =0.007, >95 % confidence interval). The significance bar (Labeled with \*\*) indicates the difference between the 0 (control) and 50  $\mu\text{g}/\text{mL}$  is very significant. b) Comparative plot showing the percentage of proliferating microglial cell for peptide concentrations 0  $\mu\text{g}/\text{mL}$  and 50  $\mu\text{g}/\text{mL}$  (Unpaired t-test, P-value =0.0394, >95 % confidence interval). The significance bar (Labeled with \*) indicates the difference between the 0 (control) and 50  $\mu\text{g}/\text{mL}$  is significant. c) Comparative plot showing the percentage of proliferating astrocytes for peptide concentrations 0  $\mu\text{g}/\text{mL}$  and 50  $\mu\text{g}/\text{mL}$  (Unpaired t-test, P-value =0.0413, >95 % confidence interval). The significance bar (Labeled with \*) indicates the difference between the 0 (control) and 50  $\mu\text{g}/\text{mL}$  is significant.

In the literature, the peptide KHIFSDDSSSE has been shown to be effective in reducing the proliferation of astrocytes in primary rat astrocyte cultures [47]. The astrocyte proliferation in the culture that contained 100  $\mu\text{g}/\text{mL}$  of this peptide was found to be ~25% less than the culture without the peptide [47]. In this work, the total glial cell proliferation in the mixed culture that contains 50  $\mu\text{g}/\text{mL}$  of this peptide was found to be ~26.6 % less than the mixed culture without the peptide. The decrease in proliferation varied with cell type; the decrease in proliferation of the microglia was greater than that of the astrocytes.

## 2.5 Peptide dependence on cell seeding density

The dependence of this peptide on cell seeding density to reduce glial cell proliferation was studied in mixed glial cultures of two seeding densities ( $8 \times 10^6$  cells/mL and  $2 \times 10^4$  cells/mL) and the results are discussed below. The plots of the percentage of proliferating glial cells for two peptide concentrations (0 and 50  $\mu\text{g/mL}$ ) at two seeding densities ( $8 \times 10^6$  cells/mL and  $2 \times 10^4$  cells/mL) are shown in Figure 2.6. The sample not treated with the peptide (*i.e.* 0  $\mu\text{g/mL}$  peptide concentration) was used as the control sample. At low cell seeding density ( $2 \times 10^4$  cells/mL), 50  $\mu\text{g/mL}$  peptide-treated samples ( $32.5 \pm 3.3$ ) has lower percentage of proliferating glial cells than the control ( $44.3 \pm 1.6$ ) (Figure 2.6 b), which is consistent with previous works [47]. But, increasing cell seeding density ( $8 \times 10^6$  cells/mL) there was no variation in percentage of proliferating glial cells between peptide-treated sample ( $6.7 \pm 0.5$ ) and control ( $6.2 \pm 0.9$ ) (Figure 2.6 a).

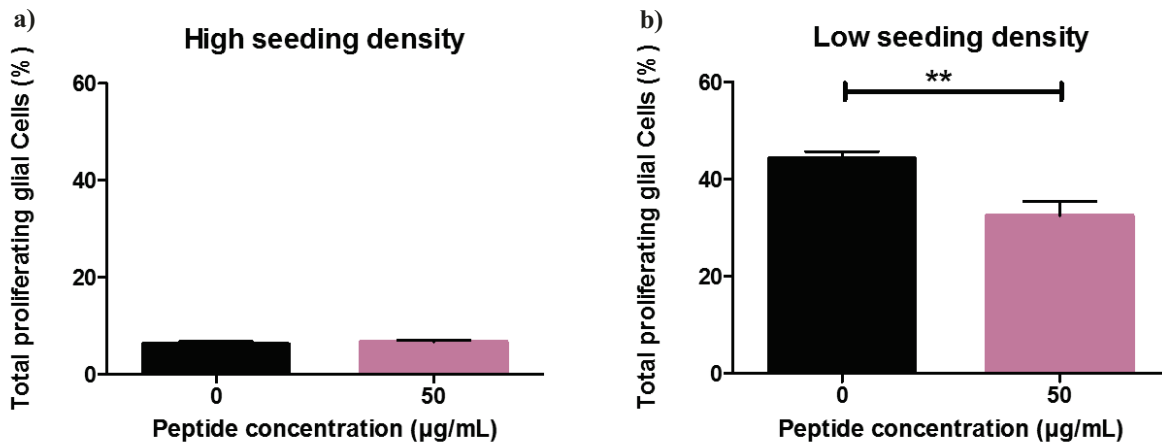


Figure 2.6: Plots showing the percentage of proliferating glial cells for peptide concentrations 0  $\mu\text{g/mL}$  and 50  $\mu\text{g/mL}$  at two seeding densities ( $8 \times 10^6$  cells/mL and  $2 \times 10^4$  cells/mL). a) High seeding density of  $8 \times 10^6$  cells/mL. The unpaired t-test showing no statistical significance in percentage of proliferating glial cells between 0  $\mu\text{g/mL}$  and 50  $\mu\text{g/mL}$  peptide concentrations ( $P=0.5028$ ,  $>95$  %confidence interval). b) Low seeding density  $2 \times 10^4$  cells/mL. The unpaired t-test showing a statistical significance in percentage of proliferating glial cells for the low seeding density raw data, and the result showing that the peptide at 50  $\mu\text{g/mL}$  peptide concentration reduces the proliferation of glial cells when compared to the sample with 0  $\mu\text{g/mL}$  peptide concentration ( $P=0.0449$ ,  $>95$  %confidence interval). The significance bar (Labeled with \*\*) indicates the difference between the 0 (control) and 50  $\mu\text{g/mL}$  is very significant.

When exposed to this peptide, cells plated at a lower cell density show greater decrease in glial cell proliferation when compared to cells plated at a higher cell density. This behavior could be due to the fact that the high cell density cultures reached confluence whereas the low cell density did not reach confluence. This phenomenon called the contact inhibition effect is shown by glial cells [47], [51]. These results show that the peptide KHIFSDDSSE (part of NCAM molecule) exhibits dependency on cell seeding density to reduce the proliferation of glial cells similar to the NCAM molecule observed by Sporns *et al.* [47].

## **2.6 Summary**

Glial cells were successfully grown in 2D cultures, and the ability of the peptide to reduce the proliferation of these cells was tested. The peptide was shown to reduce proliferation of both cell types (astrocytes and microglia). The decrease in proliferation varied with cell type; the decrease in proliferation of the microglia was greater than that of the astrocytes. The peptide also exhibited dependency on cell seeding density to reduce the proliferation of the glial cells due to the contact inhibition effect [47], [51].

Given the effect of the peptide on the behavior of the cells mainly microglia and astrocytes involved in the foreign body response, Chapter 3 focuses attaching this peptide to polyimide insulated Pt/Ir microwires (and to characterizing these coatings). In Chapter 4, the visualization techniques described here are used to visualize the response of glial cells to peptide-coated wires inserted into 3D cell cultures.

## Chapter 3.0

# Peptide attachment on the microwires

### **3.1 Introduction to peptide attachment on microwires**

This chapter describes a method to bind chemically the peptide KHIFSDDSSSE to the polyimide surface that is insulating the platinum/iridium (Pt/Ir) microwires. This was achieved by attaching an amine-terminated silane (3-Aminopropyl) triethoxysilane (APTES) to the surface of the wires. Later, the peptide was attached to the silane via a carboxyl-amine reaction (carboxyl-terminal of the peptide and amine-terminal of the silane) to form amide bond. To undertake this functionalization, it was first necessary to develop a reliable method to attach a stable silane monolayer to the wire. The effect of varying the pH during the deposition of this layer was explored, and X-ray photoelectron spectroscopy (XPS) and fluorescent microscopy were used to characterize the APTES layer and its stability after incubation in physiological conditions. Next, the peptide was attached to the amine (NH<sub>2</sub>) group of the silane. The goal of this attachment step was to get a high peptide coverage on the wire. Parameters such as reactant concentration, process time and temperature were varied to achieve this goal. The coverage of the peptide coating on the wire surface were characterized using fluorescent microscopy to image a fluorescent dye attached to the peptide. The stability of the peptide coating was also analyzed by incubating the peptide-coated wires under physiological for 10 and 14 days, and imaging the samples by fluorescent microscopy.

### **3.2 Process steps of the peptide attachment process**

The microwires of interest (used as electrodes in ISMS) are 50 µm diameter wires of platinum/iridium (Pt/Ir) metal alloy, insulated with 3 µm of polyimide. When used in ISMS, 30-70 µm [5] of the tip of each wire is de-insulated to expose the metal. The purpose of the work described in this chapter is to attach the peptide KHIFSDDSSSE to the insulating layer of polyimide, so as to try to modify the glial scarring process.

The process of peptide attachment on this microwire consist of three steps. They are: 1) oxygen plasma treatment, 2) silane (APTES) attachment, and 3) peptide attachment (Figure 3.1). Firstly, the microwire was cleaned with isopropanol and acetone (rinsed) to remove organic substances from the substrate's surface. The cleaned wire was treated with oxygen plasma for 6 minutes at a

power of 60 W, and a pressure of 150 mT (milliTorr). The oxygen plasma treatment creates hydroxyl (OH) groups on the surface of the polyimide (PI) wire (Figure 3.1 b) [49], [56].

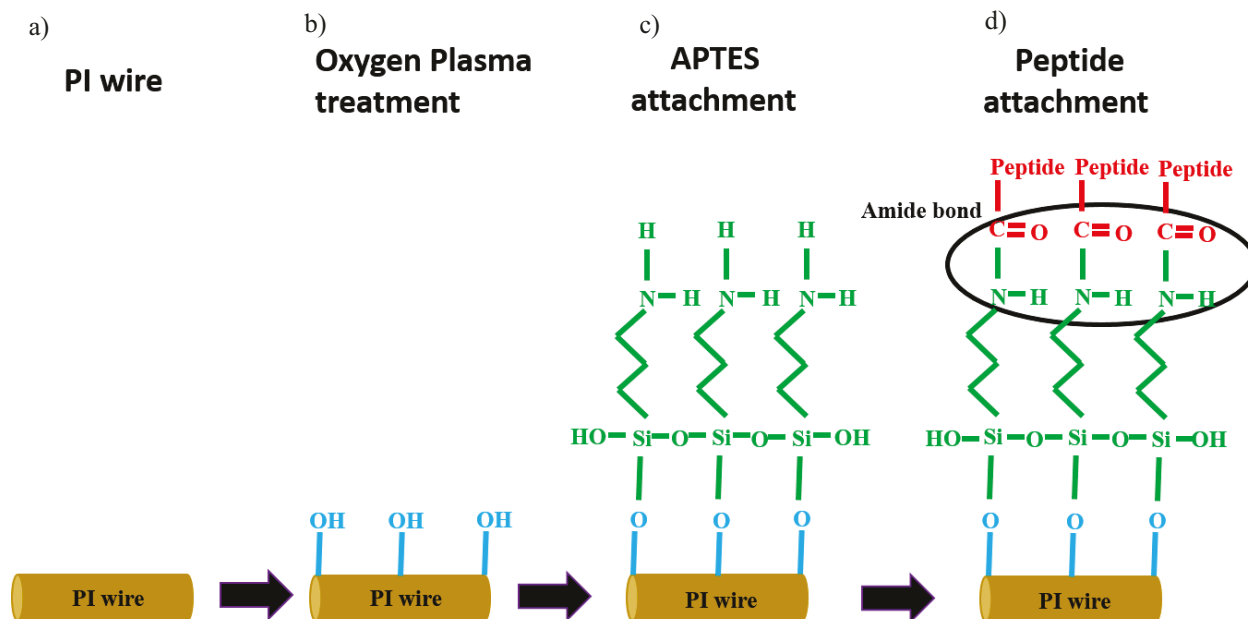


**Figure 3.1: Schematic of peptide attachment process** a) Polyimide-insulated microwire (PI wire) cleaned with isopropanol and acetone b) The oxygen plasma treatment of the polyimide wire c) The covalent bonding of silane to the oxygen plasma treated wires d) The amide bond formation ( marked by black circle ) between the peptide and the silane using EDC.

The APTES silane was hydrolyzed using aqueous ethanol (EtOH) in the presence of acetic acid; the plasma-treated wires were then immersed in the solution for 12 minutes, allowing the silane to form a chemical bond with the hydroxyl groups on the surface of the polyimide (Figure 3.1 c). The peptide was attached to the silane-functionalized surface by EDC, which forms an amide bond between amine (NH<sub>2</sub>) group of the silane and carboxyl (COOH) group of the peptide in the presence of EM (Figure 3.1 d). These steps are explained in detail in the following sections of this chapter. This work was carried out in the cleanroom of the nanoFAB facility at the University of Alberta. The goal of the peptide attachment process was to get a high peptide coverage on the surface of the microwire.

### 3.2.1 Oxygen plasma treatment step

Before plasma treatment, each microwire was first attached to a PDMS base using a Kapton tape for structural support and handling (Figure 3.2). The microwire/PDMS base pair was cleaned by rinsing with isopropanol and acetone and was placed in the chamber of the micro-etch reactive ion etch (RIE) equipment (Figure 3.2). The chamber was closed and evacuated at  $\sim 45$  mT. Oxygen was then introduced into the chamber at a pressure of 150 mT, and a radio frequency (RF) signal (to generate the plasma) with a power of 60 W was applied to the sample for 6 minutes[49], [50]. Through this process, hydroxyl groups were created on the polyimide surface [50].

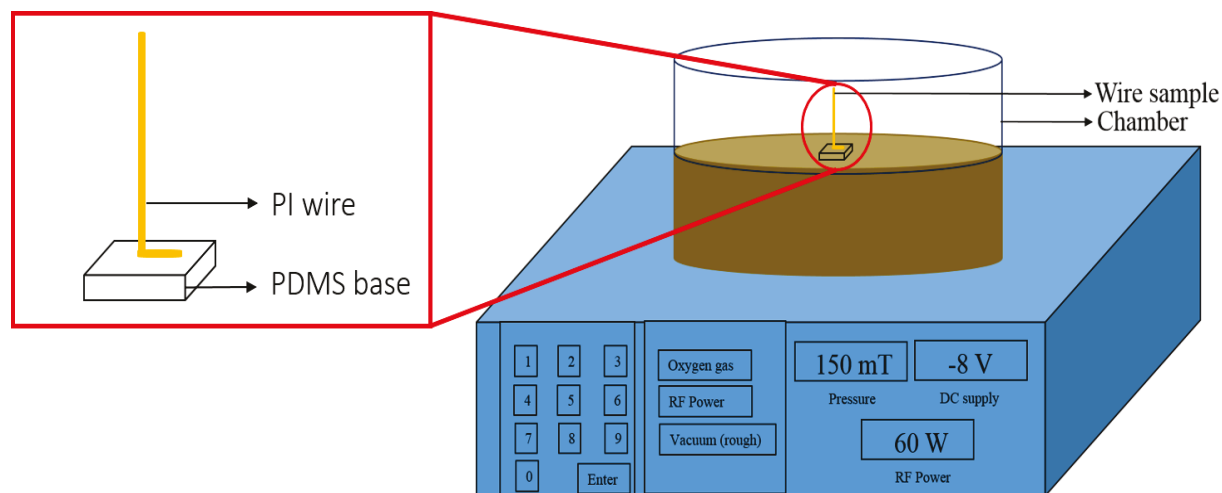


**Figure 3.2: Schematic of oxygen plasma treatment step. The image showing the schematic of micro-etch RIE equipment with the chamber containing wire sample (zoomed portion in the image).**

### 3.2.2 Silane attachment step

Prior to the plasma-treated wires attached with APTES, it was first hydrolyzed to form silanetriols or silanols ( $\text{H}_2\text{N}(\text{CH}_2)_3\text{-Si}(\text{OH})_3$ ). Upon immersion of the wires in the solution, the silanetriols condense on the plasma-treated surfaces to form hydrogen bonds. Application of heat causes water removal and the bond formation between the silane, and the plasma treated surface (Figure 3.3) [57].

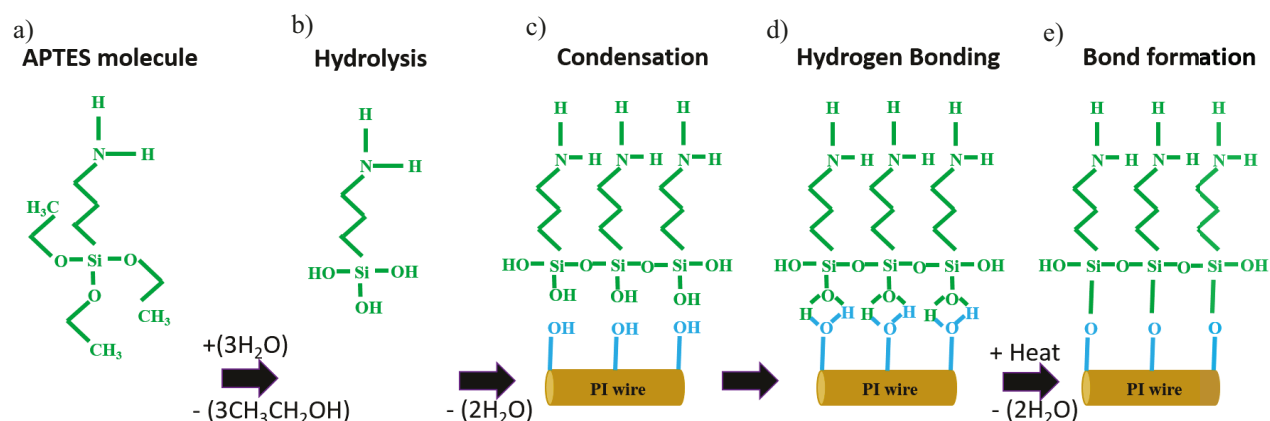


**Figure 3.3: Schematic of APTES attachment process** a) APTES molecule dissolved in ethanol and water mixture (95mL: 5mL) b) Hydrolysis of the APTES molecule produced silanols c) The condensation of two or more APTES molecules on the plasma treated PI wire after removal of water molecules d) The condensation process leads to hydrogen bond formation between hydroxyl group on the wire and the silanols e) Application of heat resulted in water removal and covalent bond formation between hydroxyl group on the wire and the silanols.

The APTES was hydrolyzed by dissolution in 95 % EtOH (95 mL of EtOH and 5 mL of distilled (DI) water) to achieve a final concentration of 2 % APTES. The processing time for the hydrolysis of APTES was 10 minutes. The plasma treated wires were placed in the 2% APTES solution for 15 minutes to allow condensation and hydrogen bond formation. The sample was then baked at 110°C for 10 minutes to remove the water.

One concern about this process was ensuring the stability of the silane layer on the plasma-treated surface. When a silane reacts with the surface, it can potentially form multilayers rather than monolayers of silane (Figure 3.4). This is undesirable because (1) multilayers formed will not be uniform across the surface [58] and (2) not all layers will be chemically bound to the surface *i.e.* they are not stable on the surface [56]. If the peptide is chemically attached to these non-bound layers of the silane, the peptide will be removed along with the non-bound silane layer in subsequent washing steps (Figure 3.3). Hence, a monolayer of silane (that is chemically bound) is required for a good stability of the silane and peptide layers (Figure 3.4). It is known from the literature that the pH of the solution can affect the silanetriols formation and thereby layer structure of silanes deposited from solution [57]. Therefore, deposition of the APTES was undertaken at two pH values: 4 and 6. As made, 2% APTES solutions in aqueous EtOH had a pH of 6. The pH could

be reduced to 4 through the addition of acetic acid. After immersing plasma had treated samples in one of these solutions for 12 minutes, physisorbed silane molecules were removed by ultrasonication of the silane-coated sample in anhydrous EtOH for 10 minutes. After ultrasonication, samples were dried with nitrogen gas and baked at 110°C for 10 minutes. The dried samples were characterized by the X-ray photoelectron spectroscopy (XPS) and a fluorescent microscope to check for a percentage of APTES coating on the surface and their stability.

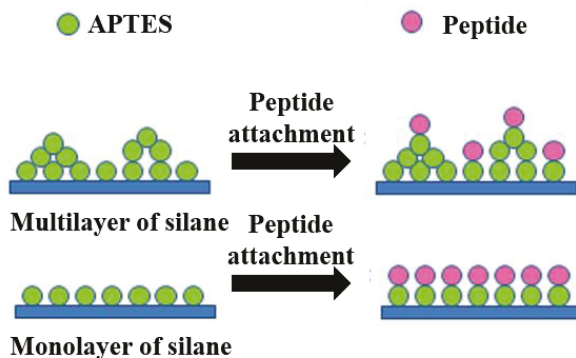


**Figure 3.4: Schematic of multilayer and monolayer silane attachment on the plasma treated the surface.**

Preliminary results showed that the quantification of the elemental composition of the APTES on a single PI wire yielded a very low signal strength (*i.e.* counts of electrons for a specific BE were not high) when characterized using XPS. This limitation was due to the cylindrical structure and the small dimensions of the wire (diameter: 50 $\mu$ m). Thus, the optimization of the APTES layer deposited under the two pH conditions was done on the surface of the glass instead of characterization on the single PI wire. The fluorescent imaging on the APTES layer deposition on the glass substrate under different pH conditions was used for validation of the XPS data and images were analyzed for a number of fluorescein isothiocyanate (FITC) dye units on the glass surface.

The optimization procedure involved depositing APTES on the surface of the glass samples under two pH conditions. These samples were then incubated in 0.9% sodium chloride (NaCl) solution conditions at 37 °C for four days (representative of physiological conditions [56]). The APTES deposited glass samples before and after incubation in NaCl solution were characterized using

XPS and the fluorescent microscope. The best suited pH condition was selected based on the stable APTES coating on the glass surface.

After selecting the right pH condition, the PI wire was coated with APTES under this pH condition. The presence of APTES on the PI wire was verified by measuring the silicon (Si) element signal that corresponds to the APTES chemical. The Si is uniquely present on the wire surface indicating presence of APTES. Since a single PI wire did not give a strong signal, an average signal of Si was measured by placing 5 PI wires very close to each other. The stability of the APTES layer (labeled with FITC) on a single PI wire under the 0.9% NaCl solution conditions at 37 °C for four days was measured using the fluorescent images. The percentage of FITC fluorescent intensity on the wire surface was measured before and after the incubation in NaCl solution.

### **3.2.2.1 X-ray photoelectron spectroscopy (XPS)**

An Axis Ultra (Kratos Analytical) X-ray photoelectron spectroscopy (XPS) was used to quantify the elemental composition of the APTES layer. The XPS spectrum of the APTES deposited sample was obtained by measuring the kinetic energy (KE) of electrons and the number of electrons that were emitted from 10 nm of the sample surface when irradiated with X-rays. The binding energy (BE) of the bonds was calculated from the KE of emitted electrons. The XPS spectra were captured over BE values ranging from 0 to 1500 electron volts (eV) with the scan rate of 2eV/second and an energy step of 400meV.

### **3.2.2.2 Fluorescence microscope**

Fluorescent imaging was used as a confirmatory test to validate the presence of the APTES layer. The APTES deposited samples were treated for 24 hours with a fluorescent dye called FITC, which was dissolved in dimethyl sulfoxide (DMSO). The FITC dye attaches to the amine-terminal of the APTES. Dye-labeled wires were imaged using a fluorescent microscope.

### 3.2.2.3 Optimization of APTES layer on the glass substrate

The goal of the XPS spectra comparisons between each pH condition was to find out which condition yields a monolayer. XPS spectra were also used to study the stability of the monolayer and the multilayer under 0.9% NaCl conditions at 37 °C for four days (representative of physiological conditions [56]).

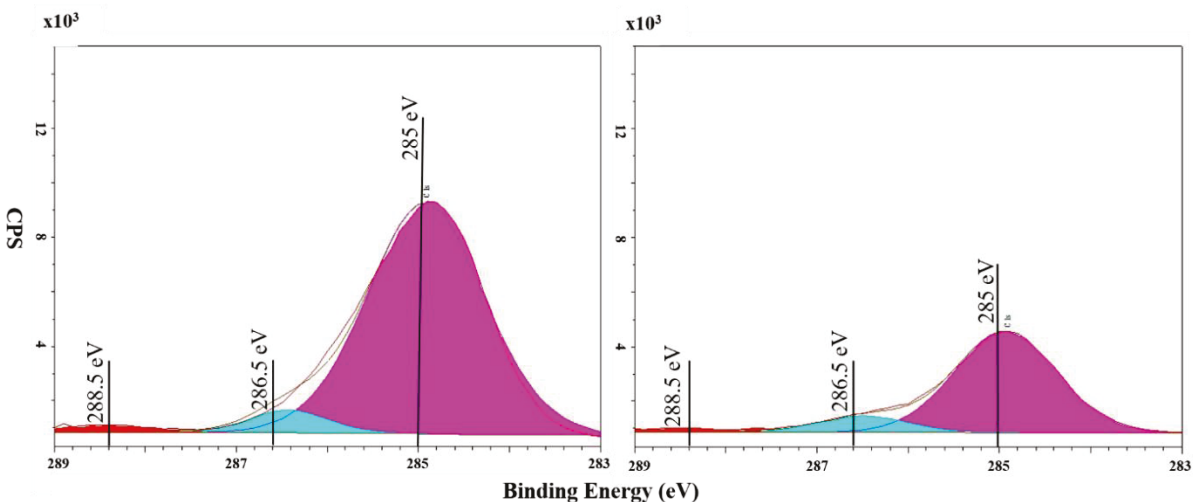
In glass samples, high-resolution carbon (C), nitrogen (N), silicon (Si) and oxygen (O) spectra were obtained for each pH condition (pH 4, and pH 6). The peak position (*i.e.* BE at the peak value of the spectra for each element) was obtained and compared with the literature values to validate the presence of APTES silane under both pH conditions. The atomic percentage nitrogen values were compared between both pH conditions. It is known from the literature that for a monolayer of silane, the atomic percentage nitrogen was close to 2 atomic percentage [58]. The ratio of atomic percentage C to Si (C/Si ratio) and the ratio of atomic percentage N to Si (N/Si ratio) was calculated. These ratios acted as a measure of a number of organosilane present on the surface of the glass [56]. The C/Si ratio and N/Si ratio of samples deposited under each pH condition was measured. These ratios were used as a measure of the stability of organosilanes. The ratios under each condition for samples before and after the incubation in 0.9% NaCl solution at 37 °C for four days were compared [56].

Table 3.1 shows the peak position of elements C, O, N, and Si (2p) of the silane-coated samples obtained for samples deposited under pH 6 condition compared to the literature values [50], [59]–[63]. The samples deposited under pH 4 condition also had peaks at similar BE value (eV) whereas their magnitude *i.e.* CPS values varied (Figure 3.5). Both the experimental values and the literature peak values were close to each other. The experimental values confirm the chemical composition of APTES on the glass surface.

Elements	BE value from the literature (eV)	BE value from the samples deposited under pH 6 (eV)
C	286 ±2 (largest peak)	285±0.5 (largest peak)
O	532±1	532±1
N	401±1	400±1
Si 2p	102±2	102±0.5

**Table 3.1: Comparative table of the BE values of the samples deposited under pH 6 to that of the BE values in the literature [50], [59]–[63] for elements like C, O, N, and Si (2p).**

The carbon spectra of the samples (BE (eV) in X axis Vs Counts per second (CPS) in Y axis) under pH 6 and 4 (with acetic acid) conditions reveals presence of peaks at  $285\pm 0.5\text{eV}$  (largest peak, pink color peak in Figure 3.5),  $286.5\pm 0.2\text{eV}$  (blue color peak in Figure 3.4), and  $288.5\pm 0.3\text{eV}$  (red color peak in Figure 3.4) and the values indicate the presence of a specific bond. The bonds such as C-C/C-H/C-Si, C-O/C-N, and C-C=O/C=O correspond to BE peak at 285eV, 286.5eV and 288.5eV respectively [59], [60], [64]. These bonds correspond with those expected for the APTES molecule.

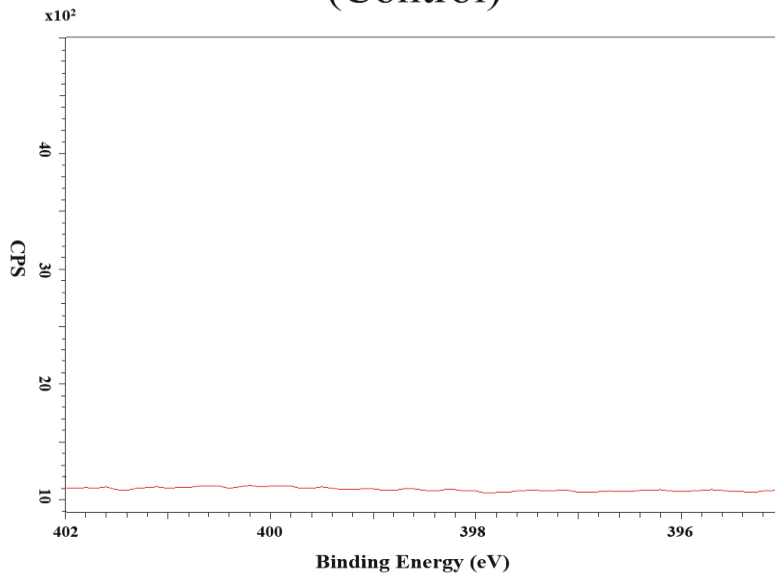


**Figure 3.5: Carbon spectra (obtained using XPS) of samples treated with (pH 6) and without (pH 4) acetic acid during treatment.**

The atomic percentage nitrogen was calculated from the nitrogen spectra of samples deposited under both pH conditions (Figure 3.6 b, c). The atomic percentage nitrogen of each pH condition was compared to that of plasma treated sample (Figure 3.6 a) and the graph is shown in Figure 3.6 d. The samples treated in the presence of acetic acid (pH 4) shows an atomic percentage nitrogen value of 2 (the atomic percentage values can vary  $\pm 10\%$  of the obtained value). This value is similar to the monolayer values obtained in the literature [58]. The atomic percentage nitrogen value of 2 for samples deposited under pH 4 show that these samples yielded a monolayer. On the other hand, samples deposited under pH 6 form multilayer of silane on the glass surface.

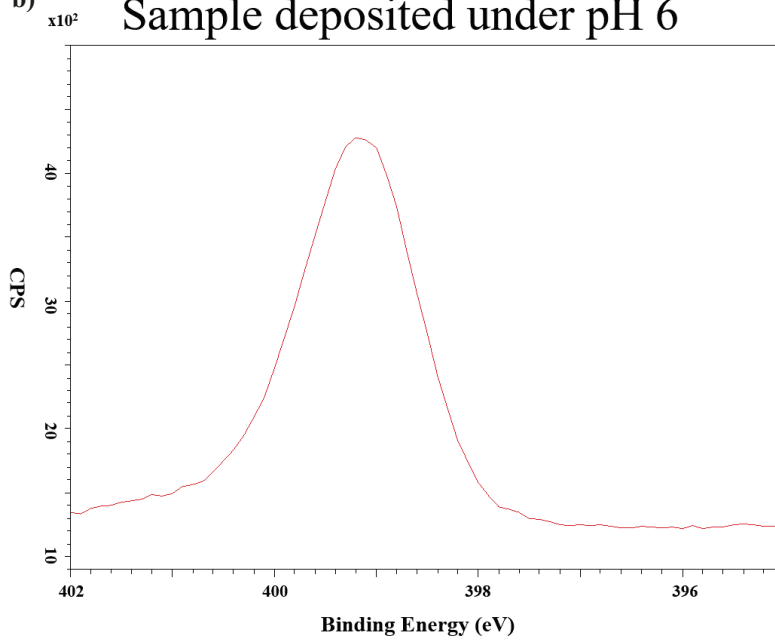
# Plasma treated sample (Control)

a)



b)

# Sample deposited under pH 6



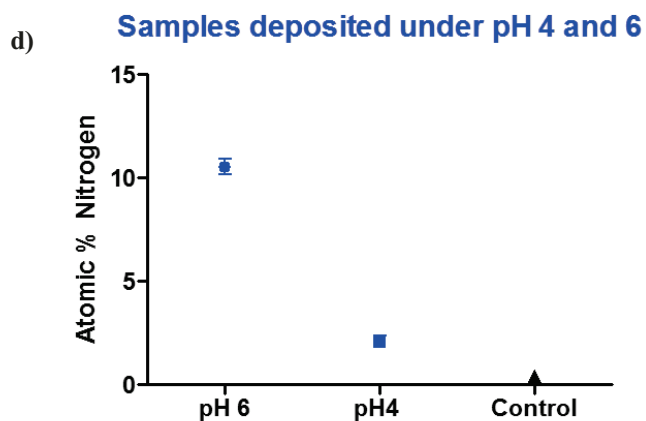
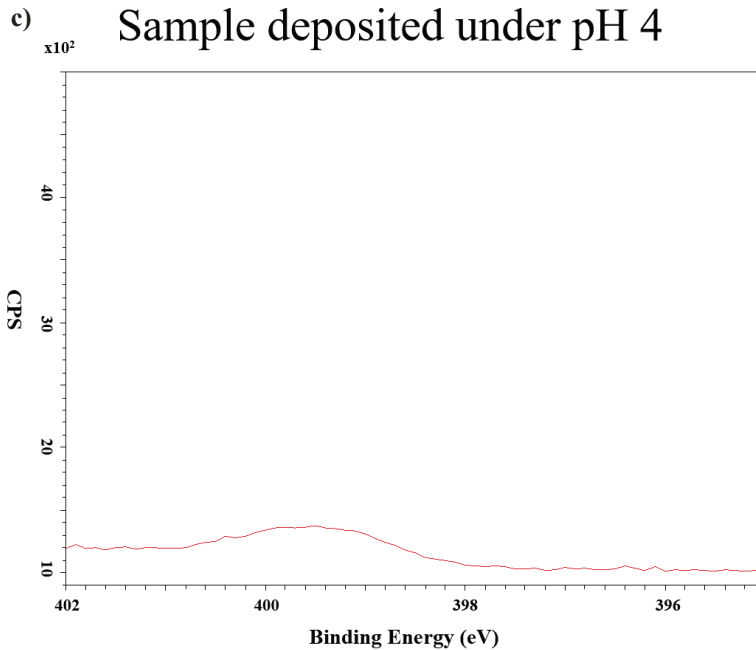
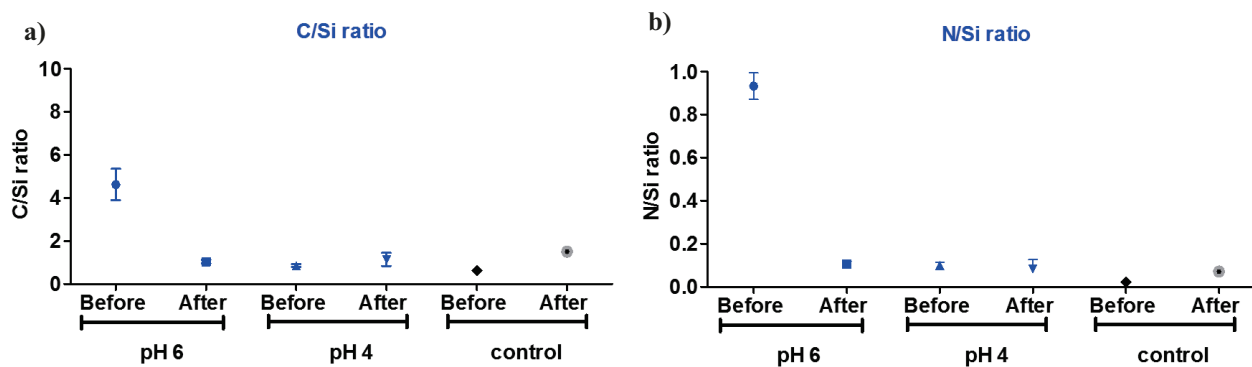


Figure 3.6: Nitrogen spectra (collected by XPS, peak at 399 eV) of a) plasma treated samples b) sample deposited under pH 6 c) sample deposited under pH 4 d) graph showing the atomic percentages of nitrogen under each condition.

The ratio of C/Si and N/Si were calculated from the C, N and Si spectra of samples and the ratios for each condition is plotted in a graph shown in Figure 3.7. The conditions shown in the graph were samples prepared under pH 6 and pH 4 (before incubation) and these samples were incubated in 0.9% NaCl solution at 37°C for four days (after incubation). The graph shows that after incubation, the C/Si, and N/Si ratios decrease for samples prepared under pH 6 but not for samples

prepared under pH 4. These results indicate that the samples prepared at pH 6 are multilayers, which do not remain stable for four days in NaCl solution.



**Figure 3.7:** Graphs showing a) the C/Si ratio and b) the N/Si ratio of samples deposited under pH 6, and pH 4, and control samples before and after incubation in 0.9 % NaCl at 37° C for four days.

The carbon (Figure 3.8) and the nitrogen (Figure 3.9) spectra show a similar trend before and after incubation in NaCl solution. The graph in Figure 3.7 was plotted based on these spectra. The results also show that the samples deposited under pH 4 had a monolayer that was stable in NaCl solution, whereas the samples deposited under pH 6 had unstable multilayers.

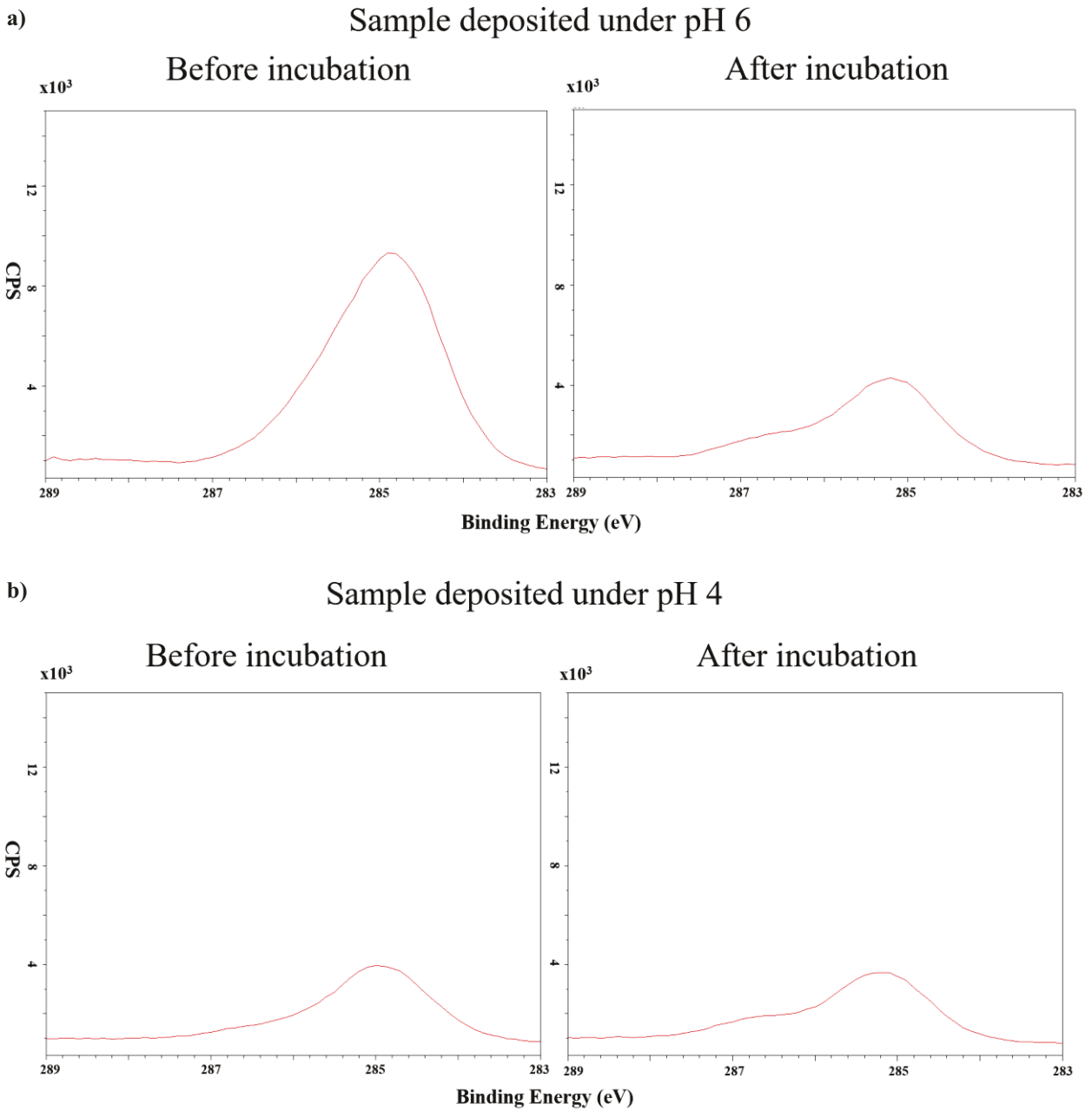


**Figure 3.8: Carbon spectra (obtained using XPS) of a) sample deposited under pH 6 condition before and after incubation in 0.9 % NaCl at 37° C for four days b) sample deposited under pH 4 condition before and after incubation in 0.9 % NaCl at 37° C for four days.**

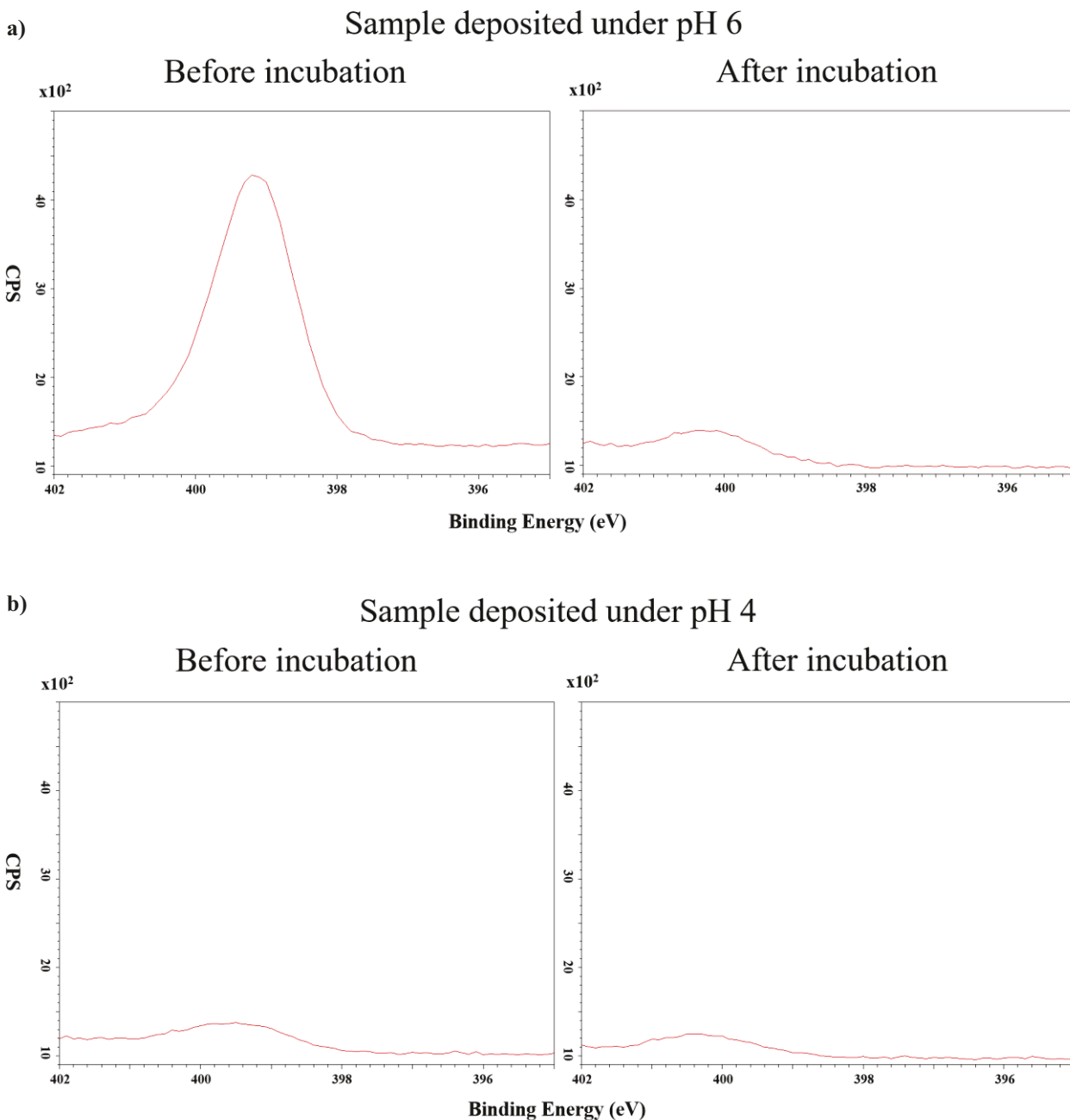


**Figure 3.9: Nitrogen spectra (obtained using XPS) of a) sample deposited under pH 6 condition before and after incubation in 0.9 % NaCl at 37° C for four days b) sample deposited under pH 6 condition before and after incubation in 0.9 % NaCl at 37° C for four days.**

To verify the stability of the APTES layer (deposited at pH 4 and 6) on glass, fluorescent microscopy was utilized to image a fluorescent dye attached to the APTES. Glass samples prepared under different pH conditions were imaged before and after four days incubation under physiological conditions to show that the APTES layer remained stable.

The dye FITC was dissolved in 1 mg dissolved in 1mL of DMSO to attach the dye to the APTES-functionalized glass. APTES-functionalized wires (prepared at both pH 6 and pH 4) were placed in the solution for 24 hours [65]. The samples were rinsed in DMSO. The fluorescence intensity of FITC dye was measured using the Leica DMI6000B inverted fluorescent microscope.

The Figure 3.10 a shows that the samples prepared at pH 6 has more FITC dye on the surface than samples treated under pH 4. This result shows that the number of silane groups on the surface of the samples prepared under pH 6 is greater than for the samples prepared under pH 4. After incubation, the samples prepared under pH 6 show a substantial decrease of FITC dye on the surface, whereas the samples prepared under pH 4 show similar amounts of FITC before and after incubation. The number of FITC dye clusters on the surfaces was counted using MATLAB program, and the results were plotted as a graph (Figure 3.10 b). The counting of FITC dye was achieved by counting the number of edges found in the fluorescent images for each of the conditions in Figure 3.10 a. For counting, the fluorescent images were converted to a grayscale image and filtered. The 7<sup>th</sup> bit plane of the gray scale image was obtained as this plane has a high signal to noise ratio (SNR). The edge image was obtained from the 7<sup>th</sup>-bit plane image. The edges in the edge image were filled and segmented out based on an intensity threshold to obtain the number of edges.

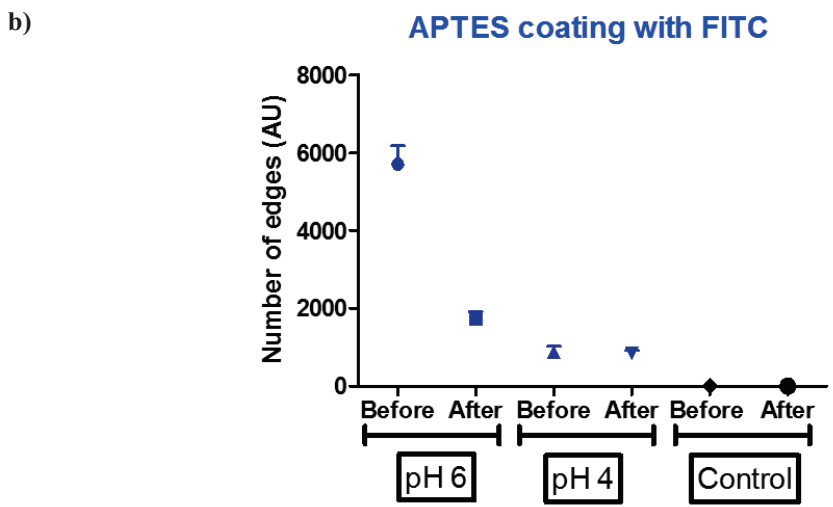
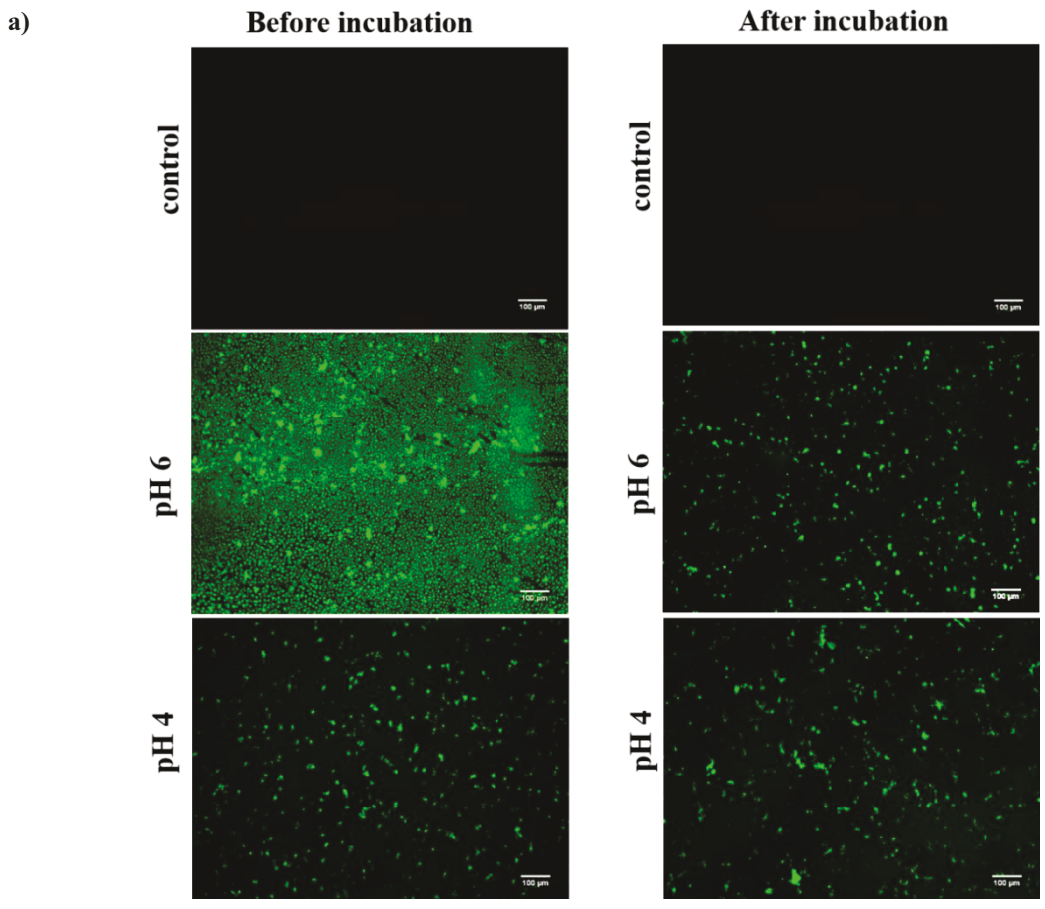


Figure 3.10: a) Fluorescent images (obtained using fluorescent microscope) of a plasma treated sample (control), and silane-treated samples deposited under pH 6 and silane-treated samples deposited under pH 4 before and after incubation in NaCl solution b) graph showing the number of edges *i.e.* corresponding to the number of FITC dye for each condition shown in the fluorescent images (Figure a of this image).

The XPS spectral data and the fluorescent microscope data show that the samples deposited under pH 4 was very stable and also formed a monolayer of silane on the glass surface. The pH 4 condition was considered for further APTES coating on the PI wire.

### **3.2.2.4 APTES deposition on PI wire**

The procedure that was developed on glass was verified by attaching the APTES layer on the PI wire under pH 4 condition. The Si element was detected on the surface of the APTES-coated wires using XPS. The stability of the silane coating on the PI wires was quantified using FITC dye. The fluorescence of the dye was measured for quantification of the silane coating before and after incubation in 0.9% NaCl at 37°C for four days.

Silane was attached to the PI wires in the presence of acetic acid (pH 4) for 15 minutes; the samples were then ultrasonicated in anhydrous EtOH and blown dry with nitrogen gas. The samples were dried at 110° C for 5 minutes (since the samples were very small) by placing the samples over a glass slide kept on a hot plate (there was no direct contact of the wires with hotplate). The measurements of Si 2p signal in the samples with and without the silane (Figure 3.11) were obtained using XPS. The average signal of 5 wires placed close to each other was obtained. Though low signals were achieved, they could be used to detect the presence of Si. The atomic percentage Si 2p for the sample without silane showed 0 % silicon whereas the samples with silane coating showed 4.5% silicon. This result proves that the PI wire has silane attached to the surface when prepared under pH 4 conditions. The stability of the silane coating on the PI wires was tested attaching the FITC dye to the silane and measuring the fluorescence intensity by fluorescence microscopy.

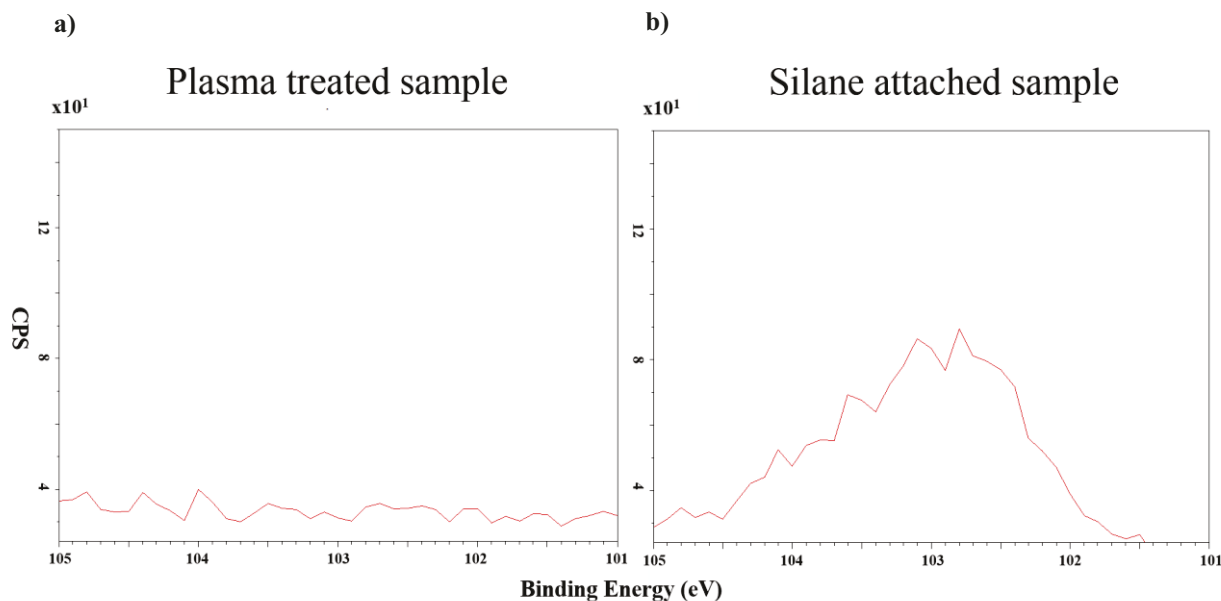


**Figure 3.11: Silicon spectra (obtained using XPS) of a) plasma treated sample without silane b) silane-attached sample deposited under pH 4 condition.**

5 mg of the FITC dye was dissolved in 1 mL of DMSO. It was then attached to the silane-coated PI wires (prepared in the presence of acetic acid). The FITC dye was attached to the samples before and after incubation under physiological conditions in 0.9 % NaCl solution at 37°C for four days (Figure 3.12). The fluorescent intensities of these samples were measured along the length of the wire. The fluorescent intensities of samples before and after incubation in physiological conditions showed the similar value of 68 % of coating throughout the wire. This result shows that the level of silane coating on the surface has not decreased, indicating that the silane-coated wires are stable for four days under physiological conditions. The reduced fluorescent intensity in both samples (~68%) could be due to quenching caused by collision of the fluorescent dye molecules and complex formation [66]. The peptide was attached to this silane coating in the next step of the peptide attachment process.

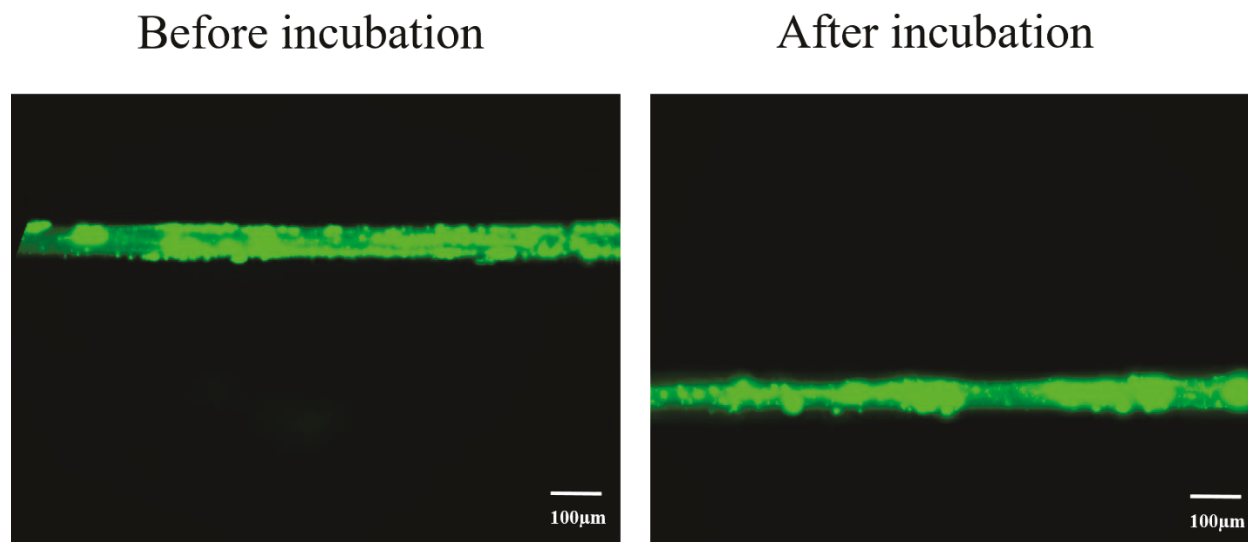


**Figure 3.12: a) Fluorescent images (obtained using fluorescent microscope) of the silane-coated sample deposited under pH 4 before and after incubation in 0.9 % NaCl solution for four days at 37°C.**

### 3.2.3 Peptide attachment step

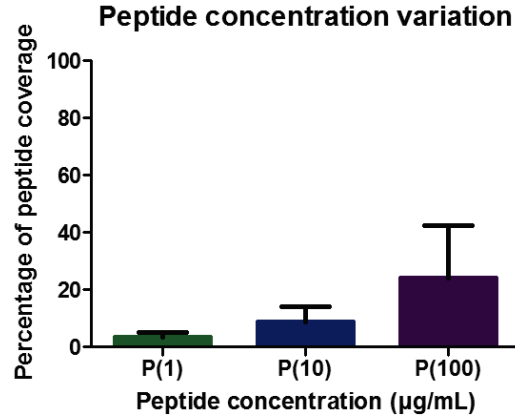
Once a procedure to attach stable silane layers to the surface of the plasma-treated wires was in place, the next step was to attach the peptide to this silane layer. The peptide KHIFSDDSSSE attached with 5-carboxytetramethylrhodamine (TAMRA) dye to the amine group in the N-terminal of the lysine molecule. The peptide was also attached with bis-N-[1-(4, 4- dimethyl-2, 6- dioxocyclohexylidene) ethyl (Dde) to the side terminal of the lysine molecule. The peptide attached with TAMRA and Dde was bought from Biomatik. This TAMRA attached peptide was built based on the solid state peptide synthesis. The purity of the peptide was 97 % (as tested with a mass spectrometer (MS), high-performance liquid chromatography (HPLC) by the supplier). Liquid chromatography-mass spectrometry (LC-MS/MS) was used to validate the sequence of the material as received from the company. The samples showed that the peptide sequence was valid and was of high purity.

This TAMRA-attached peptide was used to quantify the level of peptide coating on the surface of the PI wire. Bioactive molecules like peptides (which have a carboxylic acid group on their end) can be attached to this silane molecule with the help of crosslinker like EDC molecule [43], [48], [67]–[69]. In the EDC chemistry, EDC (dissolved in N, N-dimethylformamide (DMF)) reacts with the carboxyl group (COOH) of the peptide and forms an active O-acylisourea intermediate. This

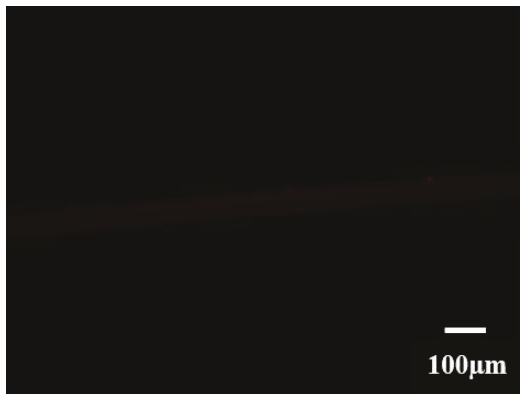
intermediate then reacts with the amine group of the silane to form the amide bond. The amine groups in the peptide were attached with the protecting group Dde (except the N-terminal of the peptide which was already attached with TAMRA dye) to avoid crosslinking between peptide molecules. The EDC and EM were added to the peptide dissolved in DMF (this constitutes the peptide mixture) and the silane-coated PI wire was placed in this peptide solution for the desired length of time (3 or 4 hours) at a specific temperature (21 or 37 °C). After the reaction, the peptide-coated samples were washed with DMF and imaged for the fluorescence using the Leica DMI6000B inverted fluorescent microscope. The goal of the peptide attachment step is to have high peptide coverage on the surface of the silane-coated PI wire. EDC concentration, process time, and process temperature were varied to obtain a maximal coverage throughout the wire surface.

The first parameter to be varied was the peptide concentration. The concentrations used were 1 µg, 10 µg and 100 µg of the peptide each dissolved in 1 mL of DMF. The EDC (1 mg in 1 mL of the DMF) and EM (486 µL) were added to each peptide concentration. The silane-coated samples were treated with the peptide mixture for 3 hours at room temperature (21°C). The peptide with the highest concentration (100µg/mL) had the highest coverage (percentage of peptide coverage on the PI wire- 24%) under these conditions (Figure 3.13 a, b).

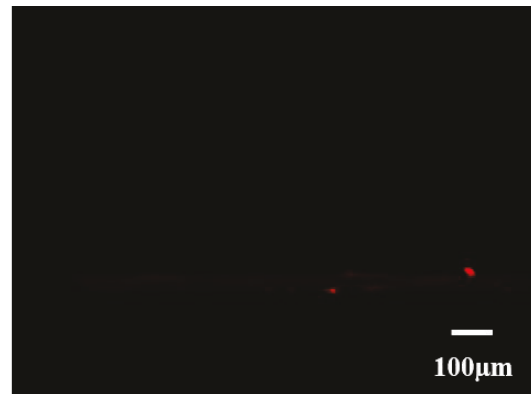
a)



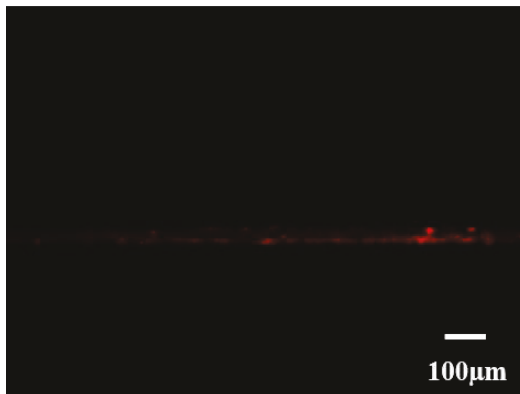
b)



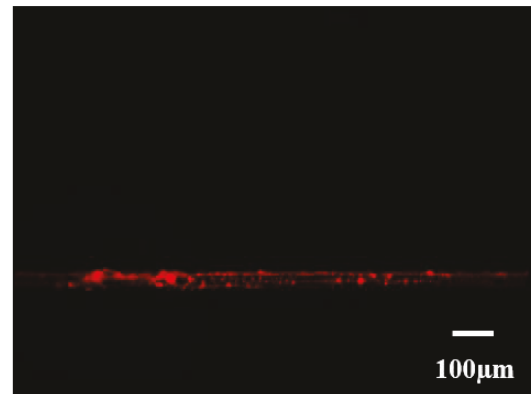
Silane coated sample without peptide



Peptide concentration = 1 µg/mL,  
EDC concentration = 1 mg/mL, Time  
= 3 hrs, Temperature = 20 ° C



Peptide concentration = 10 µg/mL,  
EDC concentration = 1 mg/mL, Time  
= 3 hrs, Temperature = 20 ° C



Peptide concentration = 100 µg/mL, EDC  
concentration = 1 mg/mL, Time = 3 hrs,  
Temperature = 20 ° C

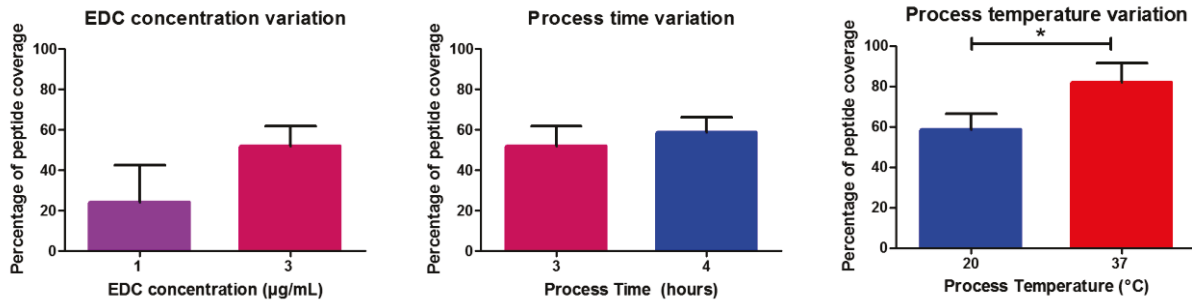
Figure 3.13: a) Graph showing the percentage of peptide coverage on the PI wire for various peptide concentrations (1 µg/mL, 10 µg/mL and 100 µg/mL) b) Fluorescent images (obtained using fluorescent microscope) of silane-coated sample (control), and the peptide-coated wires at different concentrations.

The next parameter to be varied was the EDC concentration. Since the peptide of concentration 100  $\mu\text{g}/\text{mL}$  of DMF resulted in the highest surface coverage, it was fixed as constant for other comparisons. Two EDC concentrations were compared: 1 mg of EDC/1mL of DMF and 3 mg of EDC/ 1 mL of DMF (Figure 3.14 a). Silane-coated PI wires were treated with 1 mL of peptide mixture at room temperature (21°C) for 3 hours. The fluorescent images of the wires treated with varying EDC concentrations (Figure 3.14 b) show that samples treated with the highest EDC concentration have a greater surface coverage on the wire (percentage of peptide coverage on the PI wire: 52%) when compared to the ones treated with low EDC concentration (percentage of peptide coverage on the PI wire: 24%).

In the next set of experiments, the processing time was varied to improve the surface coverage. The processing time was varied from 3 to 4 hours. The EDC concentration during this experiment was fixed at 3mg/ 1 mL of DMF, and the peptide concentration was fixed at 100  $\mu\text{g}/ 1 \text{ mL}$  of DMF. The process was carried out at room temperature (Figure 3.14 a) for both process times. The time variation did not increase the peptide coverage significantly (4 hours of process time yielded a coverage of 59% while 3 hours of process time yielded a coverage of 52%).

Finally, the process temperature was varied to improve the peptide coating. The EDC concentration was fixed at 3 mg of EDC/ 1 mL of DMF; peptide concentration was fixed at 100  $\mu\text{g}/ 1 \text{ mL}$  of DMF and the time was fixed at 4 hours. Two temperatures were compared: 21°C (room temperature) and 37 °C (samples were placed inside an incubator, and the temperature was controlled). Increasing the process temperature, the coating coverage significantly improved from  $59 \pm 8 \%$  to  $82 \pm 10 \%$  (averaged over 3 independent experiments). A t-test was performed on samples in which the process temperature was varied. The samples processed at 37°C showed a significant difference in the  $> 95 \%$  confidence interval (P value = 0.0305, \*).

a)



b)

Peptide concentration = 100 µg/mL

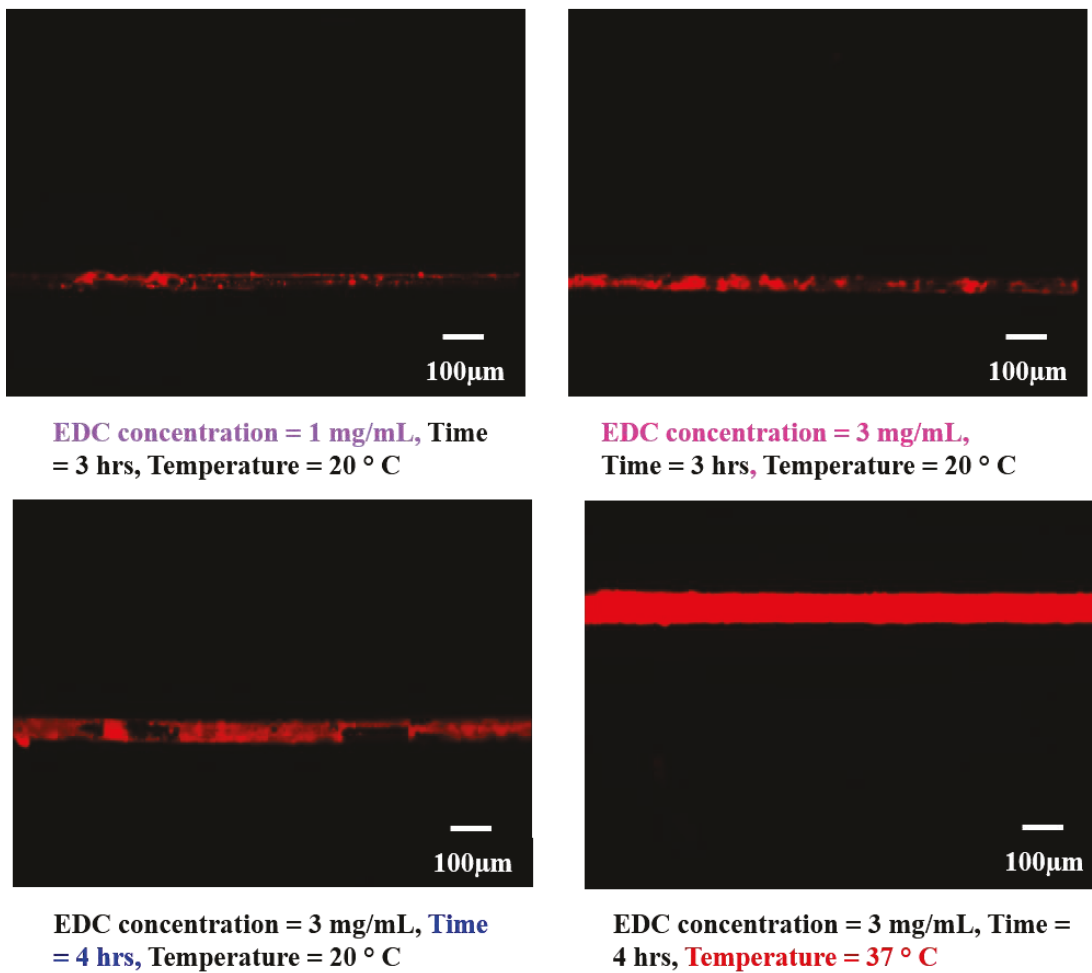
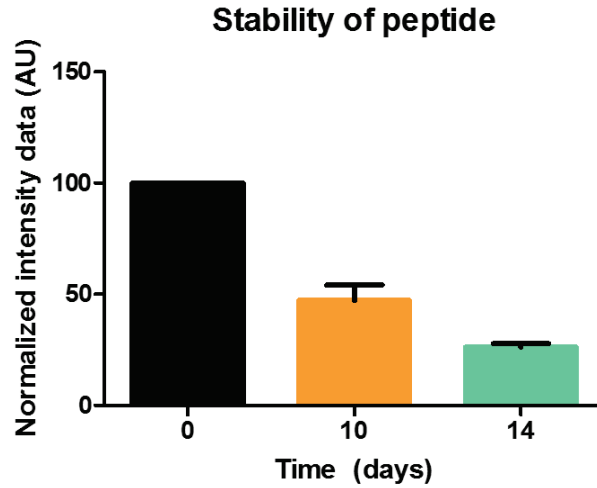


Figure 3.14: a) Graph showing the percentage of peptide coverage on the PI wire by varying reaction parameters including EDC concentration, process time and temperature for 100 µg/mL peptide concentration. b) Fluorescent images (obtained using fluorescent microscope) of peptide-coated sample for the same conditions as shown in the graph.

The sample treated with peptide mixture containing 100 µg/mL peptide and 3 mg/ mL EDC in the presence of EM for four hours at 37 °C, showed high coverage (82%) on the surface of the PI wire. The stability of the peptide attached to these samples was analyzed by placing the wires in 0.9 % NaCl solution for ten and fourteen days. The fluorescence intensity of the TAMRA dye was used to quantify the peptide stability. The samples at day 10 and day 14 post incubation in NaCl solution showed a decrease in fluorescence intensity of TAMRA (Figure 3.15 a, b) when compared to samples before incubation. The fluorescence decreased to 47% at day 10 and 27% at day 14. The decrease in TAMRA dye intensity could be due to the degradation of either the dye or peptide. Since the concentration of peptide on the PI wire is low (~ ng), the quantification of the degraded peptide products and the dye was difficult. Though the stability test results show an exponential decay in fluorescence over time incubated, this trend may be due to degradation of the dye itself. Alternatively, it might exhibit different behavior in the presence of cells. Nonetheless, peptide is still present at day 14, and it is expected that the peptide will be reasonably stable for influencing the acute response and delaying the chronic response of the CNS cells towards the PI-insulated wire electrodes.

a)



b)

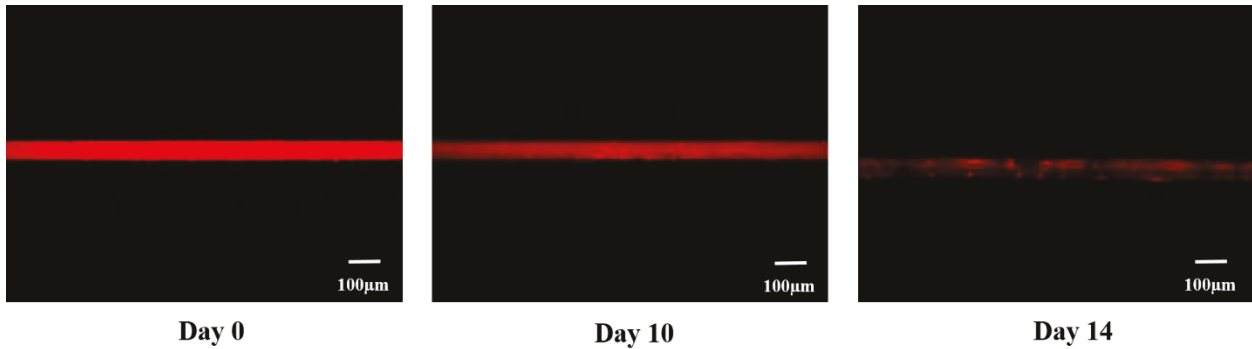


Figure 3.15: a) Graph showing the normalized fluorescent intensity data for the PI wire samples placed in 0.9 % NaCl solution at 37°C for ten and fourteen days and PI wire sample before placing in the NaCl solution (Day 0) b) Fluorescent images (obtained using fluorescent microscope) of peptide-coated sample for the same conditions as shown in the graph.

### 3.3. Summary

By varying the deposition parameters of each step of the coating process, high peptide coverage (82%) on the wires was obtained. Stable monolayers of the silane coupler were achieved at pH 4. The best peptide coatings were achieved for PI wires treated with EDC concentration of 3 mg of EDC/ 1 mL of DMF, peptide concentration of 100 µg/ 1 mL of DMF at 37 °C for 4 hours. The *in vitro* cellular response to peptide-functionalized wires (coated using the procedures described in this chapter) will be discussed in chapter 4.

## Chapter 4.0

# Testing peptide-coated wire in 3D mixed glial cultures

## **4.1 Introduction to responses of glial cells to peptide-coated wire in 3D mixed glial cultures**

This chapter investigates the responses of microglia and astrocytes in 3D hydrogel cultures to the peptide-coated wire at 1, 7 and 14 days post implantation. The 3D gels were prepared from methacrylated hyaluronic acid (HAMA). The goal of this experiment is to determine how the peptide coating affects the glial cells in the vicinity of the wire, by measuring both the number of microglia near the surface of the wire and the intensity of GFAP (antibody) signal from astrocytes attached to the wire. When a wire is inserted in the CNS, the microglial cells are the first responders and their number peaks within a week (*i.e.* as a part of the acute inflammatory response). This increase in the number of microglial cells at the electrode is followed by an increase in the number of astrocytes. The number of astrocytes near the electrode starts to increase after 7 days post insertion of the electrode (*i.e.* as a part of the chronic inflammatory response) [9], [13], [37], [70]. In this chapter, mixed glial cells (consisting of astrocytes and microglia) were seeded in a 3D HAMA gel, and the seeding parameters (cell density, gel density) were optimized to achieve high viability of cells [13]. The cells in 3D gels were incubated in media solution at 37°C and 5 % CO<sub>2</sub> for five days before inserting the peptide-coated wire. At day 4, the peptide was attached to the wires, using the method described in chapter 3 (1 µg/mL, 10 µg/mL and 100 µg/mL peptide (in DMF), 3 mg/mL EDC (in DMF), 4 hours, 37° C). At day 5, peptide-functionalized wires were inserted into the 3D gels with the cells. The samples were incubated for 1, 7 and 14 days and later the responses of the glial cells were analyzed. At each time point, samples were fixed with formalin and cells were labeled with primary and secondary antibody similar to chapter 2. The responses of the microglia and astrocytes were quantified and analyzed.

## **4.2 Glial cell extraction and their growth in 3D gels**

Mixed glial cells were extracted the same method as chapter 2 [53]–[55]. The cells were extracted from the brain tissue of postnatal day one Sprague –Dawley rat pups and they were grown in cell culture flasks treated with poly-L-lysine. The well plates were maintained in media solution (DMEM/F12 + FBS + PS) for fourteen days at 37°C in 5 % CO<sub>2</sub> humidified incubator[53]–[55].

At day 14, the cells were extracted from culture flasks and integrated with the HAMA gels. Jeffery *et al.* have developed a method of preparing cell-seeded HAMA gels; this method is summarized here [13]. Methacrylated HA (HAMA) gel was prepared by dissolving hyaluronic acid sodium salt (HA) in distilled water. Methacrylate (MA) was added to the HA solution while the pH was kept between 8 and 12 (maintained by sodium hydroxide solution (NaOH)). This mixture was left overnight at 4°C [13]. The methacrylated HA was formed and then lyophilized using a Savant SuperModulyo freeze dryer [13]. The lyophilized HAMA was stored at -25°C prior to use.

The integration of cells with the gel involved two steps, namely the rehydration of the lyophilized HAMA, and the encapsulation of cells in the gel [13]. The lyophilized HAMA was rehydrated using phosphate buffered saline (PBS) to a specific weight percentage (wt %) HAMA gel (0.5 wt% or 0.75 wt %). The cells were dissociated from the culture flask by adding 25 mL (per flask) solution containing 0.025 % Trypsin and 0.01 % Ethylenediaminetetraacetic acid (Trypsin-EDTA, Gibco). The culture flask containing trypsin-EDTA was placed in the incubator at 37°C for 10 minutes. After 10 minutes, the cells were lifted off from the bottom of the culture flask as a thin film. The film (containing cells) was collected using a 1000 µL pipette and poured into a centrifuge tube of volume 15 mL. The trypsin-EDTA solution was spun down using centrifuge for two minutes to get pellet cells [13].

The Trypsin-EDTA solution was decanted, and the cells were resuspended in 1mL of the media solution into each centrifuge tube. These cells were further dissociated into single cell suspensions via trituration. The volume of cell suspension and the volume of media solution required to achieve a specific seeding density ( $1 \times 10^7$ ,  $5 \times 10^6$  or  $1 \times 10^6$  cells/mL) were calculated using Trypan blue staining as in chapter 2. The diluted cell suspensions were centrifuged and resuspended in HAMA gel (of specific weight percentage) containing precursors 0.1 % (w/v) of triethanolamine (TEA), 0.1 % (w/v) 1-vinyl-2-pyrrolidinone (NVP) and 0.01 mM eosin Y (EY) in PBS. The cells suspended in the gel monomer were poured into a PDMS mold and photocrosslinked by exposing in LED of wavelength 520 nm for 2 minutes. The gels containing the cells were placed in 12 well-plates, covered with the media solution. The well plates were incubated at 37°C in a 5% CO<sub>2</sub> environment for five days before the wires were inserted [13].

### 4.3 Peptide coating on the wire and insertion into the gel

On the 4<sup>th</sup> day after the cells were encapsulated in the gels, peptide coatings were applied to the wires (in preparation for insertion on the 5<sup>th</sup> day). The peptide KHIFSDDSSE was functionalized with two additional groups: 9-Fluorenylmethyloxycarbonyl (FMOC) on the amine group of the N-terminal of the lysine molecule, and bis-N-[1-(4, 4- dimethyl-2, 6-dioxocyclohexylidene) ethyl (Dde) group on the side terminal of the lysine molecule. The peptide attached with FMOC and Dde was purchased from Biomatik and used as received. This peptide was built based on the solid state peptide synthesis. The purity of the peptide was 97 % and was tested with a mass spectrometer (MS), high-performance liquid chromatography (HPLC) by the company. The peptide was attached to the PI wire using the method described in Chapter 3 (1 µg/mL, 10 µg/mL and 100 µg/mL peptide (in DMF), 3 mg/mL EDC (in DMF), 4 hours, 37° C). The protecting groups FMOC and Dde were utilized to ensure that the main reaction would rather be the formation of a covalent bond between the peptide and the silane and not crosslinking between two peptide molecules. Three different concentrations of peptide were used in the preparation of the peptide solution: 1 µg, 10 µg and 100 µg of the peptide each in 1 mL of DMF. The peptide solution contained the peptide, EDC and EM dissolved in DMF. The protecting groups attached to the peptide were removed before inserting the wires into the gel containing the cells. The FMOC was removed by placing the PI wire samples in 1mL of morpholine and DMF mixture for 30 minutes [71], [72]. The morpholine and DMF mixture contains equal volumes of DMF and morpholine. The Dde group was removed using 2% hydrazine in DMF (1mL of the mixture) for 3 minutes [73], [74].

The peptide-coated wires and the uncoated PI wires (control) were inserted into the gels on the 5<sup>th</sup> day post-cell encapsulation in gels. The gels were covered with the media solution, and incubated at 37°C in a 5% CO<sub>2</sub> environment for 1, 7 and 14 days post insertion/implantation of the wires into the gel.

The responses of the cells to the peptide-coated (peptide concentrations: 1 µg/mL, 10 µg/mL and 100 µg/mL) and control wires at specific time point (1 or 7 or 14 days post insertion) were measured by labeling the microglia and astrocytes with their respective primary and secondary antibodies [13]. The procedure for attaching the antibodies is discussed below. The gels containing the cells were fixed using 10 % formalin at days 1, 7, and 14 post insertion, respectively [13]. The formalin was removed after 20 minutes treatment, and the gels were washed with PBS. After the

washing step, cells were treated with primary antibodies anti-mouse GFAP and anti-rabbit Iba1 for labeling astrocytes and microglia cells respectively. The primary antibody for the astrocytes, namely anti-mouse GFAP, was diluted 1:500 in PBS and the anti-rabbit Iba1 antibody was diluted 1:1000 in PBS. Both primary antibodies were added to the wells containing gel along with 0.1 % Triton X-100 and 1% NHS. The solution of primary antibody was added as 1.5 mL/ well (each well contains a single gel). The cells in the primary antibody solution were incubated overnight (over 18 hours) at 4°C with mild shaking [13].

A day later, the primary antibody solution was removed. The wells containing the gels were washed with PBS thrice, and the secondary antibodies such as Alexa Fluor 647 anti-mouse and Alexa Fluor 488 donkey anti-rabbit were applied. The secondary antibodies were diluted 1:250 in PBS with 1% NHS. This solution was added as 1.5 mL/well was added. The wells were again washed with PBS thrice. The wells containing secondary antibody solution were incubated overnight (over 18 hours) at 4°C with mild shaking [13]. After 18 hours, the nucleus of all the cells were also labeled using Hoechst stain (HS) with the dilution of 1:1000 in PBS and with the volume of 1.5 mL/well. The samples were left at room temperature for one hour and later washed with PBS thrice. The gels in the wells were imaged using the confocal microscope, and they were analyzed using Image J [13]. The gels were imaged through multiple z-planes. These z-planes were projected into a single image using Image J. The number of microglia near the wires, and the intensity of GFAP signal from the astrocytes attached to the wires were measured at different time points. These measurements were plotted as a graph after quantification from these images.

#### **4.4 Characterization of 3D gels with cells**

Before inserting the PI wires into the gels, the viability and the morphology of the cells within the gel were assessed by the same method as Jeffery *et al.* [13]. These assessments were done to optimize the parameters such as cell seeding densities and the weight percentage of the HAMA gel. The viability and morphology of cells in gels were measured at days 5, 12 and 18 post cell capsulation in gels. These time points were chosen to correspond the time points in which the response of the glial cells for the implanted wire would be measured *i.e.* days 1, 7 and 14 days post insertion of the wire, respectively.

The cell viability was assessed using the Syto13/SytoxOrange membrane permeability assay [13] and the procedure is discussed below. 5  $\mu$ M of Syto13 was added to each gel and incubated at 37°C for 30 minutes. At the end of 30 minutes, 0.5  $\mu$ M of SytoxOrange was added to the same gel and was again incubated for another 30 minutes at 37 °C. At the end of 60 minutes, each gel was washed with DMEM/F12 and later fixed with 10 % formalin for 20 minutes [13]. Each gel was imaged using confocal microscope within 24 hours. The gel was imaged through multiple z planes and then projected into a single image using Image J. The live and dead cells were manually counted for each gel. From the counted cells, the percentage of live cells was found and plotted in a graph for various time points [13].

The morphology of the cells was assessed using the specific primary and secondary antibodies (*i.e.* immunochemistry) respective to a cell type in the gel [13]. The gels at time points 5, 12 and 18 days post cell encapsulation were labeled with primary antibody and secondary antibody using the method discussed in section 4.3 of this chapter.

#### **4.4.1. Viability of cells in 3D gels**

The goal of the viability test is to find the optimum parameters in which the gel has maximum viable cells. Parameters such as cell seeding density and weight percentage (wt %) HAMA gel (during rehydration of the gel with PBS) were varied to achieve higher viability of cells in the gel. The viability of cells in the gels under all these conditions were assessed using the membrane permeability assay Syto13 and SytoxOrange in the method stated in section 4.4.

0.75 wt% HAMA gel was seeded with glial cells (microglia and astrocytes) of seeding densities  $1 \times 10^7$ ,  $5 \times 10^6$  and  $1 \times 10^6$  cells/mL to find the optimal seeding density. The time point to compare the viability of cells in the gel with various seeding density was 5 days post encapsulation of cells in the gel. A membrane permeability assay (section 4.4) was applied to these gels at day 5 post cell encapsulation in the gels, and they were imaged using the confocal microscope (Figure 4.1). The number of live and dead cells were counted manually, and the percentage of living cells was plotted for various cell densities (Figure 4.2).

A comparative discussion on 0.75 wt% HAMA gel with various seeding densities based on the confocal images (Figure 4.1) is done below. The confocal images of the highest cell seeding

density ( $1 \times 10^7$  cells/mL) show higher cell death (the dead cells labeled by SytoxOrange (red channel) is higher) as opposed to the other cell densities. The higher cell death could be due to greater cell clumping in these gels. The confocal images of other seeding densities show the high viability of cells. The confocal images of the lowest cell seeding density ( $1 \times 10^6$  cells/mL) show that it will not lead to a realistic foreign body response when a wire was inserted into the gel as expected due to the low number of cells present. The desired 'realistic' foreign body response include cell migration towards the wire electrodes and the interaction of those cells with the wire surface. The gel with cell seeding density of  $5 \times 10^6$  cells/mL, shows limited cell death, cell clumping, and it also shows a sufficient number of cells to get a realistic foreign body response.

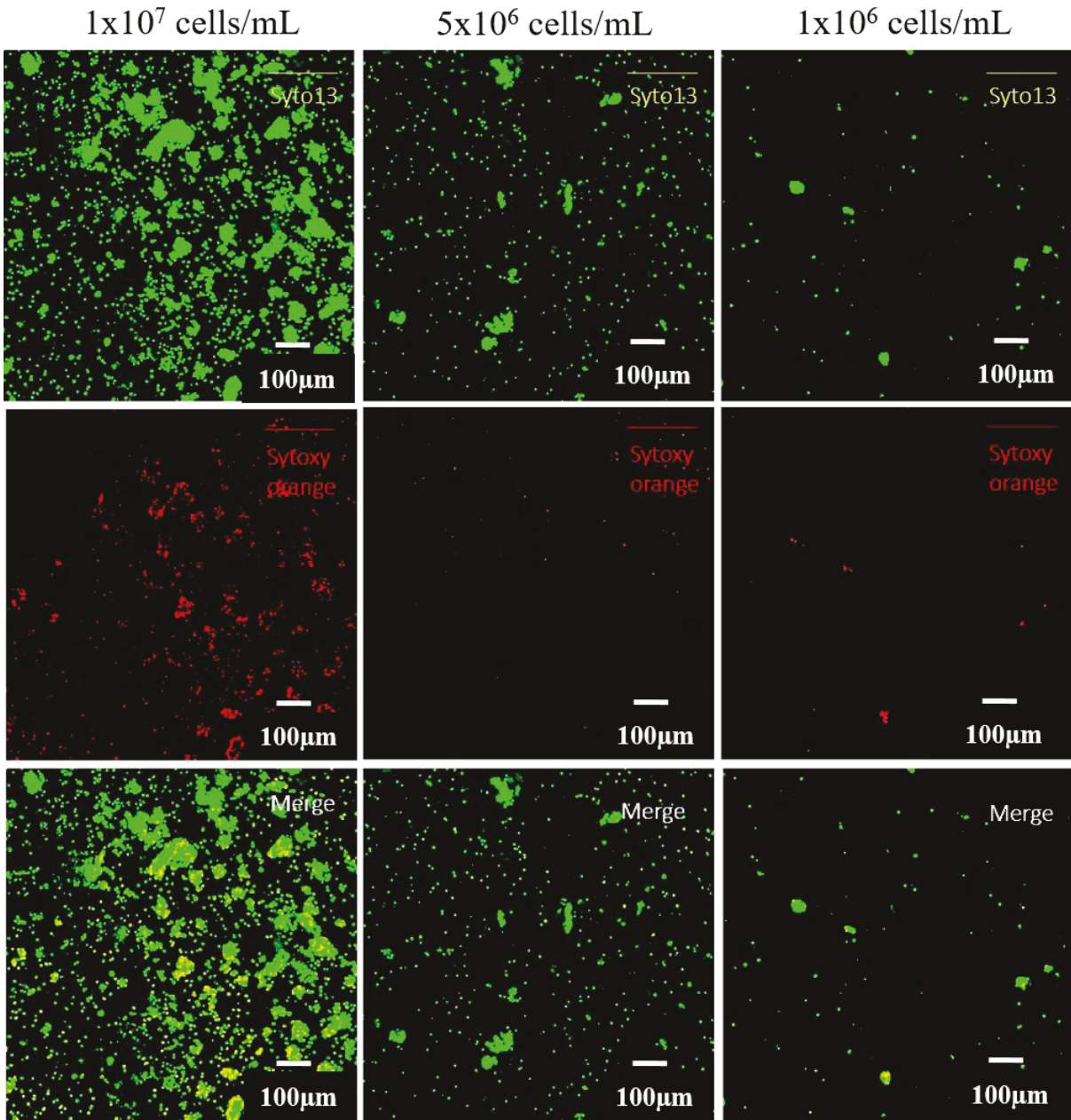
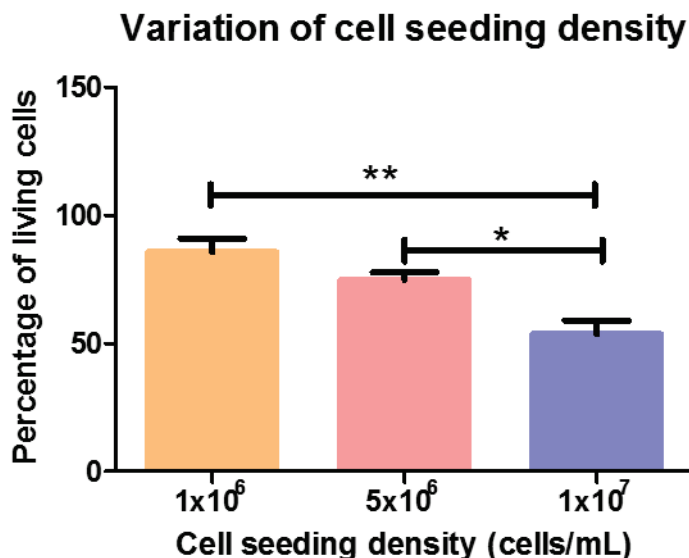


Figure 4.1: Confocal images of the 0.75 wt% HAMA gel with various cell seeding densities  $1 \times 10^7$ ,  $5 \times 10^6$  and  $1 \times 10^6$  cells/mL. The images show that the gel with seeding density  $1 \times 10^7$  has the least viability when compared to the other seeding densities.

The percentage of living cells for the 0.75 wt% HAMA gel for various seeding densities quantified from the confocal images data (Figure 4.2) are discussed below. The cell density of  $1 \times 10^6$  cells/mL has the highest percentage of live cells (86%) while the cell density of  $1 \times 10^7$  cells/mL has the least (54%). The cell seeding density of  $5 \times 10^6$  cells/mL had 74% viability. One- way ANOVA was

performed with Tukey post-test showing a significant decrease in the percentage of live cells in case of  $1 \times 10^7$  cells/mL when compared to other seeding densities (in 95% confidence interval). The cell seeding density of  $5 \times 10^6$  cells/mL had a sufficiently greater number of cells without clumping and to get a realistic foreign body response as opposed to seeding density of  $1 \times 10^6$  cells/mL. It also has a high number of viable cells (though not as high as seeding density of  $1 \times 10^6$  cells/mL). Thus, this seeding density was considered for further optimization.



**Figure 4.2:** The graph showing the quantified value of the percentage of living cells in the 0.75 wt% HAMA gel with various seeding densities of densities  $1 \times 10^7$ ,  $5 \times 10^6$  and  $1 \times 10^6$  cells/mL (independent experiments N=3). The graph showing that percentage of living cells in seeding densities  $5 \times 10^6$  and  $1 \times 10^6$  cells/mL were significantly higher than  $1 \times 10^7$  cells/mL. (One- way ANOVA with Turkey post-test was performed, and the P value was 0.0073 (<0.05) in 95 %confidence interval) The significance bar (Labeled with \*) indicates the difference between the  $5 \times 10^6$  cells/mL and  $1 \times 10^7$  cells/mL is significant and the significance bar (Labeled with \*\*) indicates the difference between the  $1 \times 10^6$  cells/mL and  $1 \times 10^7$  cells/mL is very significant.

The next parameter that was optimized was the weight percentage HAMA gel based on the rehydration of the gel with PBS before the cell encapsulation step. Two weight percentages HAMA gel that were considered: 0.5 and 0.75 wt % HAMA gel (in PBS). Both types of gels were integrated with cells of seeding density  $5 \times 10^6$  cells/mL. The Syto13 and SytoxOrange assays were used to assess cell viability at day 5 post cell encapsulation (Figure 4.3). The percentage of living cells was counted and plotted as a graph (Figure 4.4). The confocal images of the 0.5 wt % HAMA

gel shows the higher viability of cells when compared to 0.75 wt % HAMA gel (Figure 4.3). The 0.5 wt % gel shows much less clumping when compared to the 0.75 wt% HAMA gel.

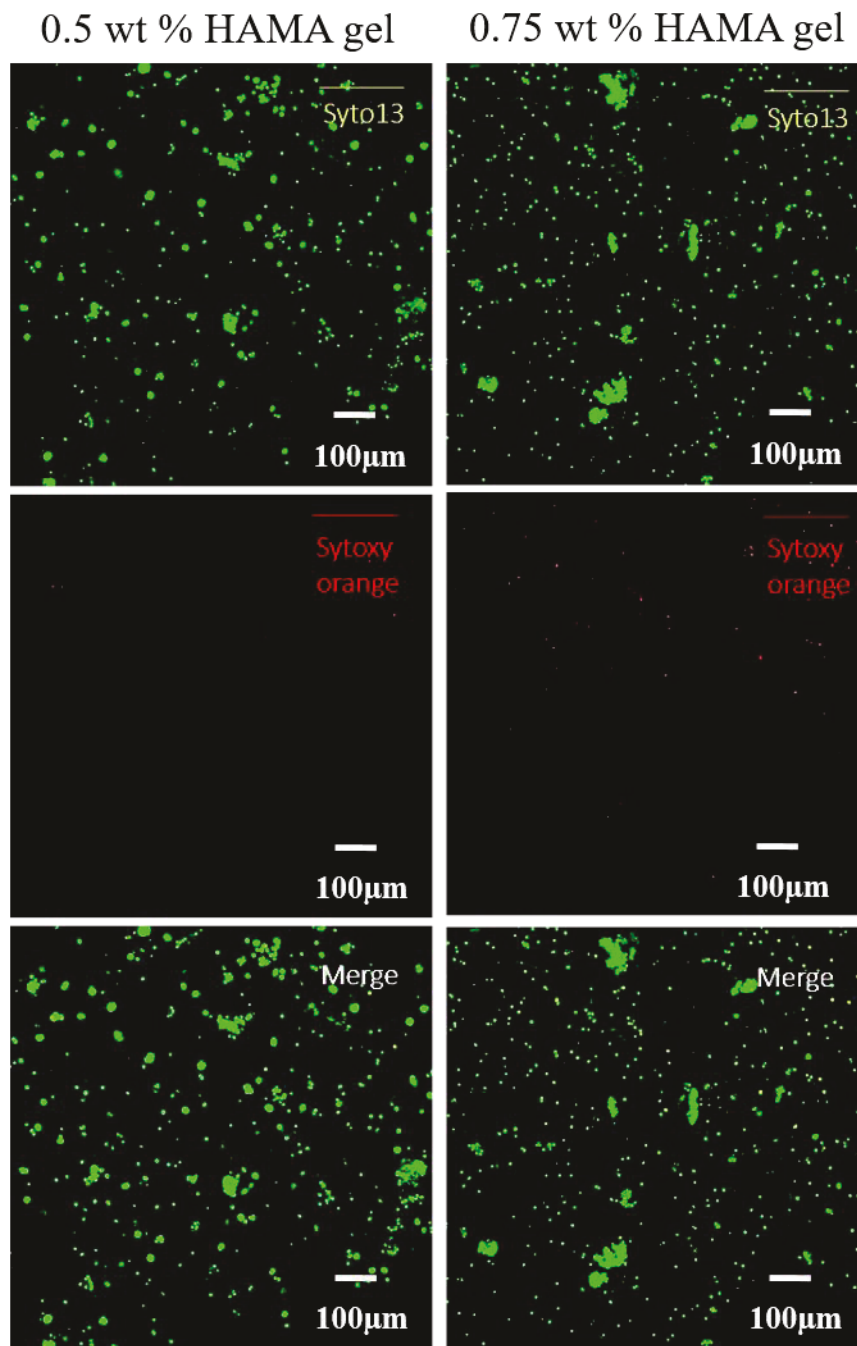


**Figure 4.3:** Confocal images of the 0.5 wt% and 0.75 wt% HAMA gels seeded with  $5 \times 10^6$  cells/mL. The images show that 0.5 wt% HAMA gel has the higher viability when compared to 0.75 wt% HAMA gel.

The percentage of living cells for the 0.5 wt% HAMA gel and 0.75 wt% HAMA gel quantified from the confocal images data (Figure 4.4) are discussed below. The 0.5 wt % HAMA gel has

94.7% of live cells whereas the 0.75 wt %HAMA gel has only 74% of live cells at day 5 post cell capsulation. The unpaired t-test confirmed the difference was significantly different when tested at the 95% confidence interval (Figure 4.4). The 0.5 wt % HAMA gel with cell seeding density of  $5 \times 10^6$  cells/mL has the highest viability at day 5 post cell encapsulation. The viability and morphology of cells in this gel was quantified and studied further at days 12 and 18 post cell encapsulation.

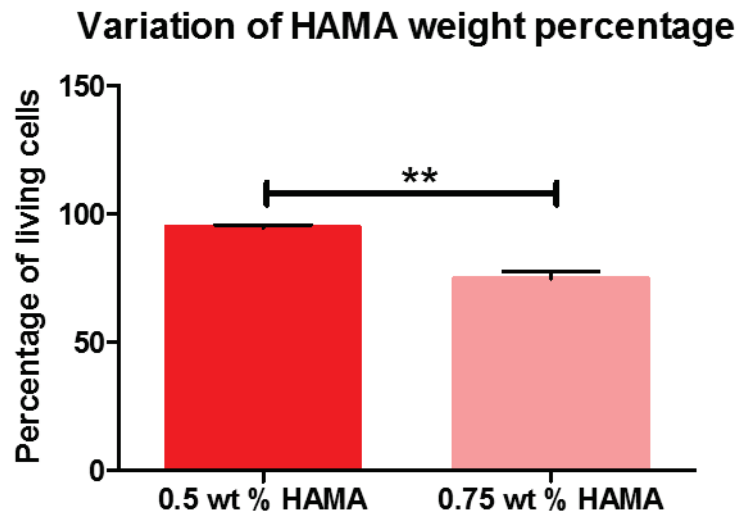


Figure 4.4: The graph showing the quantified value of the percentage of living cells in the 0.5 wt% HAMA gel and 0.75 wt% HAMA gel seeded with  $5 \times 10^6$  cells/mL (independent experiments N=3). The graph showing that the percentage of living cells in 0.5 wt% HAMA gel was significantly higher than 0.75 wt% HAMA gel. (The unpaired t-test was performed and the P value was 0.0031 ( $<0.05$ ) in 95 %confidence interval). The significance bar (Labeled with \*\*) indicates the difference between the 0.5 wt% HAMA gel and 0.75 wt% HAMA gel is very significant.

The viability of the 0.5 wt% gels seeded with  $5 \times 10^6$  cells/mL at time points 5, 12 and 18 days post cell encapsulation are discussed below. The confocal images of the 0.5 wt % HAMA gel at 5, 12 and 18 days post cell encapsulation show that the gel has high viability at all time points (Figure 4.5). The images of gel at day 18 show that the gel has the smallest number of individual cells overall. There is some clumping of these cells (at day 18) but still it had high viability (Figure 4.5).

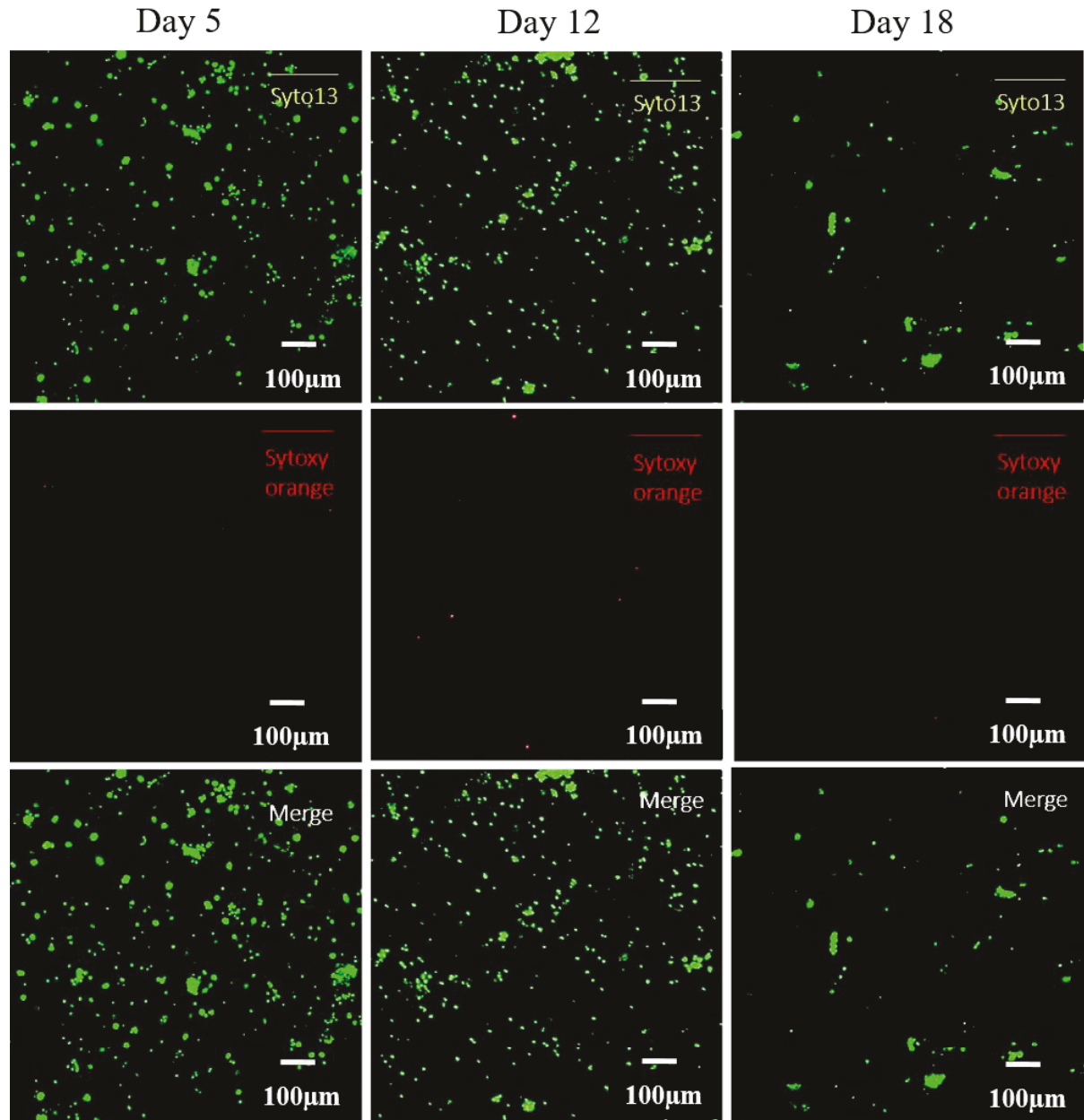
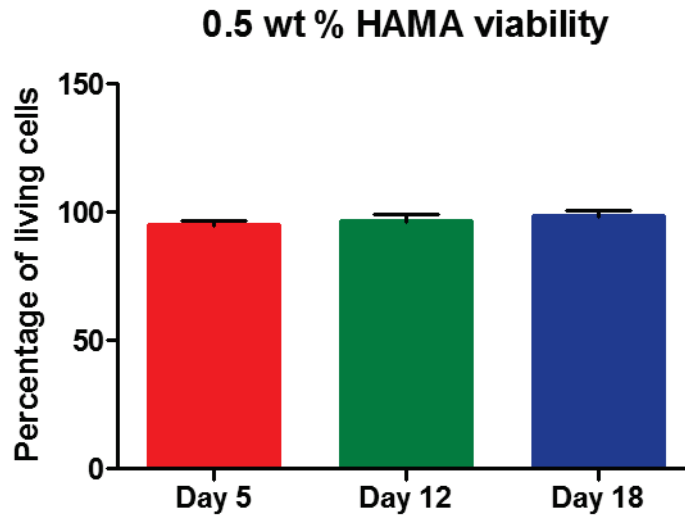


Figure 4.5: Confocal images of the 0.5 wt% HAMA gels seeded with  $5 \times 10^6$  cells/mL at various time points 5, 12 and 18 days post cell encapsulation. The images show that 0.5 wt% HAMA gel has the high viability at all time points.

The percentage of living cells for the 0.5 wt% HAMA gel seeded with  $5 \times 10^6$  cells/mL at time points 5, 12 and 18 days post cell encapsulation were quantified. The percentages were obtained from the confocal images data of the same conditions (Figure 4.6). The quantified results are

discussed below. The percentage of living cells at the time points day 5, day 12 and day 18 are 95%, 96%, and 98% respectively. The quantified values show that the viability of the 0.5 wt% HAMA gel seeded with  $5 \times 10^6$  cells/mL remains the same at all time points.



**Figure 4.6:** The graph showing the quantified value of the percentage of living cells in the 0.5 wt % HAMA gels at various time points (independent experiments N=3). The graph showing that the percentage of living cells in 0.5 wt% HAMA gel were approximately the same at all time points.

#### 4.4.2. Morphology of cells in 3D gels

The 0.5 wt% HAMA gel seeded with  $5 \times 10^6$  cells/mL at time points 5, 12 and 18 days post cell encapsulation were labeled with primary antibody and secondary antibody using the method discussed in section 4.3 of this chapter. The nuclei of all cells were labeled with Hoechst stain, and it can be seen as the **blue channel** in the confocal images (Figure 4.7). The astrocytes were immunostained for GFAP (**pink channel**) and the microglia were labeled for Iba1 (**green channel**). The nuclear staining show approximately same number of nuclei at each time point (5, 12 and 18 days). The images also show that the astrocytes and microglia start extending their processes at day 12 post cell encapsulation. These processes remain visible at day 18 (Figure 4.7).

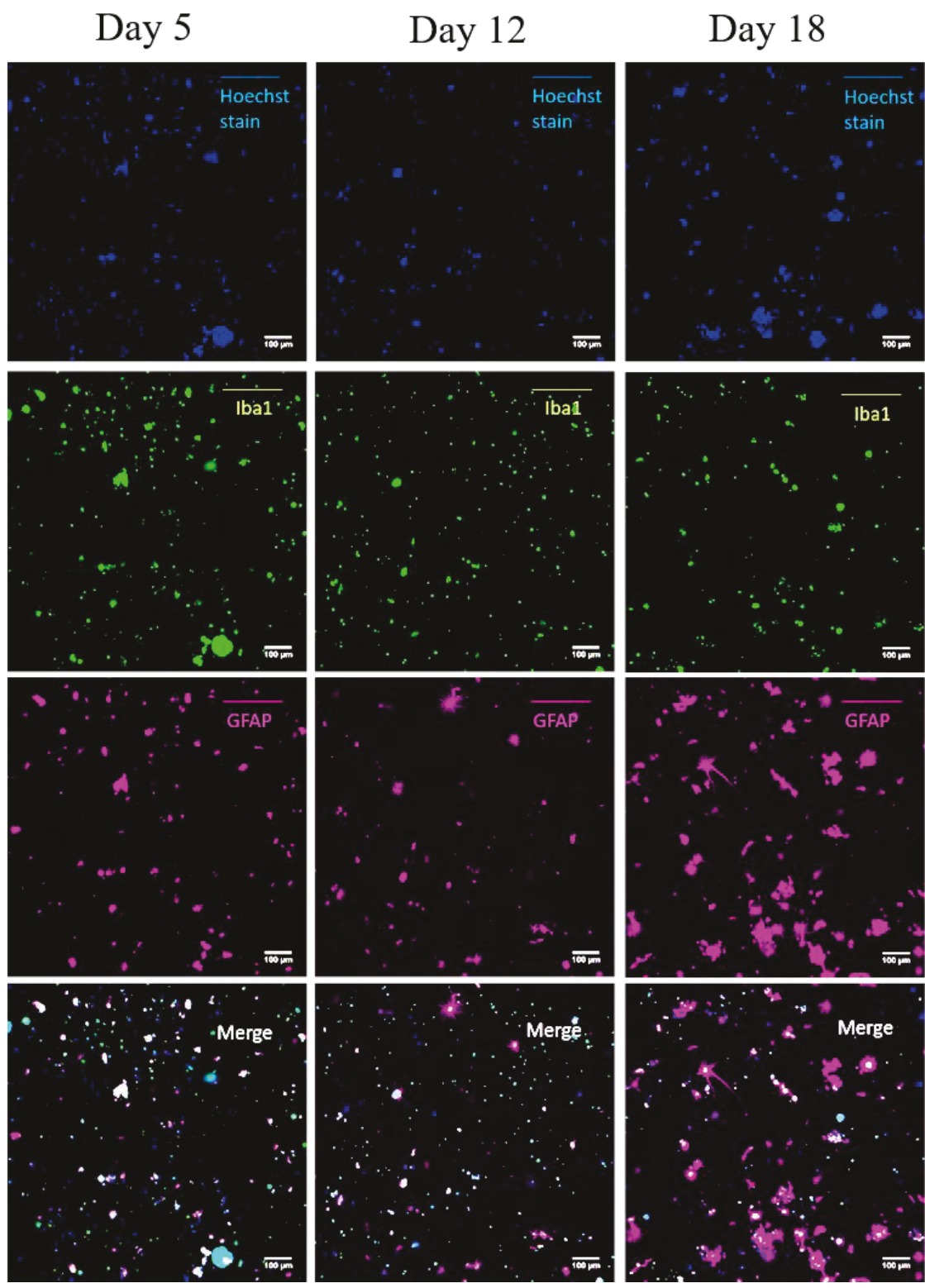


Figure 4.7: Confocal images of the 0.5 wt% HAMA gel with cell seeding density of  $5 \times 10^6$  cells/mL at days 5, 12 and 18 post cell encapsulation. The antibodies labeled for microglia (**Iba1**), astrocytes (**GFAP**) and nuclei of all cells labeled with **Hoechst stain**.

## 4.5 Responses of glial cells to the peptide-coated wire

The acute response and initial stage of the chronic response of the glial cells namely microglia and astrocytes were studied in this section. In acute response, the microglia gets activated and in the activated state these cells start the process of phagocytosis (during which they try to break down the electrode) [12]. They further recruit and activate astrocytes, signifying the start of the chronic response [13]. The activated astrocytes encapsulate electrodes by forming a compact sheath around the electrodes [9], [10].

The goal of this section is to compare the response of the glial cells between the peptide-coated wire and the control wire. The control sample was also compared with the polyimide-insulated Pt/Ir wire electrode (PI wires) studied by Jeffery *et al.* to ensure events of the acute response and initial stage of chronic response occurs with respect to the events described in the literature [13]. The number of microglia near the wires were measured and quantified to explain the acute response (starting at 3 days post insertion of electrodes into the gel and the response is mainly contributed by microglia). The intensity of GFAP signal from the astrocytes attached to the wires were measured and quantified to explain the initial stage of the chronic response (starting at 14 days post insertion of electrodes into the gel and the response is mainly contributed by astrocytes).

Confocal images of the peptide-coated wires (before insertion into the gel) were collected to aid in the analysis of the images. These images show autofluorescence signal from the Pt/Ir metal inside the wire. This signal is produced due to the reflection of incident light from the metal, and these signals were seen as solid lines (green for Iba1 and pink for GFAP, Figure 4.8).

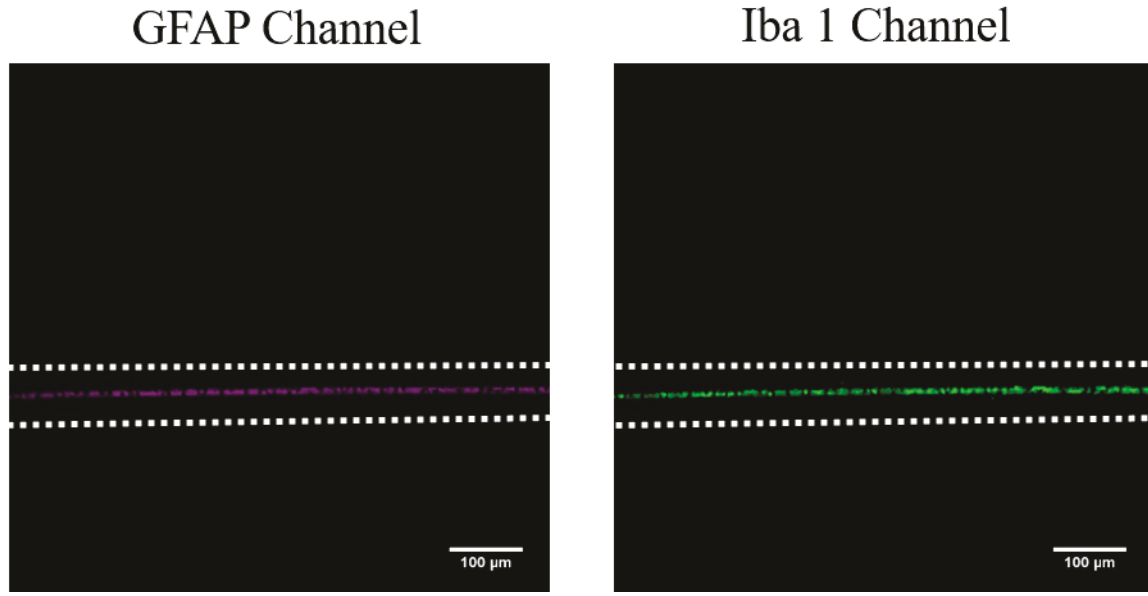


**Figure 4.8:** Confocal images showing autofluorescence signal of the Pt/Ir metal in the PI wire when looked under **Iba1** channel and **GFAP** channel and the wires were not inserted into a gel. The solid line (**Solid green line** and **solid pink line**) seen in the image correspond to the auto-fluorescence signal.

As described in section 4.3 of this chapter, the peptide-coated, and the control wires were inserted into the gels with cells on the 5<sup>th</sup> day post-cell encapsulation into the gel. The analysis was then performed at days 1, 7 and 14 (post insertion). The gel sample at each time point was repeated thrice (N=3 independent experiments *i.e.* cells from three rat brains). The gel samples with the wires were fixed after the time points (days 1, 7 and 14 post insertion) using 10% formalin. The primary and secondary antibody were attached in the same method as in section 4.3 of this chapter. The nuclei of all cells were labeled with Hoechst stain as in section 4.3. The gels were imaged through z planes of depth 102  $\mu\text{m}$  using the confocal microscope (Figure 4.9). The microglial cells near the electrode were counted, and the counts were plotted on a graph for all the various conditions (Figure 4.9). The GFAP intensity from the astrocytes for the same conditions were measured on the wire (Figure 4.9). The microglial counting was carried out per volume of the gel that was imaged *i.e.* the volume of the gel was  $6.3 \times 10^6 \mu\text{m}^3$  (length x breadth x depth=  $527.65 \times 118.17 \times 102 \mu\text{m}^3$ ). The GFAP intensity measurement from astrocytes were carried out per volume of the gel *i.e.* the volume of the gel was  $2.6 \times 10^6 \mu\text{m}^3$  (length x breadth x depth=  $527.65 \times 50 \times 102 \mu\text{m}^3$ ). 2-way ANOVA in 95 % confidence interval was carried out in both cases with Bonferroni post-test.

Figure 4.9 shows the 0.5 wt% HAMA gels (seeded with  $5 \times 10^6$  cells/mL) inserted with control wire and peptide-coated wires. The PI wires were coated with the peptide at three concentration; 1  $\mu\text{g/mL}$ , 10  $\mu\text{g/mL}$  and 100  $\mu\text{g/mL}$  of DMF. The observation from the confocal images is discussed below. Some of the wires in Figure 4.9 show autofluorescence signal similar to Figure 4.8.

The confocal images of the control wire show the following events in the acute response (7 days post implantation of the wire into the gel) and initial stage of the chronic response (14 days post implantation of the wire into the gel) (Figure 4.9). In the control sample *i.e.* the polyimide-insulated Pt/Ir wire without peptide coating, the microglia appears to peak at day 7 and appears to decrease at day 14 (Figure 4.9). The GFAP signal intensity from the astrocytes in the control sample appears to increase on day 14 from the day 1 samples and day 14 sample appears to show astrocytes encapsulation around the wire (Figure 4.9). The events discussed above is similar to the events seen by Jeffery *et al.* [13]. They have reported the events in the acute response and initial stage of the chronic response of these cells to the PI wires when it was inserted into the HAMA gel [13]. At day 6 post insertion, the number of microglia started to peak, and these microglia cells had circular morphology (the circular morphology is indicative of the activated state of the microglia) [13]. Similar to the microglial count pattern observed by Jeffery *et al.* [13], it has been reported that for stab wounds in rats, the microglia count near the wound started to peak at day 3 and remained the same till day 7 [70]. The study also showed that the number of microglia had decreased significantly after day 7 [70]. In the study by Jeffery *et al.*, the astrocytes started appearing near the wire electrode at day 6 post insertion of the wire into the gel, and the astrocytes encapsulation of the wire starts at day 11 and sustained until day 14 [13]. From the similarity of the events between the literature and the control sample in this work, it is proved that the gel can model the acute response and initial stage of the chronic response of the glial cells.

The confocal images of the peptide-coated wires (all three concentrations) show the following events in the acute response and initial stage of the chronic response (Figure 4.9). The control wire is compared with the other peptide-coated wires.

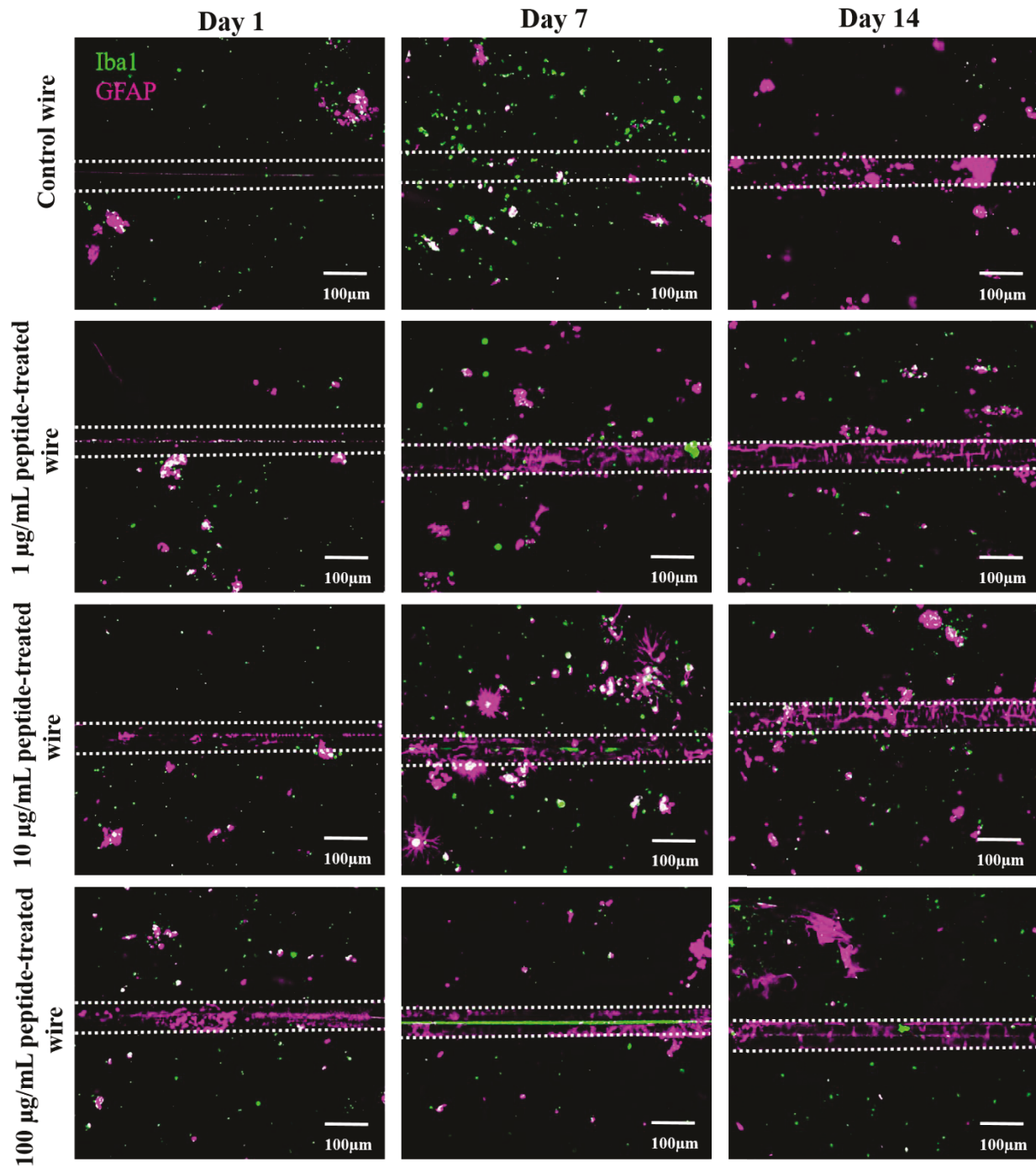


Figure 4.9: Confocal images of the 0.5 wt% HAMA gel (cell seeding density of  $5 \times 10^6$  cells/mL) with wires treated at 0 (control), 1 µg/mL, 10 µg/mL and 100 µg/mL peptide solution at days 1, 7 and 14 post cell encapsulation. The antibodies labeled for microglia (Iba1), astrocytes (GFAP).

The events in the acute response (in terms of the number of microglia near the peptide-coated wires) from the confocal images (Figure 4.9) are first considered. In Figure 4.9, the PI wires treated with 1  $\mu\text{g}/\text{mL}$  and 10  $\mu\text{g}/\text{mL}$  peptide solutions appear to show an increased number of microglia cells at day 7 (similar to control sample). The number of microglia near these wires at day 14 appear to have decreased (similar to control sample). The PI wire treated with 100  $\mu\text{g}/\text{mL}$  peptide solution appears to show less number of microglia at day 7 (much less than control sample). The number of microglia near these wires at day 14 appears to remain roughly the same as day 7.

The events in the initial stage of the chronic response (in terms of the intensity of GFAP signal from astrocytes attached to the wire) are considered next. The PI wires treated with 1  $\mu\text{g}/\text{mL}$  and 10  $\mu\text{g}/\text{mL}$  peptide solutions appear to show an increased intensity of GFAP signal from astrocytes at day 14 when compared to day 1 (similar to control sample) (Figure 4.9). The PI wire treated with 100  $\mu\text{g}/\text{mL}$  peptide solution appears to show the intensity of the GFAP signal from astrocytes even at day 1 (different from control, and the other two peptide samples). The intensity of the GFAP signal from astrocytes attached to this peptide-coated wire appears to remain roughly the same till day 14.

100  $\mu\text{g}/\text{mL}$  peptide-coated samples were treated with primary and secondary antibodies of the astrocytes (GFAP) to verify the GFAP signal from the astrocytes on the peptide-coated wires was a true signal. After treatment, the wires were imaged under the GFAP channel (Figure 4.10). A true signal from astrocytes will result from the interaction between GFAP and astrocytes and not between GFAP and the peptide. Figure 4.10 shows that the GFAP has not interacted with the peptide-coated wire, and the solid pink line seen in the image is due to the auto-fluorescence similar to the Figure 4.8. The intensities of the GFAP signal from the astrocytes were quantified using Image J and were plotted as graph under each peptide concentration.

## GFAP interaction

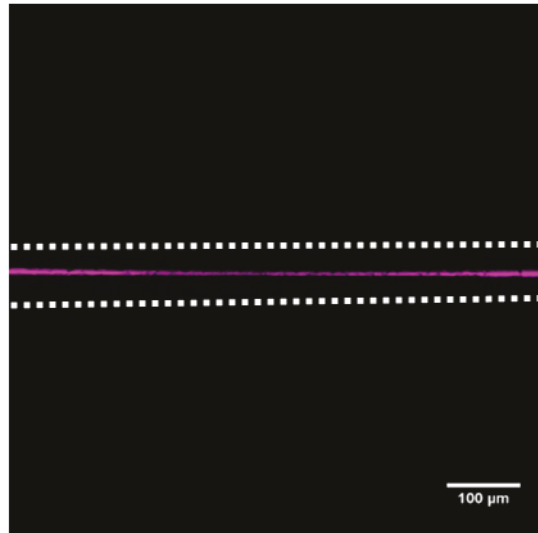


**Figure 4.10:** Confocal image showing wires treated with **GFAP** (primary and secondary antibody) and the **solid pink line** in the image is an auto-fluorescence signal of the Pt/Ir metal in **GFAP** channel (wires were not inserted into the gel).

The number of microglial cells near the PI wire and intensity of the GFAP signal from the astrocytes attached to the wire were quantified and plotted in graphs (Figure 4.11 and 4.12). The microglia cells in all these conditions were counted positive if the diameter of the cell is  $\geq 8 \mu\text{m}$  (Figure 4.11). The GFAP signal intensities from astrocytes on the different wire conditions were measured using Image J (Figure 4.12). The observations from the confocal images were verified by the quantified values in Figures 4.11 and 4.12.

### 4.5.1. Microglia counts near the wire

Figure 4.11 shows the plot of the number of microglia near the peptide-coated (wire treated with  $1 \mu\text{g/mL}$ ,  $10 \mu\text{g/mL}$  and  $100 \mu\text{g/mL}$  peptide concentrations) and control wires for day 1, 7 and 14 post implantation. As can be seen in Figure 4.11, for the control wire, the number of microglia peaks at day 7 (undergoing a significant increase from the value at day 1). The number of microglia then significantly decreases at day 14 from the peak value at day 7 to a similar value at day 1 post insertion.

The PI wire treated with 1 µg/mL peptide shows a high number of microglia at day 1 and day 7. The number of microglia around these wires at day 14 has decreased, but this decrease is not significant. The 10 µg/mL peptide-treated PI wire shows an increased microglial count at day 7 (similar to control) from day 1 but the increase is not significant. There is, however, a significant decrease in the number of microglia at day 14 when compared to the day 7 sample (similar to control). The PI wire treated with 100 µg/mL peptide solution shows a significant decrease in the number of microglia at day 7 when compared to wires treated with 1 µg/mL, 10 µg/mL peptide, and the control wire. For the 100 µg/mL peptide-treated wire, the number of microglia remains the same until day 14. A 2-way ANOVA was performed on these various conditions. 2-way ANOVA with Bonferroni post-test shows a significance in 95% confidence interval with the factors days post insertion \*\*\*(highly significant), peptide concentration \*(significant) and their interaction \*\*(very significant).

These results suggest that treating the wire with 100 µg/mL peptide can reduce the number of microglia near the wire surface as opposed to the control wire at day 7 post insertion. Since 100 µg/mL peptide-treated wire has the lowest number of microglia around it, this wire modulated acute inflammatory response (compared with the control sample and the other peptide samples, Figure 4.11). The number of microglia on the 100 µg/mL peptide-treated wire remains roughly constant at all time points (Figure 4.11). The 1 µg/mL, 10 µg/mL peptide-treated wires were not as effective as the 100 µg/mL peptide-treated wire in reducing the number of microglia surrounding the wires at day 7 post insertion into the gel.

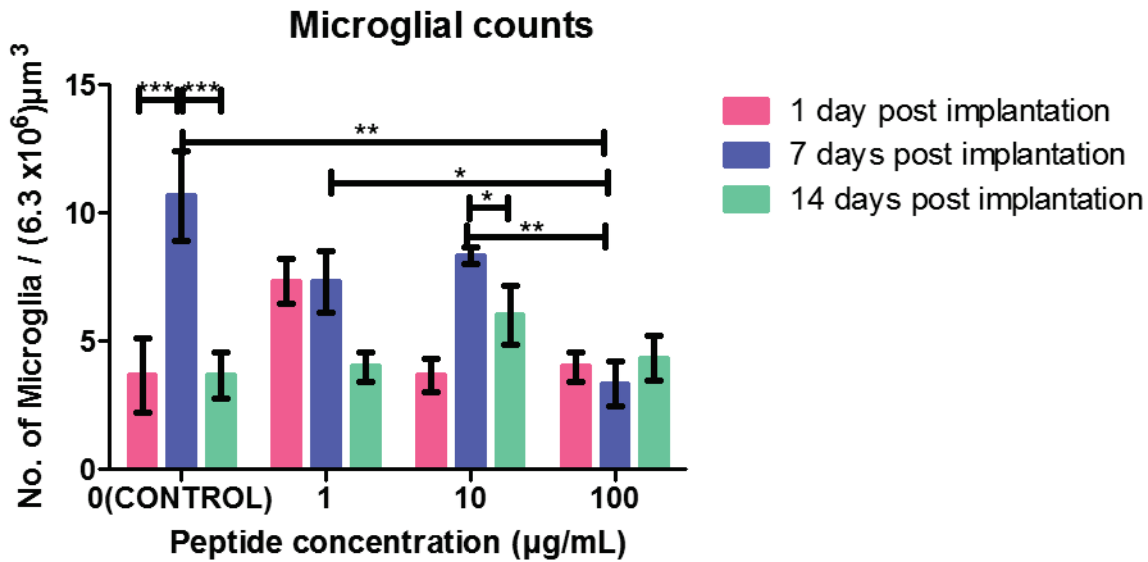


Figure 4.11: Graph showing microglial counts near the wire that is inserted into the 0.5 wt% HAMA gel with cell seeding density of  $5 \times 10^6$  cells/mL at days 1, 7 and 14 post insertion. The wires were treated with 0  $\mu\text{g/mL}$  (control), 1  $\mu\text{g/mL}$ , 10  $\mu\text{g/mL}$  and 100  $\mu\text{g/mL}$  peptide solution. 2 way ANOVA with Bonferroni post-test, significance of days post insertion \*\*\* (highly significant), peptide concentration \* (significant) and their interaction \*\* (very significant).

#### 4.5.2. GFAP signal intensity from the astrocytes attached to the wire

Figure 4.12 shows the plot of the intensity of GFAP signal from the astrocytes attached to the peptide-coated (wires treated at 1  $\mu\text{g/mL}$ , 10  $\mu\text{g/mL}$  and 100  $\mu\text{g/mL}$  peptide concentrations) and control wires for days 1, 7 and 14 post implantation. Figure 4.12 indicates that for the control sample, there is a significant increase in the intensity of the GFAP signal (from astrocytes) from day 1 to day 14. For the wire treated with 1  $\mu\text{g/mL}$  peptide, there was an increase in astrocytes intensity from day 1 to day 14, but the increase is not significant. For the wire treated with 10  $\mu\text{g/mL}$  peptide, there was a significant increase in the intensity of the GFAP signal (from astrocytes) from day 1 to day 14 (similar to the control wire). For wires treated with 1  $\mu\text{g/mL}$  and 10  $\mu\text{g/mL}$  peptide, selective attachment of astrocytes to these wires started at day 7 post insertion. For wires treated with 100  $\mu\text{g/mL}$  peptide, selective attachment of astrocytes to this wire began much earlier and is evident at even at day 1 post insertion (Figure 4.12). The intensity of GFAP signal from astrocytes attached to the 100  $\mu\text{g/mL}$  peptide-treated wires increased slightly from day 1 to day 7, and then remained the same at day 14. The intensity of the GFAP signal from astrocytes

attached to the control wire and the 100  $\mu\text{g}/\text{mL}$  peptide-treated wire samples at day 14 post implantation were approximately the same. 2-way ANOVA with Bonferroni post-test shows a significance in 95% confidence interval with the factors days post- insertion \*\*\*, peptide concentration \*. The interaction between these two factors does not show significance.

From the quantified intensity of the GFAP signal from astrocytes in the graph (Figure 4.12), the following results are concluded: astrocytes attach selectively to the 100  $\mu\text{g}/\text{mL}$  peptide-treated wires starting at day 1 post insertion. The intensity of GFAP signal from astrocytes attached to on these wires remains the same till day 14 post implantation, whereas the control wire does not have a specific attachment of astrocytes at day 1. For the control wire (and wires functionalized with lower concentrations of the peptide), the increase in astrocyte attachment is much more gradual. In the literature, astrocytes have been shown to attach selectively to KHIFSDDSSSE peptide-coated glass substrates due to the homophilic property of the peptide [41], [48]. The selective attachment of astrocytes on the 100  $\mu\text{g}/\text{mL}$  peptide-treated wires even at day 1 could be due to the homophilic binding property of the peptide as discussed in the literature [41], [48]. In the control wire, the intensity of GFAP signal from astrocytes increases significantly from day 1 to day 14. The GFAP intensity from the astrocytes remains roughly the same in the case of the 100  $\mu\text{g}/\text{mL}$  peptide-treated wire sample from day 1 to day 14. This response of astrocytes to the peptide-coated wire could be due to the property of the peptide to reduce proliferation of glial cells as discussed in Chapter 2. The wire treated with other peptide concentrations (1  $\mu\text{g}/\text{mL}$ , 10  $\mu\text{g}/\text{mL}$ ) has a selective attachment of astrocytes at day 7 but the intensity of GFAP signal from astrocytes increases similar to the control wire on day 14. Thus, the 100  $\mu\text{g}/\text{mL}$  peptide-treated wire (which was shown in Chapter 3 to be the wire with the highest coverage of peptide  $\sim 82\%$ ) is effective in modulating the response of the astrocytes when compared to 1  $\mu\text{g}/\text{mL}$ , 10  $\mu\text{g}/\text{mL}$  peptide-treated and the control wires.

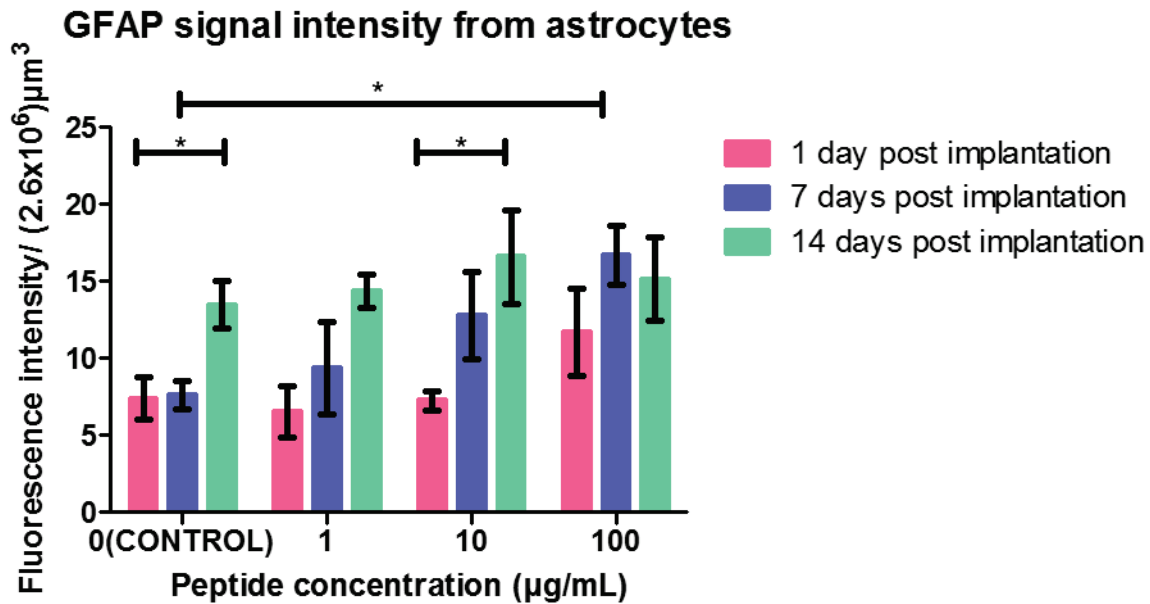


Figure 4.12: Graph showing GFAP signal intensity from the astrocytes attached to the wire that is inserted into the 0.5 wt% HAMA gel with cell seeding density of  $5 \times 10^6$  cells/mL at days 1, 7 and 14 post insertion . The wires were treated with 0  $\mu\text{g/mL}$  (control), 1  $\mu\text{g/mL}$ , 10  $\mu\text{g/mL}$  and 100  $\mu\text{g/mL}$  peptide solutions. 2 way ANOVA with Bonferroni post-test, the significance of days post insertion \*\*\* (highly significant), peptide concentration \*(significant). The interaction between the days post insertion and peptide concentration is not significant.

#### 4.5.3. Morphology of microglia and astrocytes after wire insertion

The morphology of the cells in the gel on or near the wire at various conditions was analyzed based on the zoomed confocal images (1.5 times) shown in Figure 4.13. The activated microglial phenotype in general show an amoeboid morphology (this is similar to a circular morphology). The activated microglia marks the acute response, and this activation starts from day 3 and peaks at day 7 [13]. The activated state of microglia in the gel can be qualitatively analyzed based on the circular morphology of the microglia in the gel. The activated astrocytes increase in cell volume and hence has more immunostaining for GFAP. The response of the astrocytes when activated marks the beginning of the chronic response of the CNS (which eventually forms scarring around the electrode); this typically occurs around day 14 post insertion [13]. The activated state of the astrocytes in the gel is difficult to verify qualitatively based on the analysis of the morphology of astrocytes in the gel from confocal images.

In the confocal images of Figure 4.13, the cells surrounding the peptide-coated wires and the control wire can be seen at day 7 and 14 post implantation. The microglia cells near the peptide-

coated and control wires at day 7 show a circular morphology, and this is indicative of the activated state of the microglia [9], [37]. The microglia near the peptide-coated samples (1  $\mu\text{g}/\text{mL}$ , 10  $\mu\text{g}/\text{mL}$  and 100  $\mu\text{g}/\text{mL}$ ) at day 14 also show circular morphology that is indicative of the continued activation of microglia.

From the confocal images (Figure 4.13), it appears that the astrocytes that were attached to the 100  $\mu\text{g}/\text{mL}$  peptide-treated wire were more fibrous than the control wire. However, it was not possible to determine either the morphology of the astrocytes on the wire in the gel system or the activated state of the astrocytes from the astrocytes seen in Figure 4.13. Further work would be required to do so, as discussed in the final chapter of this thesis.

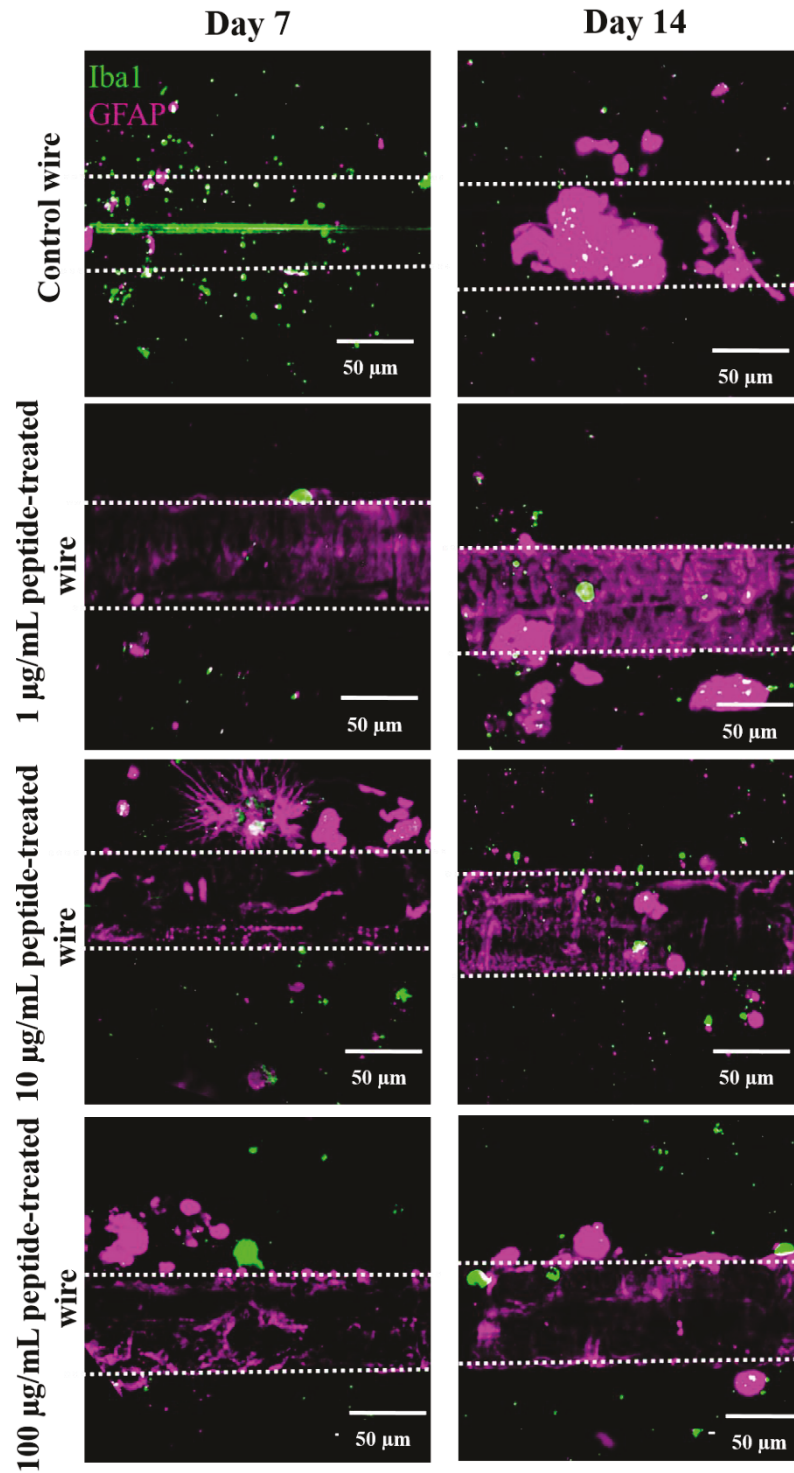


Figure 4.13: Confocal images of the 0.5 wt% HAMA gel (cell seeding density of  $5 \times 10^6$  cells/mL) with wires treated at 0  $\mu\text{g/mL}$  (control), 1  $\mu\text{g/mL}$ , 10  $\mu\text{g/mL}$  and 100  $\mu\text{g/mL}$  peptide solution at days 7 and 14 post cell encapsulation (imaged at zoom factor 1.5). The antibodies labeled for microglia (Iba1), astrocytes (GFAP).

## 4.6 Summary

In this chapter, the gel preparation, and cell integration into the gel was done based on the method developed by Jeffery *et al.* [13]. The gel was optimized (varying cell seeding density and HAMA gel wt%) to maximize the cell viability. The wires were coated with the peptide at different concentrations (1  $\mu\text{g}/\text{mL}$ , 10  $\mu\text{g}/\text{mL}$ , and 100  $\mu\text{g}/\text{mL}$ ) as described in Chapter 3. The response of the glial cells to the peptide-coated and control wires was studied. The glial cells response to the control wires was similar to the electrodes as described in the literature [9], [13], [37], [70]. The response indicates that the gel that was optimized for parameters based on the cell viability was able to model the acute response and initial stage of the chronic response.

The wires treated with the 100  $\mu\text{g}/\text{mL}$  peptide concentration were effective in reducing the number of microglia near the surface at day 7 and thereby modulating the acute response (compared with the control sample). From day 7 to day 14, the number of microglia near the wire coated from the 100  $\mu\text{g}/\text{mL}$  peptide solution remained constant (could be due to the property of the peptide to reduce the proliferation of the microglia as discussed in chapter 2). The astrocytes selectively attached to the peptide-coated wire (this could be due to homophilic binding of the peptide to the astrocyte's surface). Similarly, the intensity of GFAP signal from astrocytes attached to these wires remained roughly the same till day 14 post insertion (this could be due to the property of the due to the property of the peptide to reduce the proliferation of the microglia as discussed in chapter 2). The 100  $\mu\text{g}/\text{mL}$  peptide-treated wire is able to modulate the response of the glial cells towards the wire electrode as opposed to the control wire.

## Chapter 5.0

### Future work and conclusion

## 5.1. Overview

This thesis describes methods to coat peptide KHIFSDDSSSE on the polyimide-insulated microwires and to test the effect of the peptide-coated microwires in modulating the response of the glial cells. This chapter discusses possible future works to improve the peptide coating method and to have better understanding of the mechanisms behind the response from glial cells towards the peptide-coated microwires. Finally, the main conclusions are discussed.

## 5.2. Future work

The three possible direction for future work include 1) improving the peptide attachment process, 2) expanding the study of the stability of the peptide that is attached to the wire surface and 3) measuring indicators to determine phenotype of the glial cells, and the influence of the peptide on micromotion of the electrodes.

### 5.2.1. Improving peptide attachment process

The peptide attachment process has three steps, namely oxygen plasma treatment, silane attachment and peptide attachment (chapter 3). One possible way to improve the peptide attachment process is by using different silanes other than APTES in the silane attachment step. An organosilane namely (11-aminoundecyl) trimethoxy silane (AUTMS) can be used as a silane coating. Wang *et al.* have found that this coating had a high stability up to ten days when coated on silicon substrate under 0.9% NaCl solution at 37°C [56]. They have suggested that stability can be attributed to the molecular structure of AUTMS [56]. The molecular structure of AUTMS includes a long alkyl chain, which forms closely packed two-dimensional structure [56]. The molecular structure of AUTMS also mitigates the disrupting effect of hydrogen bonding and prevented water penetration [56]. This stable AUTMS can be applied on the polyimide-insulated microwire to improve stability.

### 5.2.2. Studies on peptide stability

The peptide stability under physiological conditions was studied in chapter 3 of this thesis. The study could not confirm if changes observed were due to the degradation of the peptide or the degradation/deattachment of the dye used to image the peptide. It is essential to find methods to quantify the peptide degradation with certainty. In this section, a new study of degradation is designed based on a study by Huh *et al.* [75]. The peptide stability in the presence of cells is also discussed.

In chapter 3 of this thesis, a study of the stability of the peptide KHIFSDDSSSE was performed. The stability of the peptide attached to the 100  $\mu\text{g}/\text{mL}$  peptide-treated wire sample was analyzed by placing these wires in 0.9 % NaCl solution for both ten and fourteen days. The fluorescence intensity of the TAMRA dye was used to quantify the peptide stability. The samples at day 10 and day 14 post incubation in NaCl solution showed an exponential decrease in fluorescence intensity of TAMRA at day 10 and day 14 when compared to samples before incubation. The fluorescence decreased to 47% at day 10 and to 27% at day 14. Though the stability test results showed an exponential decay in fluorescence over time, this trend might be due to degradation of the dye itself. The dye might not remain stable in NaCl solution for 10 or 14 days. This study could not confirm if the decrease in fluorescent intensity were due to the degradation of either the dye or peptide. A study similar to Huh *et al.* could be used to determine peptide stability[75].

Huh *et al.* have studied the stability of RGD peptide on titanium (Ti) implants (10 mm x 4mm size) [75]. They used solid, rigid polyurethane foam to mimic the bone and implanted the peptide-coated Ti implant. The RGD peptide was labeled with FITC, and this peptide-coated Ti implant was removed from the artificial bone (fixed used a customized jig) after it was rotated at 30 rotations per minute (rpm) [75]. Later, the remaining peptide from the Ti surface was eluted using 10% (v/v) ethanolamine, and they measured the fluorescent intensity of this eluted peptide using fluorescent spectroscopy. They also eluted peptide from the peptide-coated Ti implant that was not placed in the artificial bone and measured its fluorescent intensity. They compared the fluorescent intensities of both these samples to the fluorescent intensity of the uncoated Ti implant. From this comparison, they measured the peptide that had degraded from the electrode surface [75].

A method similar to the study stated above can be designed for studying the stability of peptide KHIFSDDSSSE on the microwire surface. The TAMRA-labeled peptide could be coated on the PI wire and incubated in 0.9% NaCl solution at 37 °C for few hours. The peptide-coated wires (TAMRA-labeled) without incubation in NaCl and uncoated wires would be used as negative controls. The peptide from the surface of the wire that is incubated in NaCl could be eluted using 10% (v/v) ethanolamine similar to Huh *et al.* [75] or other suitable chemicals. Similarly, the peptide from the wires that were not incubated in NaCl would be eluted. The fluorescent intensities of both these samples would be measured using fluorescent spectroscopy similar to Huh *et al.* [75]. The results could be compared with the uncoated sample, and the amount of peptide that has degraded from the PI wire could be found.

Alternatively, the degradation of the peptide might vary when the peptide is interacting with cells. The TAMRA-labeled peptide that is coated on the PI wire could be implanted into the HAMA gels with cells. The stability of the peptide could be studied using the same method describe previously.

### **5.2.3. Measurement of indicators contributing to glial scar**

The response of the glial cells in 3D gels towards the implanted peptide-coated microwire was discussed in chapter 4. From this study, the phenotypes of the glial cells were not identified. The indicators to determine the phenotype of the glial cells need to be measured. For instance, the activated microglia release oxide like nitric oxide (NO) and proinflammatory cytokine namely tumor necrosis factor alpha (TNF- $\alpha$ )[49], and these indicators need to be measured. These measurements can aid in the determination of the phenotype of the microglia *i.e.* if the microglia are activated or not.

Proinflammatory factors like IL-11 $\alpha$ , IL-1 $\beta$  and growth factors such as PDGF and BMP-2 are released by activated glial cells when an electrode is implanted *in vivo*. These factors that mimic glial scar can be added to the 3D gels. The effect of the peptide-coated wire to modulate the glial cell response can be measured and analyzed. The peptide-coated wires can be dipped in blood to mimic breaching the blood/brain barrier. Kam *et al.* have suggested that the specific astrocytes attachment on the surface of the electrode aids in the anchorage of the electrodes by preventing micromotion [41]. From chapter 4 of this thesis, astrocytes selectively attached on the 100  $\mu$ g/mL

peptide-coated microwire surface starting from day 1 post-implantation into the 3D gel containing glial cells. A study to test the effect of peptide-coated wire in reducing micromotion can help to confirm the anchorage of electrodes due to the peptide coating.

### 5.3. Conclusion

The long-term utility of any neuroprosthetic device is limited by its viability and stability within the body. These devices must be interfaced with the central nervous system (CNS) to stimulate neurons or to record neural signals. The cells of the CNS (mainly microglia and astrocytes) exhibit a foreign body response towards the implanted device. As a result of foreign body response, a scar tissue is formed around the implant. The scar tissue formation results in a loss of functionality (mainly stimulation or recording of neurons) of the device. The scar tissue causes electrical insulation of the device from the cells. Activated astrocytes secrete chemicals to inhibit neurite outgrowth in the region, thereby affecting the functionality of the device [1]. It is expected that modulation of the responses from microglia and astrocytes would enhance the compatibility of the device with CNS.

The glial cells (mainly astrocytes) of the scar tissue actively proliferate in the region. Reduction in the proliferation of glial cells is expected to influence the extent of scar tissue formed around the implant. This work focused on developing a method for modulating the responses of the microglia and astrocytes to reduce scarring around intraspinal microstimulation electrodes made of polyimide-insulated platinum (Pt) / iridium (Ir) metal alloy. The electrodes were modified with a specific peptide – with the sequence KHIFSDDSSE – to modulate the glial scar. The effect of the peptide to modulate the proliferation of the glial cells was first tested on the 2D mixed glial culture (Chapter 2). The peptide was then coated on the polyimide-insulated microwire electrodes (PI wire), and the coating was characterized (Chapter 3). The response of the glial cells to the implanted peptide-coated wire was measured and quantified *in vitro* in 3D HAMA gels containing the glial cells designed to model the foreign body response of these cells (Chapter 4).

A study examining the effects of adding peptide KHIFSDDSSE to 2D mixed glial cultures was performed (Chapter 2). Glial cells from Sprague-Dawley rat brains were successfully grown in 2D cultures. These mixed glial cultures contained microglia and astrocytes, and it represented the

more realistic heterogeneous environment in the spinal cord. In these cultures, the ability of the peptide to reduce the proliferation of these cells was tested. The number of proliferating glial cells in the presence and absence of peptide (in solution) was measured. The proliferation of glial cells was measured using a nucleotide, EdU [52] labeled with a fluorescent azide [1]. Both cell types (microglia and astrocytes) were labeled with their respective primary and secondary antibodies to specify which type of cell was proliferating. The influence of peptide (at various concentrations) on the proliferation of glial cells was studied. The peptide was shown to reduce proliferation in both cell types (astrocytes and microglia). The level of reduction varied with cell type; the proliferation of the microglia was more reduced than the proliferation of the astrocytes. This experiment was significant because this was the first time that the effect of the peptide was analyzed in mixed glial cultures, which represented more realistic heterogeneous environment in the spinal cord.

A method to covalently attach the peptide KHIFSDDSSSE to polyimide-insulated platinum (Pt) / iridium (Ir) electrodes was described in chapter 3. The peptide modification process included three steps; oxygen plasma treatment of the polyimide surface [49], [50], covalent attachment of APTES to this plasma-treated surface, and attachment of the peptide to the silane surface through EDC chemistry [43]. A variety of parameters within each step of the process was optimized to achieve high surface coverage of the peptide on the wire. Also, the stability of the coating under physiological conditions was examined, and the deposition parameters were varied to maximize stability. A reliable method to attach a stable silane monolayer to the wire was developed to undertake the effective peptide functionalization on the wire. The pH of the APTES solution was varied to obtain monolayer of silane. This method may be useful for other applications because it both optimizes the silane coating on surfaces and establishes the necessity of monolayer for further peptide functionalization in the peptide attachment process. XPS and fluorescent microscopy were used to characterize the APTES layer and its stability after incubation in physiological conditions. The samples deposited under pH 4 yielded a stable APTES layer on the wire surface when tested with 0.9 % NaCl solution at 37° C for four days. The peptide was attached to this stable APTES layer using EDC. Parameters such as EDC concentration, process time and temperature were varied to achieve high peptide coverage around the wire. Peptide coatings on the wire surface were characterized using fluorescent microscopy to image a fluorescent dye (TAMRA) attached to the peptide. The stability of the peptide coating was also analyzed by incubating the peptide-coated

wires under 0.9% NaCl solution at 37 ° C for ten and fourteen days. The dye was imaged using fluorescent microscopy. In this work, the best coatings (82% coverage) were achieved for PI wires treated with EDC concentration of 3 mg of EDC/ 1 mL of DMF, peptide concentration of 100 µg/ 1 mL of DMF at 37 °C for 4 hours. These results are important because the peptide coating on the small (50 µm in diameter) polyimide-insulated wire was high (82%) over the surface of the wire under the conditions mentioned above. The response of microglia and astrocytes in 3D hydrogel cultures to the peptide attached the wire at 1, 7 and 14 days post-implantation was measured and analyzed (Chapter 4). The 3D gels were prepared from the methacrylated hyaluronic acid (HAMA). The acute response of the microglia and the initial stage of the chronic response of the astrocytes were measured. The measured responses included the number of microglia near the surface of the wire and the intensity of GFAP signal from astrocytes attached to the wire. For this experiment, mixed glial cells (consisting of astrocytes and microglia) were extracted similar to the method in Chapter 2 and were grown in culture flasks for two weeks. The cells from the culture flasks were integrated with the 3D HAMA gel, and the cells encapsulated in gel was characterized to achieve high cell viability [13]. The wires were coated with the peptide at different concentrations (1 µg/mL, 10 µg/mL and 100 µg/mL) as described in Chapter 3. The responses of the glial cells to the peptide-coated and uncoated (control) wires were studied. The glial cell responses to the control wires were similar to the electrodes as described in the literature [9], [13], [37], [70]. This indicated the gel was able to model the acute response and initial stage of chronic response of the microglia and astrocytes.

The wires treated with the 100 µg/mL peptide concentration were effective in reducing the number of microglia near the surface at day 7 (as compared to the control wire and the wires treated with lower concentrations solutions, which had lower coverage of peptide). 100 µg/mL peptide-treated wires modulated the acute response as opposed to the control sample and the other peptide concentrations. The number of microglia near these wires remained the same within error, at all time points up to 14 days. The consistent number of microglia seen at all times could be due to the ability of the peptide to reduce the proliferation of microglia, similar to the effect of the peptide in solution as discussed in chapter 2. The astrocytes selectively attached to the 100 µg/mL peptide-coated wires, and the selective attachment could be due to homophilic binding of the peptide to the astrocyte cell surface. The intensity of GFAP signal from astrocytes attached to these wires also remained the same at days 7 and 14 post insertion. The same quantity of astrocytes at days 7

and 14 could be due to the property of the peptide to reduce the proliferation of the astrocytes similar to the effect of the peptide in solution as discussed in chapter 2. Thus, the peptide treatment at 100  $\mu\text{g}/\text{mL}$  was able to modulate the acute response and initial stage of the chronic response of the glial cells towards the wire electrodes.

This work is important because it has provided an optimized method to get high peptide (KHIFSDDSSE sequence) coverage on the polyimide-insulated microwire surface. This peptide-coated wire is shown to be effective in reducing the number of microglia -the main responders during the acute inflammatory response- near the surface of the wire. The astrocytes selectively attach to the peptide-coated wires, and their number remained the same till day 14 post insertion into the gel. The astrocytes that were attached to the peptide-coated electrodes looked more fibrous compared to the uncoated electrodes. This behavior of the astrocytes could further modulate the chronic response.

In future, measurements of indicators to determine phenotype of the glial cells will help in understanding the effectiveness of the peptide KHIFSDDSSE to modulate the acute response and chronic response of the glial cells. By addition factors (growth factors such as PDGF and BMP-2, cytokines such as IL-1 $\alpha$ , IL-1 $\beta$ , micromotion), a more accurate model of the glial scar can be built [76]–[78] and testing can be carried out to find the effectiveness of this peptide. The peptide-coated wires can be implanted in to rat brain and the responses of the glial cells to the implanted wires can be studied.

## Reference

- [1] R. J. McKeon, R. C. Schreiber, J. S. Rudge, and J. Silver, “Reduction of neurite outgrowth in a model of glial scarring following CNS injury is correlated with the expression of inhibitory molecules on reactive astrocytes.,” *J. Neurosci.*, vol. 11, no. 11, pp. 3398–3411, 1991.
- [2] O. Article, “The effect of deep brain stimulation on motor and cognitive symptoms of Parkinson ’ s disease A literature review ,” vol. 9, no. 1, pp. 24–31, 2015.
- [3] R. Yawn, J. B. Hunter, A. D. Sweeney, and M. L. Bennett, “Cochlear implantation: a biomechanical prosthesis for hearing loss,” *F1000Prime Rep.*, vol. 7, no. April, pp. 1–6, 2015.
- [4] J. M. Carmena, M. a. Lebedev, R. E. Crist, J. E. O’Doherty, D. M. Santucci, D. F. Dimitrov, P. G. Patil, C. S. Henriquez, and M. a L. Nicolelis, “Learning to control a brain-machine interface for reaching and grasping by primates,” *PLoS Biol.*, vol. 1, no. 2, pp. 193–208, 2003.
- [5] V. K. Mushahwar, D. F. Collins, and A. Prochazka, “Spinal cord microstimulation generates functional limb movements in chronically implanted cats.,” *Exp. Neurol.*, vol. 163, no. 2, pp. 422–429, 2000.
- [6] D. J. Weber, R. B. Stein, D. G. Everaert, and A. Prochazka, “Limb-state feedback from ensembles of simultaneously recorded dorsal root ganglion neurons.,” *J. Neural Eng.*, vol. 4, no. 3, pp. S168–S180, 2007.
- [7] E.-A. Ling, “The origin nature of microglia,” in *Advances in cellular neurobiology, volume 2*, S. Fedoroff and L. Hertz, Eds. Orlando: Academic Press, 1981, pp. 33–82.
- [8] Y. Oshida, *Bioscience and bioengineering of titanium materials*. Elsevier, 2010.
- [9] V. S. Polikov, P. A. Tresco, and W. M. Reichert, “Response of brain tissue to chronically implanted neural electrodes,” *J. Neurosci. Methods*, vol. 148, no. 1, pp. 1–18, 2005.

- [10] D. H. Szarowski, M. D. Andersen, S. Retterer, A. J. Spence, M. Isaacson, H. G. Craighead, J. N. Turner, and W. Shain, “Brain responses to micro-machined silicon devices,” *Brain Res.*, vol. 983, no. 1–2, pp. 23–35, 2003.
- [11] E. Nathaniel, H. J. and D. Nathaniel, R., “The reactive astrocyte,” in *Advances in cellular neurobiology, volume 2*, S. Fedoroff and L. Hertz, Eds. Orlando: Academic Press, 1981, pp. 49–301.
- [12] S. Stensaas S and J. Stensaas, L., “The reaction of the cerebral cortex to chronically implanted plastic needles,” *Acta Neuropathol*, vol. 35, pp. 187–203, 1976.
- [13] A. F. Jeffery, M. A. Churchward, V. K. Mushahwar, K. G. Todd, and A. L. Elias, “Hyaluronic acid-based 3D culture model for in vitro testing of electrode biocompatibility,” *Biomacromolecules*, vol. 15, no. 6, pp. 2157–2165, 2014.
- [14] R. W. Griffith and D. R. Humphrey, “Long-term gliosis around chronically implanted platinum electrodes in the Rhesus macaque motor cortex,” *Neurosci. Lett.*, vol. 406, no. 1–2, pp. 81–86, 2006.
- [15] J. N. Turner, W. Shain, D. H. Szarowski, M. Andersen, S. Martins, M. Isaacson, and H. Craighead, “Cerebral astrocyte response to micromachined silicon implants,” *Exp. Neurol.*, vol. 156, no. 1, pp. 33–49, 1999.
- [16] R. Biran, M. Noble, D., and P. Tresco, A., “Characterization of rat meningeal cultures on materials of differing surface chemistry,” *Biomaterials*, vol. 22, no. 23, pp. 3155–3168, 2001.
- [17] R. Biran, M. Noble, D., and P. Tresco, A., “Directed nerve outgrowth is enhanced by engineered glial substrates,” *Exp. Neurol.*, vol. 184, no. 1, pp. 141–152, 2003.
- [18] D. R. Kipke, W. Shain, G. Buzsáki, E. Fetz, J. M. Henderson, J. F. Hetke, and G. Schalk, “Advanced neurotechnologies for chronic neural interfaces: new horizons and clinical opportunities,” *J. Neurosci.*, vol. 28, no. 46, pp. 11830–11838, 2008.
- [19] A. Ersen, S. Elkabes, D. S. Freedman, and M. Sahin, “Chronic tissue response to untethered microelectrode implants in the rat brain and spinal cord,” *J. Neural Eng.*, vol. 12, no. 1, p. 16019, 2015.

- [20] T. D. Y. Kozai, N. B. Langhals, P. R. Patel, X. Deng, H. Zhang, K. L. Smith, J. Lahann, N. a Kotov, and D. R. Kipke, “Ultrasml implantable composite microelectrodes with bioactive surfaces for chronic neural interfaces.,” *Nat. Mater.*, vol. 11, no. 12, pp. 1065–73, 2012.
- [21] J. P. Seymour and D. R. Kipke, “Neural probe design for reduced tissue encapsulation in CNS,” *Biomaterials*, vol. 28, no. 25, pp. 3594–3607, 2007.
- [22] J. Thelin, H. Jörntell, E. Psouni, M. Garwicz, J. Schouenborg, N. Danielsen, and C. E. Linsmeier, “Implant size and fixation mode strongly influence tissue reactions in the CNS,” *PLoS One*, vol. 6, no. 1, 2011.
- [23] M. J. Ignatius, N. Sawhney, A. Gupta, B. M. Thibadeau, O. R. Monteiro, and I. G. Brown, “Bioactive surface coatings for nanoscale instruments: effects on CNS neurons.,” *J. Biomed. Mater. Res.*, vol. 40, no. 2, pp. 264–274, 1998.
- [24] C. Pennisi, P, M. Alcaide, S. Papaioannou, S. Meijs, A. Taylor, M. Nesladek, and V. Zachar, “Biocompatibility and electrochemical assessment of boron doped nanocrystalline diamond electrodes for neural stimulation,” *Front. Neuroeng.*, vol. 7, no. 2014, pp. 2014–2015, 2014.
- [25] C. Pennisi, P and M. Alcaide, “Nanocrystalline Diamond Films for Biomedical Applications,” *Front. Biomater.*, vol. 1, pp. 70–100, 2014.
- [26] M. Alcaide, A. Taylor, V. Zachar, and C. Pennisi, P, “Control of fibroblast growth on nanocrystalline diamond films: The effect of topography,” in *7th Annual Meeting of the Scandinavian Society for Biomaterials*, 2014.
- [27] P. J. Rousche, D. S. Pellinen, D. P. Pivin, J. C. Williams, R. J. Vetter, and D. R. Kipke, “Flexible polyimide-based intracortical electrode arrays with bioactive capability,” *IEEE Trans. Biomed. Eng.*, vol. 48, no. 3, pp. 361–370, 2001.
- [28] E. K. Purcell, J. P. Seymour, S. Yandamuri, and D. R. Kipke, “In vivo evaluation of a neural stem cell-seeded prosthesis.,” *J. Neural Eng.*, vol. 6, no. 2, p. 026005, 2009.
- [29] S. T. Retterer, K. L. Smith, C. S. Bjornsson, K. B. Neeves, A. J. H. Spence, J. N. Turner, W. Shain, and M. S. Isaacson, “Model neural prostheses with integrated microfluidics: A potential intervention strategy for controlling

- reactive cell and tissue responses,” *IEEE Trans. Biomed. Eng.*, vol. 51, no. 11, pp. 2063–2073, 2004.
- [30] M. R. Abidian and D. C. Martin, “Multifunctional nanobiomaterials for neural interfaces,” *Adv. Funct. Mater.*, vol. 19, no. 4, pp. 573–585, 2009.
- [31] D. Long, M. R. Maxwell, E. and L. French, “The effects of glucosteroids up on experimental brain edema,” in *Steroids and Brain Edema*, J. Reulen, H and K. Schihmann, Eds. Berlin: Springer Berlin Heidelberg, 1972, pp. 65–75.
- [32] C. A. R. Chapman, H. Chen, M. Stamou, J. Biener, M. M. Biener, P. J. Lein, and E. Seker, “Nanoporous Gold as a Neural Interface Coating: Effects of Topography, Surface Chemistry, and Feature Size,” *ACS Appl. Mater. Interfaces*, p. 150302143800005, 2015.
- [33] L. Rao, H. Zhou, T. Li, C. Li, and Y. Y. Duan, “Polyethylene glycol-containing polyurethane hydrogel coatings for improving the biocompatibility of neural electrodes,” *Acta Biomater.*, vol. 8, no. 6, pp. 2233–2242, 2012.
- [34] D. H. Kim, M. Abidian, and D. C. Martin, “Conducting polymers grown in hydrogel scaffolds coated on neural prosthetic devices,” *J. Biomed. Mater. Res. - Part A*, vol. 71, no. 4, pp. 577–585, 2004.
- [35] G. Ciofani, V. Raffa, T. Pizzorusso, A. Menciassi, and P. Dario, “Characterization of an alginate-based drug delivery system for neurological applications,” *Med. Eng. Phys.*, vol. 30, no. 7, pp. 848–855, 2008.
- [36] K. Kataoka, Y. Suzuki, M. Kitada, T. Hashimoto, H. Chou, H. Bai, M. Ohta, S. Wu, K. Suzuki, and C. Ide, “Alginate enhances elongation of early regenerating axons in spinal cord of young rats,” *Tissue Eng.*, vol. 10, no. 3–4, pp. 493–504, 2004.
- [37] W. He, G. C. McConnell, T. M. Schneider, and R. V. Bellamkonda, “A novel anti-inflammatory surface for neural electrodes,” *Adv. Mater.*, vol. 19, no. 21, pp. 3529–3533, 2007.
- [38] Y. Rao, X. F. Wu, J. Garipey, U. Rutishauser, and C. H. Siu, “Identification of a peptide sequence involved in homophilic binding in the Neural Cell Adhesion Molecule NCAM,” *J. Cell Biol.*, vol. 118, no. 4, pp. 937–949, 1992.

- [39] X. Cui, V. A. Lee, Y. Raphael, J. A. Wiler, J. F. Hetke, D. J. Anderson, and D. C. Martin, "Surface modification of neural recording electrodes with conducting polymer / biomolecule blends," *J. Biomed. Mater. Res.*, pp. 261–272, 2001.
- [40] S. P. Massia, M. M. Holecko, and G. R. Ehteshami, "In vitro assessment of bioactive coatings for neural implant applications.," *J. Biomed. Mater. Res. A*, vol. 68, no. 1, pp. 177–186, 2004.
- [41] L. Kam, W. Shain, J. N. Turner, and R. Bizios, "Selective adhesion of astrocytes to surfaces modified with immobilized peptides," *Biomaterials*, vol. 23, no. 2, pp. 511–515, 2002.
- [42] S. Kouvrakoglou, K. C. Dee, R. Bizios, L. V. McIntire, and K. Zygorakis, "Endothelial cell migration on surfaces modified with immobilized adhesive peptides" vol. 21, pp. 1725–1733, 2000.
- [43] K. C. Olbrich, T. T. Andersen, F. A. Blumenstock, and R. Bizios, "Surfaces modified with covalently-immobilized adhesive peptides affect fibroblast population motility," *Biomaterials*, vol. 17, no. 8, pp. 759–764, 1996.
- [44] R. A. Green, N. H. Lovell, and L. A. Poole-Warren, "Cell attachment functionality of bioactive conducting polymers for neural interfaces," *Biomaterials*, vol. 30, no. 22, pp. 3637–3644, 2009.
- [45] K. Webb, E. Budko, T. J. Neuberger, S. Chen, M. Schachner, and P. A. Tresco, "Substrate-bound human recombinant L1 selectively promotes neuronal attachment and outgrowth in the presence of astrocytes and fibroblasts," *Biomaterials*, vol. 22, no. 10, pp. 1017–1028, 2001.
- [46] X. Cui, J. Wiler, M. Dzaman, R. A. Altschuler, and D. C. Martin, "In vivo studies of polypyrrole / peptide coated neural probes," *Mater. Sci.*, vol. 24, pp. 777–787, 2003.
- [47] O. Sporns, G. M. Edelman, and K. L. Crossin, "The neural cell adhesion molecule (N-CAM) inhibits proliferation in primary cultures of rat astrocytes.," *Proc. Natl. Acad. Sci. U. S. A.*, vol. 92, no. 2, pp. 542–546, 1995.
- [48] S. Lu, A. Bansal, W. Soussou, T. W. Berger, and A. Madhukar, "Receptor-ligand-based specific cell adhesion on solid surfaces: Hippocampal neuronal

- cells on bilinker functionalized glass,” *Nano Lett.*, vol. 6, no. 9, pp. 1977–1981, 2006.
- [49] R. Polak, “Surface modification of Polymer for Improved Biocompatibility of Neural Implants Surface modification of Polymer for Improved Biocompatibility of Neural Implants,” *Main*.
- [50] L. Tang and N. Y. Lee, “A facile route for irreversible bonding of plastic-PDMS hybrid microdevices at room temperature.,” *Lab Chip*, vol. 10, no. 10, pp. 1274–1280, 2010.
- [51] G. Todaro, J. H. Green, and B. Goldberg, D, “Transformation of properties of an established cell line by SV40 and Polyoma virus,” *Proc. Natl. Acad. Sci.*, vol. 51, pp. 66–73, 1964.
- [52] F. Chehrehasa, A. C. B. Meedeniya, P. Dwyer, G. Abrahamsen, and A. Mackay-Sim, “EdU, a new thymidine analogue for labelling proliferating cells in the nervous system,” *J. Neurosci. Methods*, vol. 177, no. 1, pp. 122–130, 2009.
- [53] M. A. Churchward and K. G. Todd, “Statin treatment affects cytokine release and phagocytic activity in primary cultured microglia through two separable mechanisms,” pp. 1–12, 2014.
- [54] A. Lai, Y and K. Todd, G, “Hypoxia-Activated Microglial Mediators of Neuronal Survival Are Differentially Regulated by Tetracyclines,” *Glia*, vol. 53, pp. 809–816, 2006.
- [55] J. Saura, J. M. Tusell, and J. Serratos, “High-Yield Isolation of Murine Microglia by Mild Trypsinization,” *Glia*, vol. 44, no. 3, pp. 183–189, 2003.
- [56] A. Wang, H. Tang, T. Cao, S. O. Salley, and K. Y. S. Ng, “In vitro stability study of organosilane self-assemble monolayers and multilayers,” *J. Colloid Interface Sci.*, vol. 291, no. 2, pp. 438–447, 2005.
- [57] G. Witucki and G. Witucki, “a Silane Primer - Chemistry and Applications of Alkoxy Silanes,” *J. Coatings Technol.*, vol. 65, no. 822, pp. 57–60, 1993.
- [58] E. Metwalli, D. Haines, O. Becker, S. Conzone, and C. G. Pantano, “Surface characterizations of mono-, di-, and tri-aminosilane treated glass substrates,” *J. Colloid Interface Sci.*, vol. 298, no. 2, pp. 825–831, 2006.

- [59] R. Acres, G. A. Ellis, V. J. Alvino, C. Lenahan, E. D. Khodakov, A. G. Metha, F. and G. Andersson, G., “Molecular Structure of 3-Aminopropyltriethoxysilane Layers Formed on Silanol-Terminated Silicon Surfaces,” *J. Physical Chem. C*, vol. 116, p. 6289–6297, 2012.
- [60] A. Azioune, F. Buyl, de, and J. Pireaux, J., “Organosilane Molecular Glue for Bonding (Bio) Microchips and Sensors at Room Temperature,” in *Adhesion society*, 2006.
- [61] C. Ryu, C. Kim, and H. Chae, “Protein Patterning on a Glass Substrate with a Capillary Force Lithography Process Enhanced by Surface Treatment Processes,” *J. Korean Phys. Soc.*, vol. 51, pp. 1160–1165, 2007.
- [62] E. Vandenberg, T. L. Bertilsson, B. Liedberg, K. Uvdal, R. Erlandsson, H. Elwing, and I. Lundstorm, “Structure of 3-Aminopropyl Triethoxy Silane on Silicon Oxide,” *J. Colloid Interface Sci.*, vol. 147, pp. 103–118, 1991.
- [63] S. Xiang, G. Xing, W. Xue, C. Lua, and J. Lin, M., “Comparison of two different deposition methods of 3-aminopropyltriethoxysilane on glass slides and their application in the ThinPrep cytologic test,” *Analyst*, vol. 137, pp. 1669–1673, 2012.
- [64] R. E. Rawsterne, J. E. Gough, F. J. M. Rutten, N. T. Pham, W. C. K. Poon, S. L. Flitsch, B. Maltman, M. R. Alexander, and R. V. Ulijn, “Controlling protein retention on enzyme-responsive surfaces,” *Surf. Interface Anal.*, vol. 38, no. 11, pp. 1505–1511, 2006.
- [65] L. Jang, S and H. Liu, J, “Fabrication of protein chips based on 3-aminopropyltriethoxysilane as a monolayer,” vol. 11, pp. 331–338, 2009.
- [66] J. R. Lakowicz, “Quenching of Fluorescence,” in *Principles of Fluorescence Spectroscopy*, L. R. J, Ed. Springer US, 2006, pp. 277–300.
- [67] K. C. Dee, T. T. Andersen, and R. Bizios, “Enhanced endothelialization of substrates modified with immobilized bioactive peptides,” *Tissue Eng.*, vol. 1, no. 2, pp. 135–145, 1995.
- [68] K. C. Dee, D. C. Rueger, T. T. Andersen, and R. Bizios, “Conditions which promote mineralization at the bone-implant interface: a model in vitro study,” *Biomaterials*, vol. 17, no. 2, pp. 209–215, 1996.

- [69] J. L. West, "Modification of materials with bioactive peptides.," *Methods Mol. Biol.*, vol. 238, no. 8, pp. 113–122, 2004.
- [70] T. Fujita and et al, "Cellular dynamics of macrophages and microglial cells in reaction to stab wounds in rat cerebral cortex," *Acta Neurochir. (Wien)*, vol. 140, p. 275-279, 1998.
- [71] G. Fields, B, "Methods for Removing the Fmoc Group," in *Methods in Molecular Biology, Peptide Synthesis Protocols*, M. Pennington, W and B. Dunn , M, Eds. Humana Press Inc., 1994, p. 35.
- [72] A. Isidro-Ilobet and A. Mercedes, "Amino Acid-Protecting Groups," pp. 2455–2504, 2009.
- [73] B. Bycroft, W, W. Chan, C, S. Chhabra, R, and N. Hone, D, "A novel lysine-protecting procedure for continuous-flow solid-phase synthesis of branched peptides," *J. Chem. Soc. Chem. Commun.*, vol. 9, pp. 778–779, 1993.
- [74] W. Chan, C, B. Bycroft, W, D. Evans, J, and P. White, D, "Novel protecting group for Fmoc/tBu solid-phase synthesis of side-chain carboxy-modified peptides," *J. Chem. Soc. Chem. Commun.*, vol. 23, pp. 153–154, 1995.
- [75] J.-B. Huh, J.-Y. Lee, Y.-C. Jeon, S.-W. Shin, J.-S. Ahn, and J.-J. Ryu, "Physical stability of arginine-glycine-aspartic acid peptide coated on anodized implants after installation.," *J. Adv. Prosthodont.*, vol. 5, no. 2, pp. 84–91, 2013.
- [76] G. Garden, A and M. T, "Microglia biology in health and disease," *J. NeuroImmune Pharmacology*, vol. 1, pp. 127–137, 2006.
- [77] V. Polikov, S, J. Hong, S, and W. Reichert, M, "Soluble factor effects on glial cell reactivity at the surface of gel-coated microwires," *J. Neuroscience Methods*, vol. 190, pp. 180–187, 2010.
- [78] M. Yenari, A, T. Kauppinen, M, and R. Swanson, A, "Microglia activation in stroke: Therapeutic targets," *Am. Soc. Experimental Neurother.*, vol. 7, pp. 378–391, 2010.